The Economics of Future Membrane Desalination Processes and Applications

by

Ronan Killian McGovern

B.E., University College Dublin (2010)
S.M., Massachusetts Institute of Technology (2012)

Submitted to the Department of Mechanical Engineering
in partial fulfillment of the requirements for the degree of

Doctor of Philosophy in Mechanical Engineering

at the

MASSACHUSETTS INSTITUTE OF TECHNOLOGY

June 2014

Signature redacted

Author .....
Department of Mechanical Engineering
May 20th, 2014

Signature redacted

Certified by ..
John H. Lienhard V
Collins Professor of Mechanical Engineering
Thesis Supervisor

Signature redacted

Accepted by .....
David E. Hardt
Chairman, Committee for Graduate Studies

The Economics of Future Membrane Desalination Processes and Applications

by

Ronan Killian McGovern

Submitted to the Department of Mechanical Engineering
on May 20th, 2014, in partial fulfillment of the
requirements for the degree of
Doctor of Philosophy in Mechanical Engineering

Abstract

Seawater desalination, the desalination of waters flowing back from hydraulic fracturing processes and brackish water desalination constitute important desalination applications. These have a combined market size in excess of $25 billion per annum and a combined water production rate equivalent to the domestic consumption of over 300 million people. Each application offers its own distinct challenge. Reductions in energy consumption are key to driving down seawater desalination costs. The optimisation of water treatment in tandem with the formulation of fracturing fluids is key to reducing water management costs and environmental impacts in hydraulic fracturing. The development of desalination technologies that allow for high water recovery and high product purity is key to meeting industrial and municipal needs from brackish water sources. This thesis develops and investigates three emerging technologies: forward osmosis, electrodialysis at high salinity and hybrid electrodialysis-reverse osmosis with a view to addressing the three above challenges.

Forward osmosis has often been viewed as a technology with the potential to reduce energy consumption in seawater desalination. An analysis is therefore undertaken into the theoretical limits upon its energy requirements paying particular attention to the energy penalty involved in drawing water from the feed stream into a more concentrated solution. Although unaddressed in literature this energy penalty is an important and distinguishing factor between FO and other desalination technologies. In the case of seawater, it is shown to put FO at a disadvantage that makes it difficult to compete with reverse osmosis. Consequently, it is argued that forward osmosis research should be reoriented away from seawater desalination to focus on alternate applications where salinities are above those which reverse osmosis can handle or where draw solution regeneration is not required. For these alternate applications a new framework is provided that explains the influence of the membrane orientation upon water flux through the membrane, an insight that is of particular use in considering the trade-off between water flux and fouling.

The conventional view of electrodialysis is that it is most cost effective for the desalination of low salinity waters, and less so for moderate and high salinities, such

as those encountered in waters that flow back from hydraulic fracturing processes. A thermoeconomic analysis of the effect of salinity upon cost reveals a different picture whereby electrodialysis is most cost effective removing salt from streams with between 1,000 ppm and 20,000 ppm of total dissolved solids. At lower salinities performance is hampered by low solution conductivity and low salt removal rates. At higher salinities the process is thermodynamically inefficient as the chemical potential of salt is raised only by a small amount when transported into the concentrate stream. The conclusion is that applications requiring salt removal within this 'sweet spot' for electrodialysis, such as the treatment of waste waters from flue-gas desulphurisation and coal-bed methane production, merit accelerated investigation.

Incumbent technologies for the recycling of water produced from shales are currently inefficient and expensive. A study of electrodialysis energy requirements and equipment costs indicates that they are similar to, or even lower than, those for distillation. By developing a numerical model of system performance, which was validated over the range of 250 ppm to 192,000 ppm NaCl, it was possible to optimise the electrodialysis stack voltage and bring about cost savings of up to 30% in certain cases. These results and this numerical model warrant and will guide further investigations of electrodialysis under field conditions.

Finally, a hybrid electrodialysis-reverse osmosis system was designed and optimised such that the reverse osmosis unit shifts salt removal in the electrodialysis unit into its sweet spot. The combination of these two technologies results in a system that provides enhanced product purity and product recovery at reduced cost. A simple rule of thumb is provided to guide practitioners in their choice between hybrid and standalone systems. This rule allows a choice to be made based on the relative cost of water from electrodialysis and reverse osmosis.

Thesis Supervisor: John H. Lienhard V
Title: Collins Professor of Mechanical Engineering

Acknowledgments

I thank my co-authors, who contributed to this work: David Cohen-Tanugi, Shreya Dave, Prof. Jeffrey Grossman, Jordan Mizerak and others whom I will mention below. I thank current and former members of Prof. Lienhard's research group: Karan, Ed, Jacob, Mohamad, Charlene, Kishor, Urmi, Christine, David, Bader, Seongpil, Mohit, Jai, Karim, John and Emily. In particular, I thank Chester, Lige and Adam, with whom it was a pleasure to work on the electrodialysis project. I thank Adam for teaching me about baseball, Leo for teaching me jazz, Prakash for teaching me how to write patents and Greg, a friend whom I greatly trust. I thank my committee members, Prof. Evelyn Wang and Prof. Jongyoon Han, for their enthusiastic support for my plan of study, and Prof. Syed Zubair, for spending significant time with me when visiting and providing great encouragement. I thank Jim Freedman of the Technology Licensing Office with whom it has been a pleasure to work. I thank my advisor Prof. John Lienhard V. His courage and flexibility in allowing me to pursue and take responsibility for new research ideas allowed me to learn rapidly at MIT and his continuous support and responsiveness is greatly appreciated. I thank Ivonne, Anne-Marie, Faddy, Gabriel and Audren for the time we have spent together since we all arrived in the USA. I thank my parents, Jim and Stephanie, my sister, Aoife, and my brother, Fergal. In Irish we say 'Níl aon tinteán mar do thinteán fèin', meaning 'There's no place like home'. My family has always made me feel at home, even when I'm away. I've learned greatly and will remember fondly my time at MIT. We may have Twitter and Facebook to keep in touch but technology is no replacement for tears. Technology is no replacement for tears and with desalination those tears will always be fresh.

Sponsors supporting this work

I thank the U.S. Department of State for support through the Fulbright Science and Technology program, the Hugh Hampton Young Memorial Fund for support through a graduate fellowship, the King Fahd University of Petroleum and Minerals for funding through the Center for Clean Water and Clean Energy at MIT and KFUPM, the Martin Family for support through the Martin Fellowship for Sustainability and the International Desalination Assocation for support through the Channabasappa Memorial Scholarship.

Contents

Chapter 1

Introduction

This thesis addresses the development of technology for three significant desalination applications: seawater desalination, produced water recycling for the hydraulic fracturing of shales and brackish water desalination. The emphasis is placed on addressing a core challenge faced in each of these applications. These core challenges are summarised in this introductory section.

1.1 Seawater desalination: The challenge of reducing energy consumption

In the last twenty years, approximately 42,000,000 m^3/day of seawater desalination plant capacity had been installed worldwide[1]. Based on estimated per capita water withdrawals associated with public water supply of 574 litres per day in 2005[2], this capacity would satisfy the needs of approximately 73 million people. Increasingly, the preferred technology for seawater desalination is the membrane based pressure-driven process of reverse osmosis[3], which accounted for approximately 59% of total seawater desalination plant capacity that came online in the past 20 years[1].

The cost of desalinated water[4,5] currently lies roughly in the region of 0.5-1.5 $\$/m^3$, excluding distribution costs. Significant efforts to reduce these costs rest on reducing the energy demands of the desalination process. Depending on the price of

electricity, water costs attributable to energy (Fig. 1-1) can account for a significant portion of total water costs. Interestingly, though energy costs may seem high, energy requirements have already fallen drastically, in fact energy requirements twenty five years ago were more than double what they are today[17]. Improvements in membrane permeability and the emergence of pressure recovery devices have succeeded in capturing energy savings that constituted the 'low lying fruit'. Now, membrane development is at such a stage that further improvements in permeability are unlikely to bring about significant energy savings[3], as shown in Fig. 1-2. This recent work on the benefits of higher membrane permeability suggests that instead improvements will come about through a redesign of the reverse osmosis process. Such a redesign might entail a move towards batch rather than continuous processes, as suggested by a recent study[6] showing that energy savings of up to 7% are achievable while maintaining the water production rate constant (Fig. 1-3).

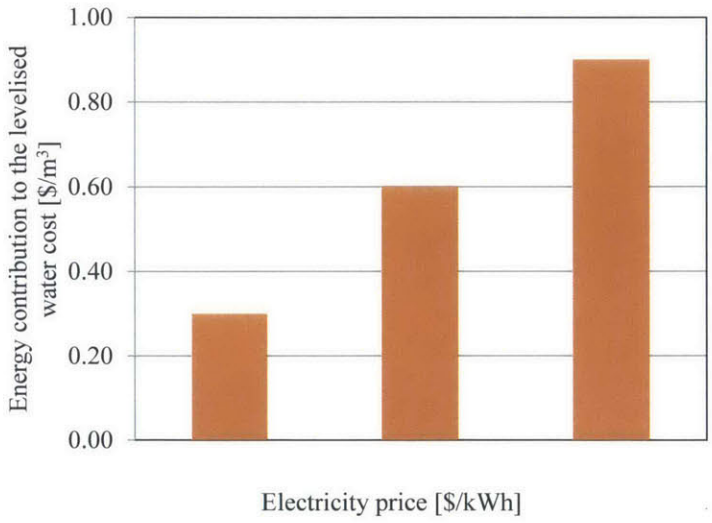

Figure 1-1 Given desalinated water prices vary from 0.50-1.50 $/m^3, energy accounts for a significant portion of costs, even when electricity prices are low. This plot is based upon reverse osmosis energy consumption[5] of 3 kWh/m^3

Thus, one of the great open questions in seawater desalination is whether another technology might someday outperform reverse osmosis and achieve lower energy consumption. Chapter 2 of this thesis addresses this question by analysing whether

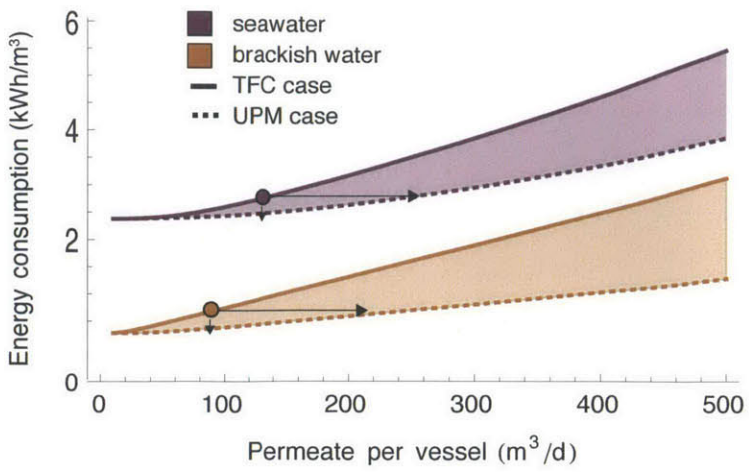

Figure 1-2 Specific energy consumption of RO vs. permeate production per vessel, for conventional thin film composite (TFC) membranes (solid) and ultra permeable membranes (UPM) at 3X greater permeability (dashed). Circles depict the baseline case, and the arrows indicate how each RO system could operate given the availability of UPMs. Feed flowrate is held fixed while pressure increases as a function of permeate production. The potential improvement in energy consumption is limited as current systems already operate with the hydraulic pressure close to the osmotic pressure of concentrated brine exiting the RO module. Image taken from Cohen-Tanugi et al.[3]

forward osmosis, an emerging membrane desalination process, might be able to compete. Chapter 3 follows up by addressing alternate forward osmosis applications other than seawater desalination focusing on how water transport can be maximised through optimisation of the membrane orientation.

1.2 Desalination of produced waters from hydraulic fracturing: The challenge of integrating desalination into water reuse

Due to a lack of comprehensive data, it is difficult to estimate the quantity of water that flows to the surface in the US each day as a result of the hydraulic fracturing of shales for oil and gas extraction. However, given that the quantity of water produced in the long term varies from roughly 200-1,000 gallons per MMCF of natural gas[7] (27-135 m^3 water per million cubic meters of gas) and roughly 26 trillion cubic feet (736

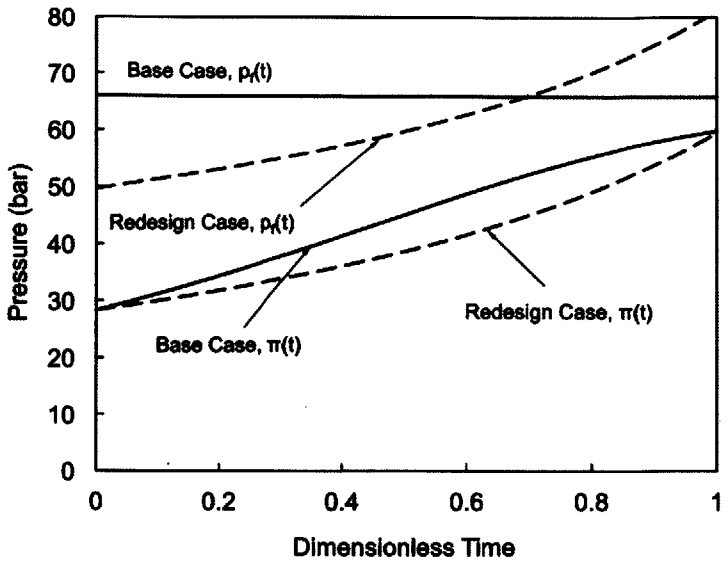

Figure 1-3 Hydraulic and osmotic pressure profiles vs. dimensionless time elapsed in the batch process. Solid lines show the pressure profiles for the base case where the hydraulic pressure is maintained constant. Dashed lines correspond to a batch process where the hydraulic pressure is increased at a rate that matches the osmotic pressure. The feed solution in each case is 35,000 ppm NaCl and the recovery ratio is 50%. The mean driving pressure difference is equal in both cases but the variance in driving pressure difference is lower in the redesigned case. Image taken from Thiel et al.[6]

billion m^3) of gas were produced from shales in the US in 2012[8], this puts produced water volumes in the long run at between 340,000 and 1,700,000 bbls/day or between 54,000 and 270,000 m^3/day.

By and large these waters are disposed of, often through injection underground, or recycled as a source of water for subsequent fracturing processes[11]. The rates of reuse vary geographically and depend upon freshwater costs, transport costs, wastewater disposal costs (Fig. 1-4) in the locality. Central to the viability of water reuse is an understanding of how recycled water quality affects the chemistry and performance of fluids used in the fracturing process. The composition of waters flowing to the surface varies geographically (Fig. 1-4) with total dissolved solids reaching levels above 300,000 ppm in certain cases. At the present time various approaches to water treatment exist with some advocating direct reuse high salinity waters, even up to 270,000 ppm[9], while others prefer total dissolved solids to be limited to 90,000 ppm

or even lower[10]. The key challenge in the long run is therefore to design a water treatment process whose costs, in addition to the costs of formulating the fracturing fluid, are minimised.

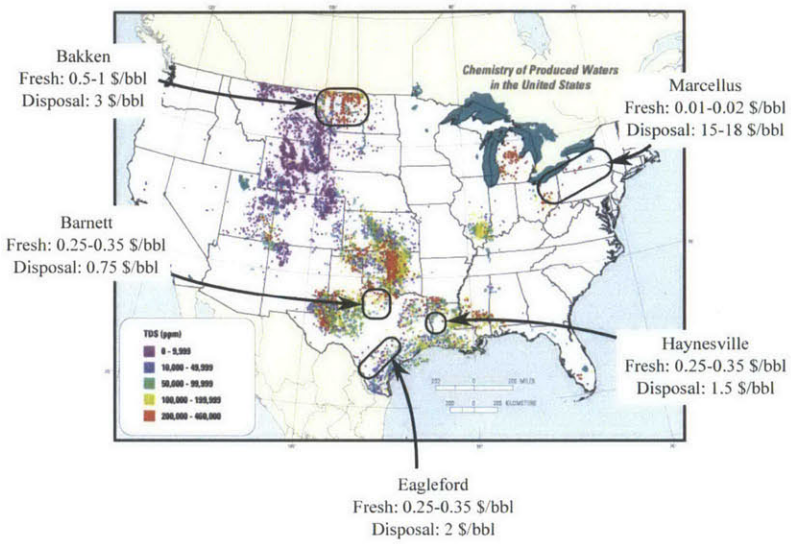

Figure 1-4 Map illustrating the ranges of produced water total dissolved solids concentrations from the U.S. Geological Survey's Produced Waters Database augmented with estimates of fresh water and disposal costs in major shale plays[11,12].

By and large, the current options for water treatment[11] are primary treatment (involving solids and oil removal) at circa $1/bbl and distillation (providing a highly pure product) at circa $3.5-6.25/bbl. Chapters 4 to 6 explore the possibility of a third option; partial desalination using electrodialysis to a level of purity that falls between the extremes of primary treatment and complete desalination through distillation. Chapter 4 provides a framework to understand the range of salinities where electrodialysis operates most cost effectively. Chapter 5 addresses the design and operational aspects of a high salinity electrodialysis process (operating in conjunction with reverse osmosis). Finally, Chapter 6 provides an experimental and economic study of electrodialysis over a range of salinities from 500 ppm to 192,000 ppm NaCl.

1.3 Brackish and industrial water desalination: The challenges of high purity and high recovery

In the last 20 years, 6.3 million m^3/day of brackish desalination plant capacity came online treating waters containing between 500 ppm and 3,000 ppm of total dissolved solids. These volumes are equivalent to the domestic consumption of approximately 110 million people. The cost of water[4] from these plants, of which 94% employed reverse osmosis or nanofiltration technology[1], ranged between 0.1 and 1 $\$/m^3$. Of particular importance is the large fraction of plants that provide high purity water to industry. Figure 1-5 shows that 46% of product water contained less than 10 ppm of total dissolved solids, which is 50 times more stringent than World Health Organisation guidelines for drinking water[13].

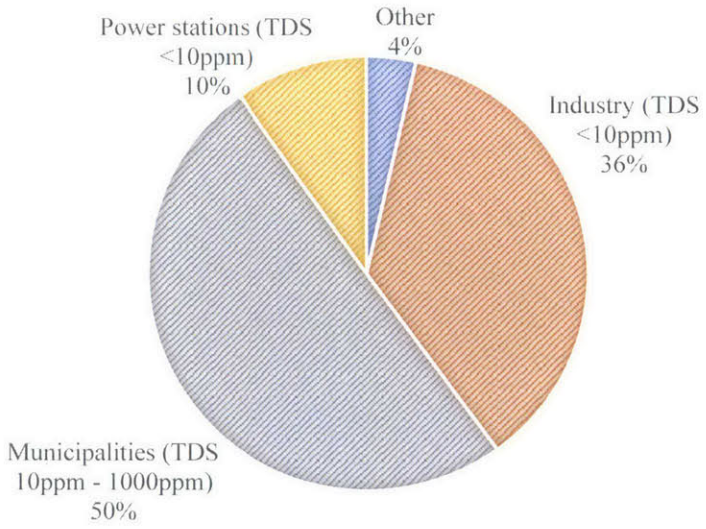

Figure 1-5 Breakdown of brackish desalination plants online in the years 1994-2014 treating waters between 500 and 3,000 ppm TDS[1].

While high purity is one desirable aspect of a brackish desalination technology, a high ratio of water recovered to feed water, known as the recovery ratio, is a second. High recovery ratios reduce feed water requirements and also reduce the volume of waste that must be disposed of after the desalination process. One of the major challenges faced in brackish desalination is thus the design of a process that can simul-

taneously achieve the goals of high product purity and high product recovery. The two primary brackish desalination technologies, reverse osmosis and electrodialysis (which accounts for 4% of installed capacity in Fig. 1-5), have undergone and are still undergoing adaptation to meet these goals. Traditional reverse osmosis technologies, which are based on water removal, achieve excellent product purity but require multiple membrane stages to remove high percentages of water. Adaptation of the process is currently taking place in the form of a batch reverse osmosis process, which can be implemented within the same stage[14]. Electrodialysis, by contrast, easily achieves high water recovery as only salt is removed. However, high levels of purity are challenging to achieve due to low electrical conductivity. In the case of electrodialysis, adaptation has involved the use of ion-conductivity spacers within flow channels in a process known as electrodeionisation[15,16].

Rather than focus on either of the dominant brackish technologies alone Chapter 7 explores the idea of hybridising reverse osmosis and electrodialysis processes. The objective is to leverage the synergy of water removal and salt removal technologies and achieve high purity high recovery processes at reduced cost.

1.4 In summary

The scale, cost, and economic significance of desalination is well illustrated by considering the volume of water produced, its cost, and the product of these two quantites: the approximate market size. Figure 1-6 summarises this information and sets out the challenges and potential solutions according to the order with which they are addressed in Chapters 2 through 7.

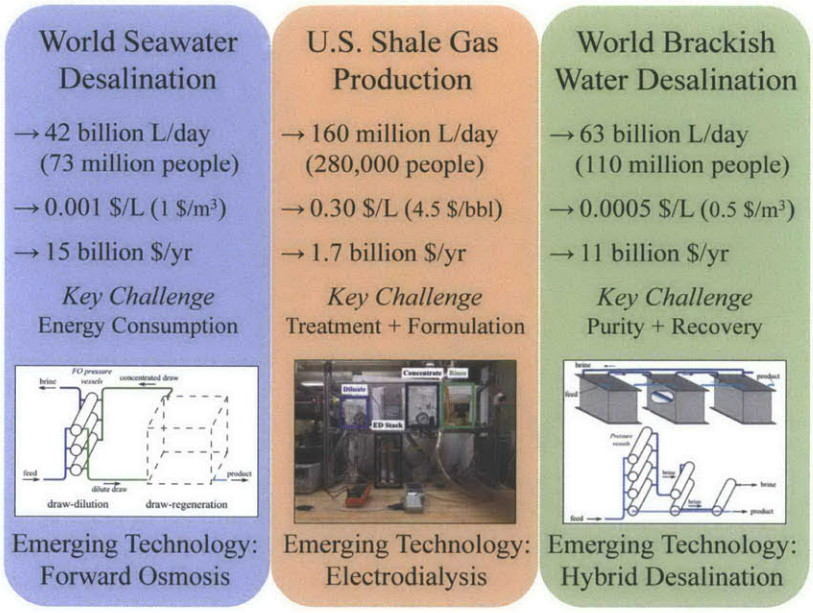

Figure 1-6 Illustration of the water volumes, water costs, challenges faced in three key desalination applications along with the solutions investigated within this thesis. Water volume and cost data are intended as a rough guide. Ranges for these values are provided in Sect. 1.1, 1.2 and 1.2. Per person water use is based on an average U.S. domestic water consumption of 336 litres per day in 2005[2]

Bibliography

[1] Desaldata. Analysis, 2014. desaldata.com.

[2] Joan F Kenny, Nancy L Barber, Susan S Hutson, Kristin S Linsey, John K Lovelace, and Molly A Maupin. *Estimated use of water in the United States in 2005.* US Geological Survey Reston, VA, 2009.

[3] David Cohen-Tanugi, Ronan K McGovern, Shreya H Dave, John H Lienhard, and Jeffrey C Grossman. Quantifying the potential of ultra-permeable membranes for water desalination. *Energy & Environmental Science*, 7(3):1134–1141, 2014.

[4] Lauren F Greenlee, Desmond F Lawler, Benny D Freeman, Benoit Marrot, and Philippe Moulin. Reverse osmosis desalination: water sources, technology, and today's challenges. *Water research*, 43(9):2317–2348, 2009.

[5] Sunny Wang Srinivas (Vasu) Veerapaneni, Ben Klayman and Rick Bond. Desalination facility design and operation for maximum efficiency. Technical report, Water Research Foundation, 2011.

[6] Gregory P Thiel, Ronan K McGovern, Syed M Zubair, and John H Lienhard V. Thermodynamic equipartition for increased second law efficiency. *Applied Energy*, 118:292–299, 2014.

[7] Matthew E Mantell. Produced water reuse and recycling challenges and opportunities across major shale plays. In *Proceedings of the Technical Workshops for the Hydraulic Fracturing Study: Water Resources Management. EPA*, volume 600, pages 49–57, 2011.

[8] U.S. Energy Information Administration. Technically recoverable shale oil and shale gas resources: An assessment of 137 shale formations in 41 countries outside the united states, June 2013.

[9] Renee LeBas, P Lord, D Luna, and T Shahan. Development and use of high-tds recycled produced water for crosslinked-gel-based hydraulic fracturing. In *2013 SPE Hydraulic Fracturing Technology Conference*, 2013.

[10] *Proceedings and Minutes of the Hydraulic Fracturing Expert Panel XTO Facilities, Fort Worth September 26*, 2007.

[11] James A Slutz, Jeffery A Anderson, Richard Broderick, Patrick Harold Horner, et al. Key shale gas water management strategies: An economic assessment. In *International Conference on Health Safety and Environment in Oil and Gas Exploration and Production*. Society of Petroleum Engineers, 2012.

[12] Shawn Shipman, Drew McConnell, Morgan Paul Mccutchan, Kushal Seth, et al. Maximizing flowback reuse and reducing freshwater demand: Case studies from the challenging marcellus shale. In *SPE Eastern Regional Meeting*. Society of Petroleum Engineers, 2013.

[13] World Health Organization. *Guidelines for drinking-water quality: recommendations*, volume 1. World Health Organization, 2004.

[14] Avi Efraty. Closed circuit desalination series no-4: High recovery low energy desalination of brackish water by a new single stage method without any loss of brine energy. *Desalination and Water Treatment*, 42(1-3):262–268, 2012.

[15] Jonathan Wood, Joseph Gifford, John Arba, and Michael Shaw. Production of ultrapure water by continuous electrodeionization. *Desalination*, 250(3):973–976, 2010.

[16] GC Ganzi. Electrodeionization for high purity water production. In *AIChE Symposium series*, volume 84, 1988.

[17] Menachem Elimelech and William A. Phillip. The future of seawater desalination: energy, technology, and the environment. *Science*, 333(6043):712–717, 2011.

Chapter 2

On the potential of forward osmosis to energetically outperform reverse osmosis desalination

Abstract

We provide a comparison of the theoretical and actual energy requirements of forward osmosis and reverse osmosis seawater desalination. We argue that reverse osmosis is significantly more energy efficient and that forward osmosis research efforts would best be fully oriented towards alternate applications. The underlying reason for the inefficiency of forward osmosis is the draw-dilution step, which increases the theoretical and actual energy requirements for draw regeneration. As a consequence, for a forward osmosis technology to compete with reverse osmosis, the regeneration process must be significantly more efficient than reverse osmosis. However, even considering the optimisation of the draw solution and the benefits of reduced fouling during regeneration, the efficiency of an optimal draw regeneration process and of reverse osmosis are unlikely to differ significantly, meaning the energy efficiency of direct desalination with reverse osmosis is likely to be superior.

Contributions

This chapter was co-authored by Prof. John Lienhard V and received financial support from the Hugh Hampton Young Memorial Fellowship.

2.1 Introduction

Energy consumption accounts for approximately 20-35% of the total cost of water in reverse osmosis desalination of seawater[1], and a greater fraction when the price of electricity is high. In this context, forward osmosis, a technology with the benefit of operating at low pressures[2–9], has been promoted as an alternative to reverse osmosis. Indeed, seawater desalination is very frequently cited as a motivating application for the study of forward osmosis; 17 of the 20 most cited articles that include the words 'forward' and 'osmosis' within their titles on the Thomson Reuters Web of Science Database address seawater desalination[2,4,5,8,10–25]. This level of interest in forward osmosis for seawater desalination is surprising given that FO processes have higher theoretical and actual energy requirements than reverse osmosis, though this is seldom acknowledged[26] or analysed.

In this context, we perform an energetic comparison of reverse osmosis, the most energy efficient commercial desalination technology[1], and forward osmosis, an indirect means of desalination, consisting of two steps; the dilution of a concentrated draw solution, and, its subsequent regeneration (Fig. 2-1). We outline how the draw-dilution step of Fig. 2-1 influences the theoretical and actual energy consumption of draw-regeneration, we assess how efficient draw-regeneration need be for forward osmosis to compete with reverse osmosis, and we outline what efficiency might be achievable by the most efficient draw-regeneration systems.

2.2 Thermodynamic limits upon draw regeneration

The minimum theoretical energy[a] required for the direct desalination of a feed stream depends upon the feed composition and the recovery ratio. For a seawater feed of 35,000 ppm total dissolved solids and a recovery of 50%, the theoretical energy

[a]The 'minimum theoretical energy requirement', which may also be termed the 'minimum thermodynamic energy requirement' or the 'reversible work requirement' will from here on, for brevity, be referred to as the 'theoretical energy'.

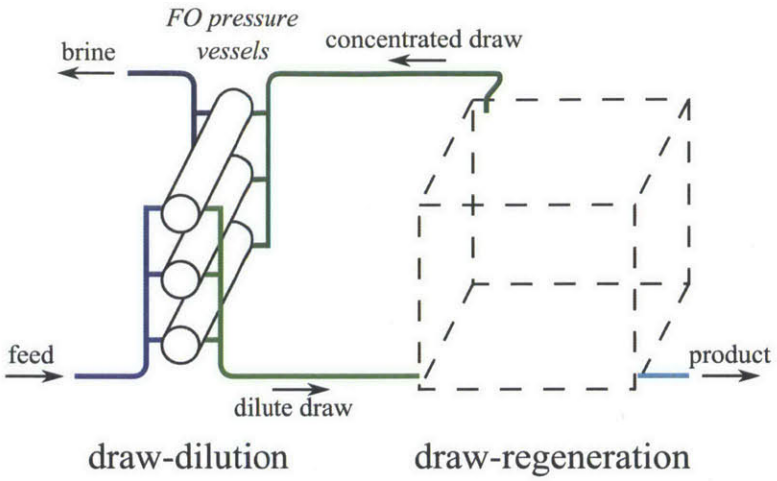

Figure 2-1 A two step desalination involving draw dilution by forward osmosis and a draw regeneration process

requirement[27] of 1.05 kWh/m^3 places single-stage seawater reverse osmosis, with an energy consumption[1] of about 2.5 kWh/m^3, at a thermodynamic efficiency of about 42% (if pre-treatment, raw and treated water conveyance are excluded).

Since forward osmosis involves the initial transfer of water from the feed to a draw solution of higher osmotic pressure, the theoretical energy required for regeneration is different. Specifically, the theoretical energy required to remove an infinitesimal volume of pure water dV_p from a solution at an osmotic pressure of π is πdV_P. On a volumetric basis, say in J/m^3 (equivalent to pascals), the minimum energy required is given by the osmotic pressure π. Thus, by first drawing water from a feed solution at π_F into a draw solution at π_D, the theoretical energy required to produce pure water increases by a factor of π_D/π_F.

The same arguments hold for a desalination process where a finite recovery (*e.g.*, greater than infinitesimal) of the feed stream is desired. Figure 2-2 illustrates a counter-flow draw dilution process where the relative mass flow ratio of the feed and draw are controlled to facilitate a driving osmotic pressure difference that is close to uniform. The feed salinity is a 35,000 ppm NaCl solution and the inlet draw osmotic pressure is 78.5 bar. The draw solution in this case is modelled as NaCl, though this is in-consequent as an almost identical osmotic pressure profile may be

obtained with almost any draw solution[b] by tailoring the mass flow rate ratio. To calculate the theoretical energy for water production, the product of osmotic pressure and permeate production are integrated over the process:

$$E_T = \frac{1}{\dot{V}_P^{tot}} \int_0^{\dot{V}_p^{tot}} \pi(\dot{V}_P)\, \mathrm{d}\dot{V}_P \tag{2.1}$$

$$= \frac{1}{RR^{tot}} \int_0^{RR^{tot}} \pi(RR)\, \mathrm{d}RR \tag{2.2}$$

Figure 2-3 illustrates the effect of the mean osmotic pressure ratio (π_D/π_F — averaged over water permeation through the membrane) in Fig. 2-2 upon the theoretical energy required for draw solution regeneration. The theoretical energy penalty is the difference between the theoretical energy required for direct desalination and the theoretical energy for draw regeneration. Both the magnitude of this energy penalty, and the total theoretical energy required for draw solution regeneration depend only on the osmotic pressure of the draw solution and not on its chemical composition.

The magnitude of the energy penalty increases rapidly with an increasing osmotic pressure ratio. At a mean pressure ratio of 2.3 (mean osmotic pressure differential of 50 bar), the theoretical energy requirements for a forward osmosis process reach 2.5 kWh/m^3 — the *actual* energy requirement of energy efficient reverse osmosis plants. Therefore, if forward osmosis systems are to achieve energy efficiency that is comparable to RO, low osmotic pressure ratios during draw-dilution are a necessity.

2.3 An energetic comparison of FO and RO

While reverse osmosis is typically electrically driven, the regeneration process in forward osmosis may also be thermally or chemically driven. Rather than delve into the amortised equipment (*e.g.* solar collectors or waste-heat exchangers) and fuel costs for various different direct desalination and draw regeneration processes, we compare

[b]The saturation osmotic pressure of the draw must be above the maximum desired osmotic pressure

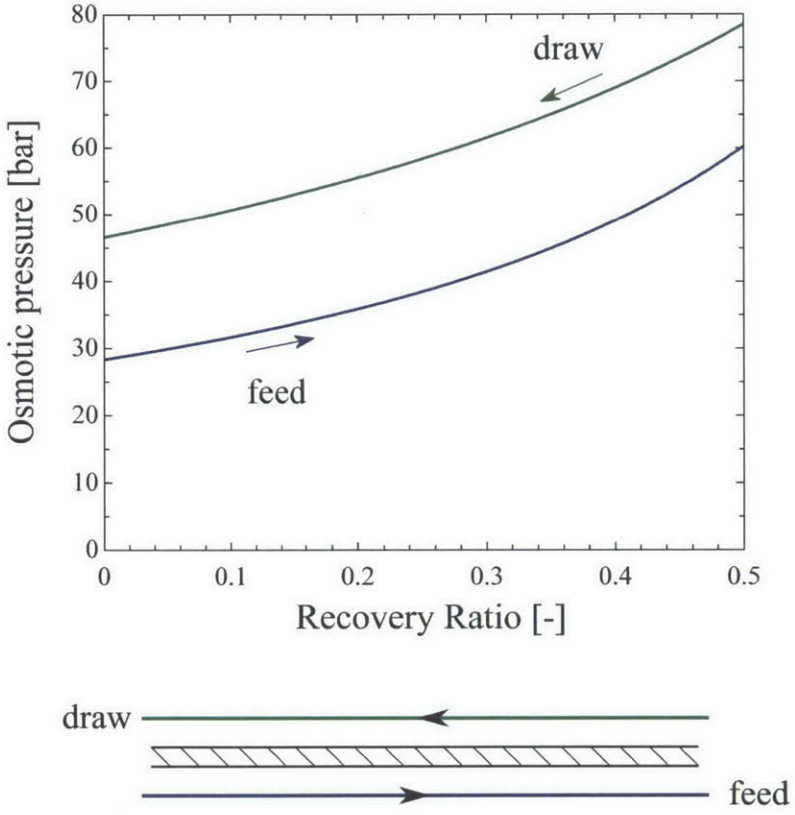

Figure 2-2 Counterflow feed concentration and draw solution dilution forward osmosis process. Feed stream of 35,000 ppm NaCl at 25°C. Draw solution of aqueous NaCl at an inlet osmotic pressure of 67.3 bar. Osmotic coefficients taken from Robinson and Stokes[28].

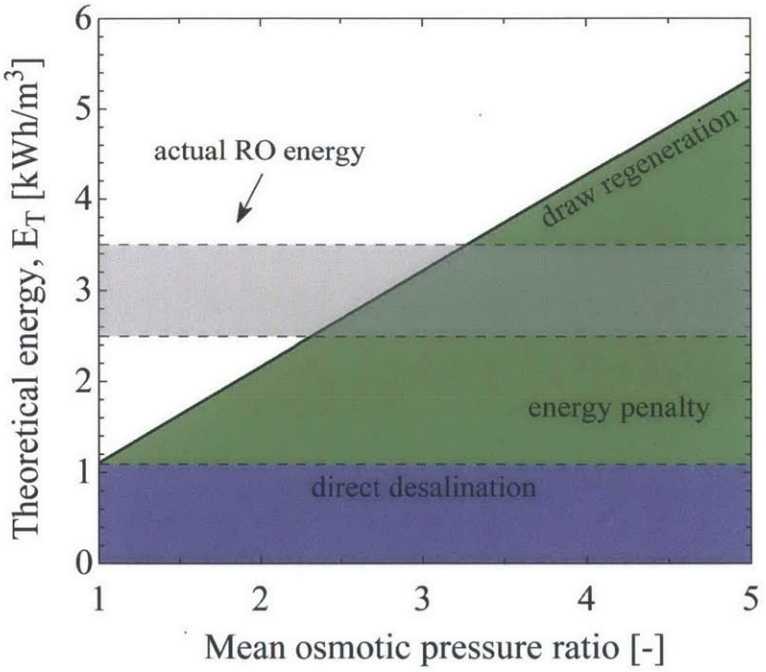

Figure 2-3 Effect of the mean osmotic pressure ratio upon the energy penalty imposed by draw solution dilution. Feed stream as in Fig. 2-2. Draw solution of aqueous NaCl with the inlet osmotic pressure and mass flow rate varied to achieve desired mean osmotic pressure ratio.

FO and RO systems on the basis of their thermodynamic efficiencies. For the reverse osmosis process, the thermodynamic efficiency, η_R, is the ratio of the theoretical energy required to recover a defined portion of the feed water as a pure water product, E_T to the actual energy (or more strictly exergy[29]), E, required:

$$\eta_R^{RO} = \frac{E_T^{RO}}{E^{RO}} = \frac{\frac{1}{RR^{tot,RO}} \int_0^{RR^{tot,RO}} \pi_{sw}(RR)\,\mathrm{d}RR}{E}. \tag{2.3}$$

For a draw regeneration process η_R^{regen} differs only in that osmotic pressure of the draw solution, rather than of seawater, is integrated over the recovery ratio of the draw regeneration process:

$$\eta_R^{RO} = \frac{E_T^{regen}}{E^{regen}} = \frac{\frac{1}{RR^{tot,regen}} \int_0^{RR^{tot,regen}} \pi_{draw}(RR)\,\mathrm{d}RR}{E^{regen}}. \tag{2.4}$$

E^{regen} is the exergy required to drive the actual regeneration process, which for an electrically driven process equals the electrical energy required and for a thermally driven process is related, by the dead state temperature, T^0, and the temperature, T^{source}, at which heat, Q^{regen}, is supplied, by:

$$E^{regen} = \left(1 - \frac{T^0}{T^{source}}\right) Q^{regen}. \tag{2.5}$$

Thus, for a draw regeneration process, η_R^{regen} relates the theoretical energy required to restore the draw solution from its most diluted to its most concentrated state, to the actual energy required (again on a Second Law basis).

In our comparison, we parametrise the thermodynamic efficiency of both reverse osmosis and draw regeneration using η_R. We consider the desalination of a 35,000 ppm stream of NaCl, with RO and FO systems at a recovery of 50%. For the draw dilution process we consider a mean osmotic pressure difference of 19.4 bar (osmotic pressure ratio of approximately 1.5). This driving force is based on the net driving pressure for a typical seawater reverse osmosis system, 2.A. A larger (smaller) osmotic

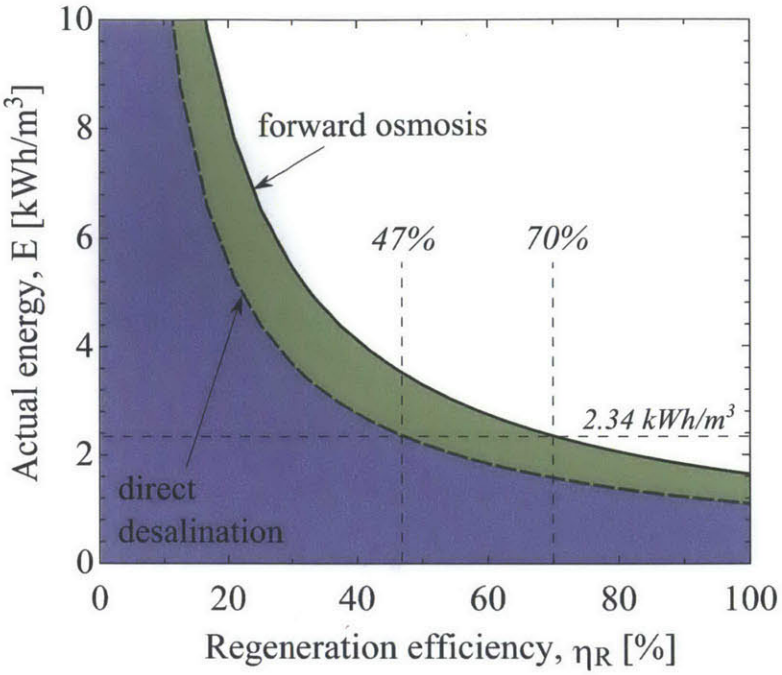

Figure 2-4 Effect of the efficiency of the draw regeneration process upon overall energy consumption. Feed stream of 35,000 ppm NaCl at 25°C and recovery ratio of 50% in all cases. Draw solution of aqueous NaCl with inlet osmotic pressure of 78.5 bar. The energy consumption of a typical single pass reverse osmosis system is indicated.

pressure difference would result in a lower (higher) forward osmosis capital costs but higher (lower) theoretical and actual energy penalties. Setting the mean driving force in forward osmosis equal to that in reverse osmosis is perhaps conservative since flux is lower in FO (at the same driving pressure difference) due to concentration polarisation[12] and thus area requirements would be higher[30].

Figure 2-4 illustrates the actual energy consumption of the RO and FO systems. Whereas the theoretical energy penalty for a draw dilution desalination process is shown in Fig. 2-3, the actual energy penalty is shown, in green, in Fig. 2-4. The actual energy penalty is calculated as the theoretical energy penalty divided by the regeneration/direct-desalination efficiency. Its presence means that the actual energy consumption of forward osmosis is always above that of reverse osmosis if reverse osmosis and the draw regeneration process operate at the same efficiency.

To perform a more complete comparison we can compare the energy consumption for a forward osmosis system and a two-pass reverse osmosis system that includes

Table 2.1 Comparison of two-pass reverse osmosis with forward osmosis assuming 47% efficiency for the first RO pass and for draw regeneration. 35,000 ppm NaCl feed @ 50% recovery.

Two-pass RO		FO	
	kWh/m^3		kWh/m^3
Ultra-filtration	0.16	Draw dilut.	0.10
RO - 1st Pass	2.34	Draw regen.	3.48
RO - 2nd Pass	0.50	-	-
Total	3.00	Total	3.58

pre-treatment, Table 2-3. Experiments suggest that forward osmosis exhibits lower rates of irreversible fouling than reverse osmosis[31] and thus might be expected to cope with lower levels of pre-treatment. As a limiting case we can neglect pre-treatment for forward osmosis and consider ultrafiltration pretreatment for reverse osmosis, estimating pumping power consumption of 0.1 and 0.3 kWh/m^3 respectively 2.B. Assuming the FO draw regeneration process to be just as efficient as RO leads to an energy requirement of 3.48 kWh/m^3 for draw regeneration, compared to 2.34 kWh/m^3 for the first pass of reverse osmosis (from Fig. 2-4). Thus, even allowing for the additional energy typically consumed in a second pass of reverse osmosis (0.5 kWh/m^3)[32,33], the total energy consumption of reverse osmosis remains lower than forward osmosis.

2.4 An analysis of RO as a regeneration process for FO

According to Fig. 2-4, a single pass RO system must operate at an efficiency of η_R=47% to achieve a specific energy consumption of 2.34 kWh/m^3 (the energy consumption of a representative seawater RO process, see 2.A). To match this performance, the regeneration portion of a forward osmosis system must achieve regeneration at an efficiency of η_R=70% — an increase of 23 percentage points. Since RO is currently the most energy efficient of desalination systems[27] (thermal regeneration

systems are estimated to achieve about 6-8% efficiency[c] and, in the case of a thermally regenerated ammonia-carbon dioxide solution, energy requirements for a final reverse osmosis purification step may further reduce efficiency[35].) it is therefore important to analyse whether reverse osmosis, operating as a draw regeneration system, can significantly outperform reverse osmosis as a direct desalination system[36]. Five factors to consider include the possibilities of:

1. employing higher permeability nano-filtration membranes.

2. increasing permeability through optimisation of the draw solution composition;

3. increasing permeability by optimising temperature;

4. lower levels of fouling as a result of treating a clean draw rather than feed seawater; and

5. reducing feed flow rates per vessel (and thus energy consumption) due to lower fouling.

Although nano-filtration membranes offer superior permeability, they exhibit inferior solute rejection to reverse osmosis membranes. For example, the nominal $CaCl_2$ rejection of nanofiltration membranes is typically in the range of 89%[37], compared to normalised NaCl rejections of 99.8%[38] for RO membranes. Thus, the use of nanofiltration necessitates multiple passes of filtration[39] or draw solutes that are large in size[40]. Unfortunately, larger molecules (such as sucrose and glucose) typically exhibit lower diffusivities than NaCl, which result in stronger concentration polarisation and reduced flux in the draw dilution step. This is particularly true when the FO membrane is oriented in forward osmosis mode[41], as is typically necessary to minimise

[c]For seawater desalination at 50% recovery, Semiat et al. estimated energy requirements of 13 kWh/m^3, leading to an efficiency of 1.1/13 = 8%[34]. For 50% recovery of a 73,000 ppm NaCl feed stream in pure form, an actual auxilliary system power of 8.5 kWh/m^3 and an electrical input of 21 kWh/m^3 for mechanical vapor compression was reported by McGinnis[35]. Based upon a theoretical minimum requirement of 1.9 kWh/m^3 this suggests an efficiency of 6%. While the use of low temperature waste heat may reduce fuel costs, the capital costs of heat exchangers required to capture waste heat are typically prohibitive (see 2.C).

Table 2.2 Influence of temperature, fouling and cross-flow optimisation on reverse osmosis efficiency, computed using membrane projection software[44] with a 35,000 ppm NaCl feed and operating at 50% recovery (see 2.A).

	temp. [° C]	fouling factor [-]	membranes/ vessel [-]	average flux [lmh]	theoretical spec. energy [kWh/m^3]	actual spec. energy [kWh/m^3]	efficiency [-]
direct desalination	25	0.8	6	13.5	1.1	2.34	47%
temperature	40	0.8	6	13.5	1.1	2.27	+1.4% pts
fouling	25	0.91	6	13.5	1.1	2.30	+0.8% pts
cross-flow	25	0.8	5	13.5	1.1	2.33	+0.2% pts

fouling[17,42]. Thus, while large solutes such as glucose may allow the use of nanofiltration membranes, flux in the draw-dilution step is significantly reduced compared to using an NaCl draw solution of the same osmotic pressure[39].

An analysis of the effect of feed solution chemistry on the permeability of reverse osmosis membranes[43] revealed that permeability decreased with increasing ionic strength. Since the draw solution must be of higher concentration than the feed water, and thus typically of higher ionic strength, this suggests that RO regeneration is at a disadvantage compared to direct reverse osmosis treatment of the feed; at least if the draw solution is ionic. As previously discussed, non-ionic draw solutes (such as glucose and sucrose) are undesirable as they increase the membrane area required in the draw dilution step.

To analyse the effects of temperature, fouling and cross-flow optimisation upon energy consumption we perform comparative analyses of RO systems using membrane projection software[44]. Holding constant the feed composition and recovery ratio we vary the feed temperature, the fouling factor and the number of membrane elements per vessel one by one, as indicated in Table 2.2.

In FO-RO processes, since the draw solution is recirculated it can potentially be maintained at a temperature above that of the feed[45], with the objective of increasing membrane permeability. However, this effect is mitigated, particularly at temperatures above 25°C, by the increase in osmotic pressure with temperature[46]. Thus, the overall enhancement in efficiency in going from 25 to 40°C, 1.4% pts, is small.

When operating as a draw regeneration process, RO benefits from lower fouling rates than a direct seawater desalination process. The levels of fouling (flux reduced to 91% of nominal after 3 years[44]) might be considered similar to that of the second pass in a two pass RO system[45], rather than the levels of fouling seen when treating seawater from an open intake (flux reduced to 80% of nominal after 3 years[44]). A comparison of the energy consumption reveals that the improvement in efficiency, of 0.8% pts, remains small. While this analysis focuses on energy consumption it is true that there may be cost benefits if membrane replacement is reduced in hybrid FO-RO processes. However, the contribution of energy to the cost of water can be five times more important than the cost of membrane replacement, as seen in the analysis of Reddy and Ghaffour[47].

A further benefit arising from reduced fouling is a relaxation of the requirement for a minimum brine cross-flow velocity to reduce fouling[44] in the reverse osmosis unit used for draw regeneration. Holding the average flux constant, this would allow for operation with a larger number of shorter pressure vessels (fewer elements per vessel). The reduced viscous pressure drop within shorter vessels with reduced flow rates can allow for a slight reduction in feed pressure and energy consumption. However the improvement in efficiency, +0.2% pts, is small, in part due to the strengthening of concentration polarisation at lower cross flow velocities.

Ultimately, the draw-dilution step requires draw regeneration to be significantly more efficient (+23% pts) than direct reverse osmosis desalination if the overall energy consumption of forward osmosis is to be comparable. Though reductions in fouling and the optimisation of temperature can enhance the regeneration efficiency, these effects are an order of magnitude smaller than what is required. It appears, therefore, that forward osmosis is better suited to applications other than seawater desalination, particularly those where reverse osmosis cannot directly compete.

2.5 Comments on alternate forward osmosis applications

One implication of the energy penalty, imposed by draw dilution, is that forward osmosis research might increasingly focus on regeneration-free applications[48], *e.g.*, where the draw solution is a nutrient containing drink[49], a concentrated fertilizer[50], or a kill fluid for hydraulic fracturing[51]. Forward osmosis processes that dilute rather than concentrate the feed stream are a second option, whereby forward osmosis is used to dilute seawater feeds, prior to reverse osmosis desalination, by employing a low salinity 'impaired' source of water[52]. This dilution provides an energy benefit compared to direct desalination of seawater but an energy penalty compared to the direct desalination of the impaired stream. Perhaps the viability of pre-dilution will be decided by weighing the benefits of a dual-barrier FO-RO system versus the benefits of avoiding the energy penalty of draw-dilution in single-barrier RO desalination of the impaired stream[53].

Desalination applications where the osmotic pressures of feeds are too great for existing reverse osmosis technologies are also potentially promising for forward osmosis[54,55]. Here, the alternatives to forward osmosis that desalinate feed streams directly are primarily evaporative technologies with efficiencies that draw regeneration processes can potentially surpass[35]. Meanwhile, evaporative technologies may well improve in efficiency[56,57] and reverse osmosis may increase its reach in terms of osmotic pressure, perhaps through tiered processes[58], but until then forward osmosis may offer energetic advantages at salinities higher than seawater.

2.6 Conclusion

The draw dilution step in forward osmosis desalination systems places the draw regeneration process at a significant energetic disadvantage compared to direct desalination of the feed stream with reverse osmosis. Even with optimisation of the draw solution, and the benefit of reduced fouling in the regeneration step, the overall forward osmosis

Table 2.3 Seawater reverse osmosis projection[44]

Feed source	open seawater intake
Feed TDS	35,000 ppm NaCl
Feed temperature	25°C
Recovery	50%
Membranes	SWC5
Elements/vessel	6
Pressure recovery	isobaric
Average flux	13.5 lmh
Net driving pressure	19.4 bar
Specific energy	2.34 kWh/m^3

process is unlikely to approach the energy efficiency of reverse osmosis for seawater desalination. In this light, it appears best for forward osmosis research to focus fully on high salinity applications and applications that do not require draw regeneration, where reverse osmosis cannot compete.

2.A Seawater Reverse Osmosis Example

Basic input parameters for the base seawater reverse osmosis case are provided in Tab. 2.3. A detailed list of parameters is provided in the Supplementary Electronic Information for this base case as well as the three other cases of Tab. 2.2.

2.B Ultrafiltration and forward osmosis pumping power estimations

The maximum transmembrane pressure in ultrafiltration is in the region of 2 bar[59]. Assuming close to 100% recovery of water from the ultrafiltration unit and a pump efficiency of 70% this leads to power consumption of approximately 0.16 kWh/m^3 of product water from the entire system.

To estimate the pressure difference between the feed inlet and outlet and the draw inlet and outlet we employ the pressure difference of 0.6 bar between the feed inlet and the brine outlet in the RO base example of 2.A. Assuming a pump efficiency of

70% this leads to an energy consumption of approximately 0.10 kWh/m^3.

2.C Evaluation of heat exchanger costs in waste heat driven forward osmosis applications

Fuel costs may be minimal when low temperature waste heat is employed to drive a desalination process. However, the cost of heat exchangers required to capture waste heat is significant. This is largely because the lower the temperature of the heat source, the lower its exergy, and, consequently, the larger the amount of heat required and the higher the heat exchanger costs. For example, if we consider a draw solution regeneration process requiring E^{regen}=13 kWh of exergy per m^3 of product water desalinated (the electrical energy requirement computed by Semiat et al. for a thermally regenerated seawater forward osmosis process[34]), we can compute the heat exchanger size, p_{HX} [in kW$_t$/(m^3/day)] theoretically required for the process to be thermally driven by a heat source at temperature T^{source}:

$$p_{HX} = \frac{E^{regen}}{1 - \frac{T^0}{T^{source}}} \times \frac{\text{day}}{\text{hr}}, \tag{2.6}$$

where T^0 is the ambient temperature. The capital cost of the heat exchangers required can then be obtained by considering the cost of heat exchangers on a \$/kW$_t$ basis, which, according to a recent report, can fall roughly[d] within the range of \$500-2,000/kW$_t$[60]. In Fig. 2-5 we illustrate how the cost and size of the heat exchangers required depends upon the heat source temperature assuming, conservatively, a heat exchanger cost of \$500/kW$_t$. At low temperatures, the capital cost of heat exchangers becomes very large, in fact, much larger than the capital costs of multi-effect distillation plants[47] (or reverse osmosis plants for that matter, typically \$600-800/(m^3/day)[47]). Thus, unless low temperature draw regeneration (or desalination) processes can be developed with significantly lower exergetic requirements (or

[d]This range depends in part on whether heat exchange occurs between two liquids, a liquid and a condensing fluid or a liquid and an evaporating fluid.

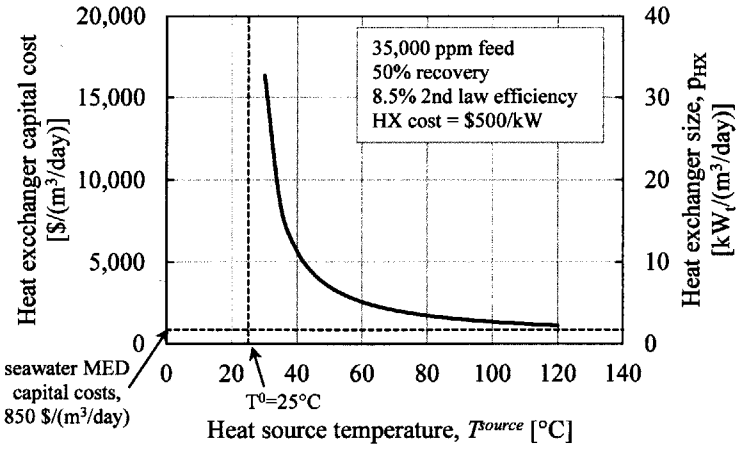

Figure 2-5 When using low temperature heat sources to drive desalination the total heat input required, and thus heat exchanger size and costs, become very large. Here, heat exchanger costs are compared to typical capital costs for large scale multi-effect distillation systems[47].

equivalently, significantly higher 2nd law efficiencies than existing thermal processes such as those documented by Mistry et al.[29]) heat exchanger costs pose a major barrier to desalination using waste heat.

Bibliography

[1] S. W. Srinivas (Vasu) Veerapaneni, Ben Klayman, R. Bond, Desalination facility design and operation for maximum efficiency, Tech. rep., Water Research Foundation (2011).

[2] Q. Yang, K. Y. Wang, T.-S. Chung, Dual-layer hollow fibers with enhanced flux as novel forward osmosis membranes for water production, Environmental science & technology 43 (8) (2009) 2800–2805.

[3] M. M. Ling, K. Y. Wang, T.-S. Chung, Highly water-soluble magnetic nanoparticles as novel draw solutes in forward osmosis for water reuse, Industrial & Engineering Chemistry Research 49 (12) (2010) 5869–5876.

[4] W. A. Phillip, J. S. Yong, M. Elimelech, Reverse draw solute permeation in forward osmosis: modeling and experiments, Environmental science & technology 44 (13) (2010) 5170–5176.

[5] R. Wang, L. Shi, C. Y. Tang, S. Chou, C. Qiu, A. G. Fane, Characterization of novel forward osmosis hollow fiber membranes, Journal of Membrane Science 355 (1) (2010) 158–167.

[6] T.-S. Chung, S. Zhang, K. Y. Wang, J. Su, M. M. Ling, Forward osmosis processes: yesterday, today and tomorrow, Desalination 287 (2012) 78–81.

[7] J.-J. Qin, W. C. L. Lay, K. A. Kekre, Recent developments and future challenges of forward osmosis for desalination: a review, Desalination and Water Treatment 39 (1-3) (2012) 123–136.

[8] S. Zhao, L. Zou, C. Y. Tang, D. Mulcahy, Recent developments in forward osmosis: Opportunities and challenges, Journal of Membrane Science 396 (2012) 1–21.

[9] C. Boo, S. Lee, M. Elimelech, Z. Meng, S. Hong, Colloidal fouling in forward osmosis: role of reverse salt diffusion, Journal of Membrane Science 390 (2012) 277–284.

[10] T. Y. Cath, A. E. Childress, M. Elimelech, Forward osmosis: Principles, applications, and recent developments, Journal of membrane science 281 (1) (2006) 70–87.

[11] J. R. McCutcheon, R. L. McGinnis, M. Elimelech, A novel ammoniacarbon dioxide forward (direct) osmosis desalination process, Desalination 174 (1) (2005) 1–11.

[12] J. McCutcheon, M. Elimelech, Influence of concentrative and dilutive internal concentration polarization on flux behavior in forward osmosis, Journal of Membrane Science 284 (1) (2006) 237–247.

[13] J. R. McCutcheon, R. L. McGinnis, M. Elimelech, Desalination by ammonia–carbon dioxide forward osmosis: influence of draw and feed solution concentrations on process performance, Journal of Membrane Science 278 (1) (2006) 114–123.

[14] N. Y. Yip, A. Tiraferri, W. A. Phillip, J. D. Schiffman, M. Elimelech, High performance thin-film composite forward osmosis membrane, Environmental Science & Technology 44 (10) (2010) 3812–3818.

[15] G. T. Gray, J. R. McCutcheon, M. Elimelech, Internal concentration polarization in forward osmosis: role of membrane orientation, Desalination 197 (1) (2006) 1–8.

[16] R. W. Holloway, A. E. Childress, K. E. Dennett, T. Y. Cath, Forward osmosis

for concentration of anaerobic digester centrate, Water Research 41 (17) (2007) 4005–4014.

[17] B. Mi, M. Elimelech, Chemical and physical aspects of organic fouling of forward osmosis membranes, Journal of Membrane Science 320 (1) (2008) 292–302.

[18] C. Y. Tang, Q. She, W. C. Lay, R. Wang, A. G. Fane, Coupled effects of internal concentration polarization and fouling on flux behavior of forward osmosis membranes during humic acid filtration, Journal of Membrane Science 354 (1) (2010) 123–133.

[19] E. Cornelissen, D. Harmsen, K. De Korte, C. Ruiken, J.-J. Qin, H. Oo, L. Wessels, Membrane fouling and process performance of forward osmosis membranes on activated sludge, Journal of Membrane Science 319 (1) (2008) 158–168.

[20] A. Achilli, T. Y. Cath, E. A. Marchand, A. E. Childress, The forward osmosis membrane bioreactor: a low fouling alternative to mbr processes, Desalination 239 (1) (2009) 10–21.

[21] B. Mi, M. Elimelech, Organic fouling of forward osmosis membranes: Fouling reversibility and cleaning without chemical reagents, Journal of membrane science 348 (1) (2010) 337–345.

[22] R. L. McGinnis, M. Elimelech, Energy requirements of ammonia–carbon dioxide forward osmosis desalination, Desalination 207 (1) (2007) 370–382.

[23] K. Y. Wang, T.-S. Chung, J.-J. Qin, Polybenzimidazole (pbi) nanofiltration hollow fiber membranes applied in forward osmosis process, Journal of Membrane Science 300 (1) (2007) 6–12.

[24] A. Tiraferri, N. Y. Yip, W. A. Phillip, J. D. Schiffman, M. Elimelech, Relating performance of thin-film composite forward osmosis membranes to support layer formation and structure, Journal of Membrane Science 367 (1) (2011) 340–352.

[25] J. R. Mccutcheon, M. Elimelech, Modeling water flux in forward osmosis: Implications for improved membrane design, AIChE Journal 53 (7) (2007) 1736–1744.

[26] R. Semiat, Energy issues in desalination processes, Environmental science & technology 42 (22) (2008) 8193–8201.

[27] K. H. Mistry, R. K. McGovern, G. P. Thiel, E. K. Summers, S. M. Zubair, J. H. Lienhard V, Entropy generation analysis of desalination technologies, Entropy 13 (10) (2011) 1829–1864. doi:10.3390/e13101829.
URL http://www.mdpi.com/1099-4300/13/10/1829/

[28] R. Robinson, R. Stokes, Electrolyte Solutions, Courier Dover Publications, 2002.

[29] K. H. Mistry, J. H. Lienhard, Generalized least energy of separation for desalination and other chemical separation processes, Entropy 15 (6) (2013) 2046–2080.

[30] D. L. Shaffer, N. Y. Yip, J. Gilron, M. Elimelech, Seawater desalination for agriculture by integrated forward and reverse osmosis: Improved product water quality for potentially less energy, Journal of Membrane Science 415 (2012) 1–8.

[31] S. Lee, C. Boo, M. Elimelech, S. Hong, Comparison of fouling behavior in forward osmosis (fo) and reverse osmosis (ro), Journal of Membrane Science 365 (1) (2010) 34–39.

[32] P. Glueckstern, M. Priel, Optimization of boron removal in old and new swro systems, Desalination 156 (1) (2003) 219–228.

[33] S. Rybar, R. Boda, C. Bartels, Split partial second pass design for swro plants, Desalination and Water Treatment 13 (1-3) (2010) 186–194.

[34] R. Semiat, J. Sapoznik, D. Hasson, Energy aspects in osmotic processes, Desalination and Water Treatment 15 (1-3) (2010) 228–235.

[35] R. L. McGinnis, N. T. Hancock, M. S. Nowosielski-Slepowron, G. D. McGurgan, Pilot demonstration of the nh_3co_2 forward osmosis desalination process on high salinity brines, Desalination 312 (2013) 67–74.

[36] A. Altaee, G. Zaragoza, H. R. van Tonningen, Comparison between forward osmosis-reverse osmosis and reverse osmosis processes for seawater desalination, Desalination 336 (2014) 50–57.

[37] Hydranautics, Esna1-lf (2014).

[38] Hydranautics, Swc5 (2014).

[39] C. Tan, H. Ng, A novel hybrid forward osmosis-nanofiltration (fo-nf) process for seawater desalination: draw solution selection and system configuration, Desalination and water treatment 13 (1-3) (2010) 356–361.

[40] J. Su, T.-S. Chung, B. J. Helmer, J. S. de Wit, Enhanced double-skinned fo membranes with inner dense layer for wastewater treatment and macromolecule recycle using sucrose as draw solute, Journal of Membrane Science 396 (2012) 92–100.

[41] C. H. Tan, H. Y. Ng, Revised external and internal concentration polarization models to improve flux prediction in forward osmosis process, Desalination 309 (2013) 125 – 140.

[42] S. Zhao, L. Zou, D. Mulcahy, Effects of membrane orientation on process performance in forward osmosis applications, Journal of Membrane Science 382 (1) (2011) 308–315.

[43] J. Wang, Y. Mo, S. Mahendra, E. Hoek, Effects of water chemistry on structure and performance of polyamide composite membranes, Journal of Membrane Science 452 (2014) 415–425.

[44] Hydranautics, Integrated membrane solution design, imsdb3 v. 63 (2011).

[45] P. G. Nicoll, Forward osmosis as a pre-treatment to reverse osmosis, The International Desalination Association World Congress on Desalination and Water Reuse 2013 / Tianjin, China.

[46] R. Franks, S. Chilekar, C. R. Bartels, The unexpected performance of highly permeable swro membranes at high temperatures, IDA Journal of Desalination and Water Reuse 4 (1) (2012) 52–56.

[47] K. Reddy, N. Ghaffour, Overview of the cost of desalinated water and costing methodologies, Desalination 205 (1) (2007) 340–353.

[48] L. A. Hoover, W. A. Phillip, A. Tiraferri, N. Y. Yip, M. Elimelech, Forward with osmosis: Emerging applications for greater sustainability, Environmental science & technology 45 (23) (2011) 9824–9830.

[49] J. Kessler, C. Moody, Drinking water from sea water by forward osmosis, Desalination 18 (3) (1976) 297–306.

[50] S. Phuntsho, H. K. Shon, S. Hong, S. Lee, S. Vigneswaran, A novel low energy fertilizer driven forward osmosis desalination for direct fertigation: Evaluating the performance of fertilizer draw solutions, Journal of Membrane Science 375 (1) (2011) 172–181.

[51] N. Hutchings, E. Appleton, R. McGinnis, Making high quality frac water out of oilfield waste, in: SPE Annual Technical Conference and Exhibition, 2010.

[52] T. Cath, C. Lundin, J. Drewes, A dual-barrier and energy saving osmosis-assisted desalination process for drinking water augmentation, AwwaRF Project 4150 (2009) N/A.

[53] R. K. McGovern, J. Mizerak, S. M. Zubair, J. H. Lienhard, Three dimensionless parameters influencing the optimal membrane orientation for forward osmosis, Journal of Membrane Science.

[54] N. T. Hancock, M. S. Nowosielski-Slepowron, L. S. Marchewka, Application of forward osmosis based membrane brine concentrators for produced water, The International Desalination Association World Congress on Desalination and Water Reuse 2013 / Tianjin, China.

[55] B. D. Coday, P. Xu, E. G. Beaudry, J. Herron, K. Lampi, N. T. Hancock, T. Y. Cath, The sweet spot of forward osmosis: Treatment of produced water, drilling wastewater, and other complex and difficult liquid streams, Desalination 333 (1) (2014) 23–35.

[56] R. K. McGovern, G. Prakash Narayan, J. H. Lienhard V, Analysis of reversible ejectors and definition of an ejector efficiency, International Journal of Thermal Sciences 54 (2012) 153–166.

[57] R. K. McGovern, K. V. Bulusu, M. A. Antar, J. H. Lienhard V, One-dimensional model of an optimal ejector and parametric study of ejector efficiency, Proceedings of ECOS (2012) 26–29.

[58] C. Wohlert, Apparatus and methods for solution processing using reverse osmosis, US Patent App. 12/455,998 (US2010032377A1), uS Patent App. 12/455,998.

[59] Dow, Dow ultrafiltration modules (2014).

[60] R. Hackl, S. Harvey, Identification, cost estimation and economic performance of common heat recovery systems for the chemical cluster in stenungsund, Tech. rep., Chalmers University of Technology (2013).

Chapter 3

Three dimensionless parameters influencing the optimal membrane orientation for forward osmosis

Abstract

In many forward osmosis applications, flux is maximised (and capital costs minimised) when the membrane is oriented such that the feed solution faces the support layer (PRO mode). Here, a framework is developed to understand the factors that determine the membrane orientation that maximises flux. In the absence of fouling, a dimensionless form of the water transport equations reveals the importance of three dimensionless groups: the ratio of draw to feed osmotic pressure; the ratio of draw to feed solute diffusivity; and the resistance to water transport of the support layer relative to the active layer. A parametric study of these parameters and an application of the dimensionless equations to three important FO processes, reveals that having the draw solution face the support layer (FO mode) can maximise flux in specific instances. Interestingly, this implies operation in FO mode can both maximise flux and minimise fouling for fertigation applications and the concentration of flowback waters from hydraulic fracturing.

Contributions

This chapter was co-authored by Jordan Mizerak, Prof. Syed Zubair and Prof. John Lienhard V. The work received financial support from the Hugh Hampton Young Memorial Fund Fellowship, the International Desalination Association's Channabasappa Memorial Scholarship, the MIT Martin Fellowship for Sustainability and the King Fahd University of Petroleum and Minerals through the Center for Clean Water and Clean Energy at MIT and KFUPM under project number R15-CW-11.

3.1 Introduction

Forward osmosis involves water being drawn from a solution of lower osmotic pressure, through a semi-permeable membrane, into a solution of higher osmotic pressure[a]. The flux of water through the membrane is important, as it determines the amount of membrane area and number of membrane pressure vessels required for a given process. Via modelling[2,3] and experimental validation[4,5], three factors have been identified as retarding the rate of water transport: the resistance of the salt-rejecting active layer to water transport, the build up of a high (or low, depending on membrane orientation) concentration region within the support layer (internal concentration polarisation, ICP) and the build up of high and low concentration regions within the solutions on either side of the membrane (external concentration polarisation, ECP). Of the three factors, internal concentration polarisation is regarded as most detrimental to water flux[5], since the lack of crossflow within the support layer results in a significant transverse concentration difference.

The existence of internal concentration polarisation has important implications when optimising the membrane orientation. Membranes are typically asymmetric and consist of a porous support layer and a salt-rejecting active layer. It is well known in literature that the degree of concentration polarisation depends on whether the support layer is facing the feed or the draw solution[1] (Fig. 3-1). When the feed is facing the active layer and the draw faces the support layer this is commonly known as the forward mode, forward osmosis mode or FO mode. When the feed is facing the support layer and draw faces the active layer this is commonly known as the reverse mode or PRO (Pressure Retarded Osmosis) mode. Given the same feed and draw solution chemistries, flux is often maximised with the support layer facing the feed[6–8b].

Beyond this observation, examinations of the optimal membrane orientation have largely focused upon considerations of fouling in both FO and PRO mode, where

[a]See Figs. 1 & 9 in[1] for the principle of operation and a typical spiral-wound membrane implementation.

[b]Fig. 5 in Mehta and Loeb[6], Fig. 4a in Gray et al.[7] and Fig. 4a in Tang et al.[8]

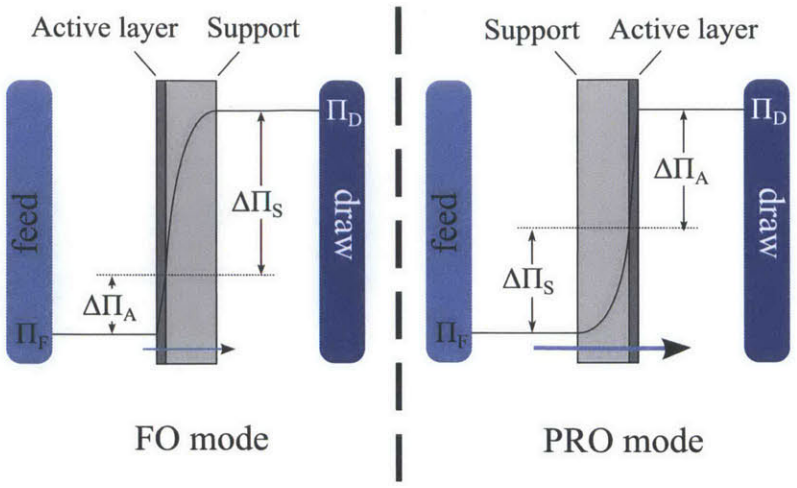

Figure 3-1 In FO mode, the orientation of the support layer towards the solution of higher concentration (the draw) results in stronger internal concentration polarisation, a lower osmotic driving force across the active layer and lower water flux. The effects of external concentration polarisation are not shown.

the rate of fouling and the dependence post-cleaning flux recovery upon membrane orientation (often better in the support-to-draw orientation[9,10]) dictate the optimal membrane orientation for a given application. Specifically, experimental results indicate that flux decline is indifferent to membrane orientation for alginate fouling[9,11] but that flux decline is more significant with the feed facing the support layer for gypsum[10], bovine serum albumin[9,10] and Aldrich humic acid[9].

Finally, draw solution diffusivity has also been recognised as an important factor influencing water flux. Tests conducted to compare the water flux using different draw solutions at the same osmotic pressure, with the membrane support layer facing the draw solution, reveal that draw solutions with higher solute diffusivity bring about higher water flux[7,10,12–14]. As a result diffusivities will effect the optimal membrane orientation.

To summarise, operation in FO mode tends to favour reduced fouling, while PRO mode tends to favour enhanced flux. This suggests a fouling-flux dilemma where the choice of membrane orientation requires a compromise between low fouling resistance and higher flux (at least before fouling sets in). However, with draw solutes of higher diffusivity, it is worth asking whether operation in FO mode may, in some instances,

maximise flux. Examination of the literature on the effects of draw solution diffusivity, feed and draw solution osmotic pressure and membrane orientation, shows that a framework has not yet been developed to understand the combined roles of these factors on water flux. Here, setting considerations of fouling aside, we develop such a framework and apply it to three commercial forward osmosis processes in order to identify scenarios where operation in FO mode maximises flux.

3.2 Dimensionless water transport equations

Since the effects of internal concentration polarisation typically dominate over external concentration polarisation, we adopt a model for membrane flux that incorporates the permeability of the active layer and concentration polarisation within the support layer. Considering a forward osmosis membrane with perfect salt rejection, we model water transport in the FO and the PRO orientations using equations from literature[2,3]:

$$J_w^{FO} = A_m \left[\pi_D \exp\left(-J_w K^{FO}\right) - \pi_F\right] \tag{3.1}$$

$$J_w^{PRO} = A_m \left[\pi_D - \pi_F \exp\left(J_w K^{PRO}\right)\right] \tag{3.2}$$

Here, J_w is the water flux, A_m the permeability of the active layer, and π_D and π_F are the osmotic pressure of the draw and feed solutions respectively. K^{FO} and K^{PRO} are the solute resistivities of the support layer[2,3] when the draw and the feed, respectively, are facing the support. K may be formulated as:

$$K = t'/D_s \tag{3.3}$$

where t'[c] represents the effective thickness of the support layer[15] and D_s represents the solute self diffusion coefficient within the porous support layer. Dividing across by the membrane permeability and the osmotic pressure of the feed solution gives the

[c]The effective thickness may be modelled as $t\tau/\epsilon$ where t is the support layer thickness, τ the support layer tortuosity and ϵ the porosity[2].

same equations in dimensionless form:

$$\bar{J}_w^{FO} = \Pi \exp\left(-\bar{J}_w^{FO}\bar{K}^{FO}\right) - 1 \tag{3.4}$$

$$\bar{J}_w^{PRO} = \Pi - \exp\left(\bar{J}_w^{PRO}\bar{K}^{PRO}\right) \tag{3.5}$$

In these equations, $\bar{J}_w$ is the dimensionless water flux, defined as

$$\bar{J}_w \equiv \frac{J_w}{A_m \pi_F}, \tag{3.6}$$

Π is the draw-to-feed osmotic pressure ratio, defined as

$$\Pi \equiv \frac{\pi_D}{\pi_F}, \tag{3.7}$$

and $\bar{K}$ is the dimensionless support layer mass transfer coefficient, defined as

$$\bar{K} \equiv K A_m \pi_F. \tag{3.8}$$

$\bar{K}$ represents the resistance of the support layer to water transport relative to the active layer ($1/A_m\pi_F$ is the resistance of the active layer to water transport). To analyse the effect of membrane orientation we consider the ratio $\bar{J}_w^{FO}/\bar{J}_w^{PRO}$ by comparing Eq. 3.4 to Eq. 3.5. In doing so, we examine the dependence of this ratio upon three dimensionless parameters: Π, the osmotic pressure ratio; $\bar{K}^{PRO}$, the relative resistance of the support layer to water transport when the support layer faces the feed; and $\bar{K}^{PRO}/\bar{K}^{FO}$, the ratio of solute resistivities in the two membrane orientations. Using a non-linear solver[16], we study the dependence of the flux ratio upon these three parameters.

Figure 3-2 illustrates how the ratio of flux in the FO and PRO mode depends upon the osmotic pressure ratio, the relative resistance of the support layer to water transport and the ratio of solute resistivities in the two orientations. Left-to-right consideration of Fig. 3-2a to c, reveals an important trend:

1. When the relative resistance of the support layer, $\bar{K}^{PRO}$, is small, the os-

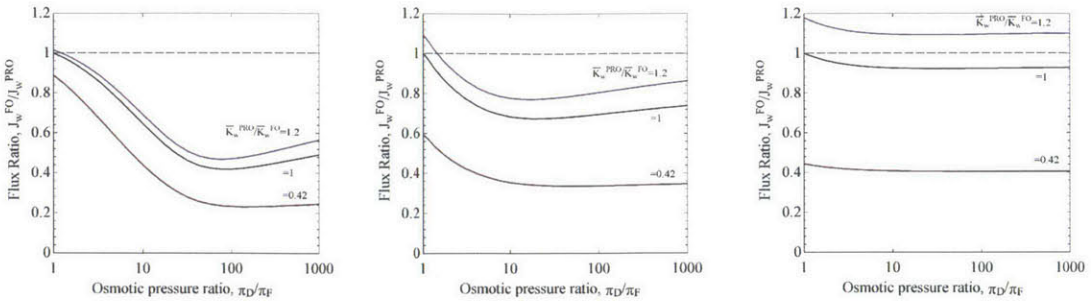

(a) $\bar{K}^{PRO} = 0.1$ **(b)** $\bar{K}^{PRO} = 1$ **(c)** $\bar{K}^{PRO} = 10$

Figure 3-2 Influence of the three dimensionless parameters upon the ratio of flux in FO mode to flux in PRO mode. A resistivity ratio of 1 implies that the feed and draw have similar solute diffusivities. The resistivity ratios of 1.2 and 0.42 are representative of processes with higher and lower diffusivity draw solutes, selected to be in line with the flowback concentration and hydration applications considered in Section 3.3.

motic pressure has a strong effect upon flux. Even at high resistivity ratios ($\bar{K}^{PRO}/\bar{K}^{FO} \approx D^{F,S}/D^{D,S}$), the possibility of enhanced flux in FO mode is small and limited to very low osmotic pressure ratios[d].

2. At high values of $\bar{K}^{PRO}$, the resistivity ratio has a strong effect on flux and allows for higher flux in the FO mode, provided $\bar{K}^{PRO}/\bar{K}^{FO}$ is above unity and the osmotic pressure ratio is sufficiently small.

We conclude from Fig. 3-2 that for processes with $\bar{K}^{PRO}$ values of approximately unity or less, PRO mode will maximise flux. Secondly, for $\bar{K}^{PRO}/\bar{K}^{FO}$ values of unity or less, PRO mode will again maximise flux. Only for values of $\bar{K}^{PRO}$ and $\bar{K}^{PRO}/\bar{K}^{FO}$ above unity (and in certain cases sufficiently low values of the osmotic pressure ratio) can the FO mode of operation maximise flux.

3.3 Application to FO Processes

To demonstrate the implications of the above analysis we apply the theory to three FO processes: the concentration of flowback water from hydraulic fracturing[17], the

[d]This approximation is affected by the variation of the effective thickness t' with solution composition and concentration. These effects, which involve ion-support layer interactions are complex to model and represent the subject of ongoing work[10].

Table 3.1 Numerical values for the three dimensionless parameters influencing the role of membrane orientation upon flux in Fig. 3-4. Data are computed using osmotic coefficients[24], limiting diffusivities[24,25], and a representative membrane permeability and support layer structural parameter[17]. Further information is provided in Appendix 3.A.

Application	**Aqueous Feed**	**Aqueous Draw**	**Osmotic Ratio** $(\Pi_D/\Pi_F)_{max}$	**Relative Resistivity** $\bar{K}^{PRO}$	**Resistivity Ratio** $\bar{K}^{PRO}/\bar{K}^{FO}$
Flowback	NaCl (7.5% wt)	NH_4-CO_2 6 M, N:C=2:1	5.4×10^{0}	1.2×10^{1}	1.1
Fertigation	NaCl (3.5% wt)	NH_4NO_3 (68% wt)	2.4×10^{1}	5.3×10^{0}	1.2
Hydration	NaCl (500 ppm)	Glucose (48% wt)	3.4×10^{2}	7.8×10^{-2}	0.42

dilution of concentrated fertilisers for subsequent irrigation (fertigation)[18,19] and the filtration of impaired waters for personal hydration[20] (*e.g.* the production of a hydration drink.). These three processes exhibit a clear energetic advantage over competing filtration processes[21], either because regeneration of the draw solution is unnecessary (fertigation or personal hydration) or because draw regeneration is competitive with an alternate direct desalination processes[17] (flowback water concentration, where the primary competing technologies are based on evaporation).

For flowback concentration, we consider a feed stream of 75,000 ppm total dissolved solids (7.5% by wt) and an ammonia-carbon-dioxide draw solution[22]. We consider fertigation with source water provided by the sea and using an ammonium nitrate fertiliser. Nitrogen fertilisers account for the largest portion of fertilisers used in the United States by mass[23]. Of fertilisers that satisfy the requirement of generating significant osmotic pressure at a close to neutral pH[14], ammonium nitrate provides a high percentage of nitrogen (34%). For personal hydration, we consider source water of low total dissolved solids content and a dextrose (glucose) draw solution, in line with the Hydropack[20], where dextrose is the most abundant ingredient by weight. Figure 3-3 illustrates the osmotic pressures and limiting diffusivities of the solutions considered while Table 3-4 provides numerical values of the three dimensionless parameters.

Figure 3-4 illustrates, for each of the three processes in question, the role of the osmotic pressure ratio upon the ratio of flux in FO mode to flux in PRO mode. From the figure, we may identify the orientation that maximises flux in the absence of

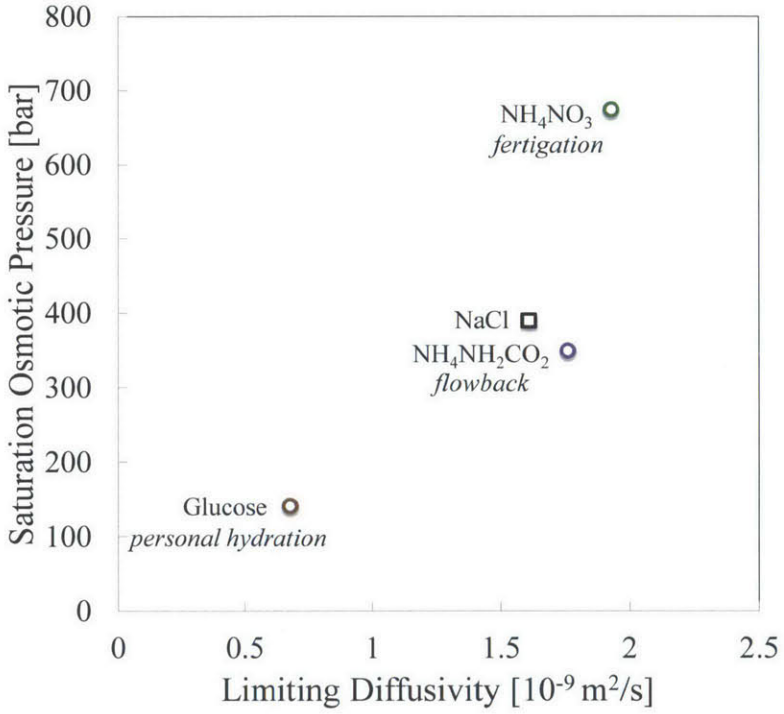

Figure 3-3 Osmotic pressure at saturation versus the limiting salt diffusivity[24,25]. See Appendix 3.A for numerical values and a detailed description.

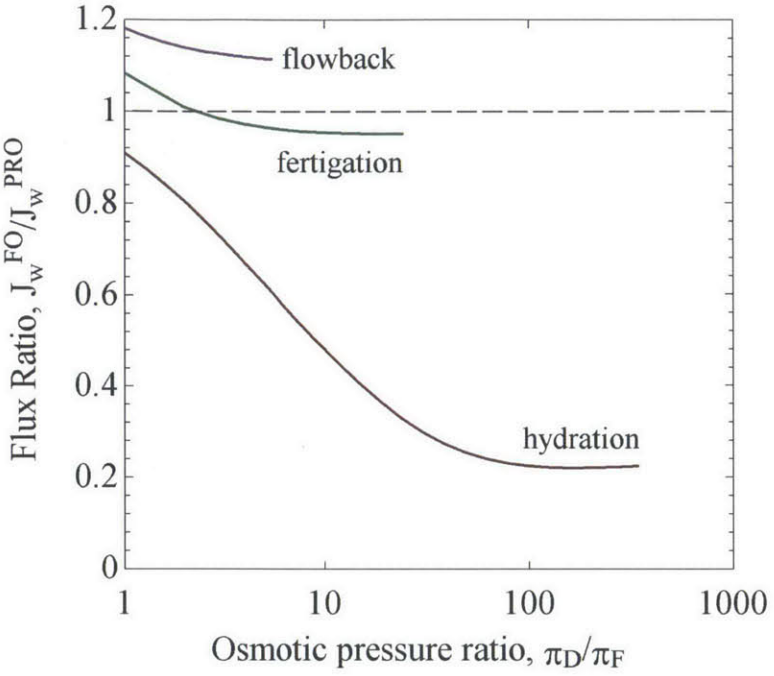

Figure 3-4 Role of the osmotic pressure ratio (abscissa) on influencing the optimal membrane orientation (ordinate)

fouling. For the flowback and fertigation processes flux is greatest when operating in FO mode, provided that the fertigation process is operated at a low osmotic pressure ratio. The relative resistivity $\bar{K}^{PRO}$ is greater than unity in both cases, meaning the resistivity ratio has a more significant effect than the osmotic pressure ratio, although as in Fig. 3-2c, the flux ratio does fall with the osmotic pressure ratio. For the hydration process, flux is greatest operating in PRO mode because the resistivity ratio is less than unity: the draw solute is less diffusive than the feed solute. The solute resistivity $\bar{K}^{PRO}$ is also much smaller than unity, meaning the osmotic pressure ratio has a strong influence upon flux.

3.4 Implications for the design of flowback, fertigation and hydration processes

Most often, flux is greatest when operating in PRO rather than in FO mode. As discussed in Section 3.1, this is somewhat unfortunate since fouling occurs more readily when the feed is facing the porous support layer rather than the active layer. However, when the draw solute is more diffusive than the feed solute[e] and when the relative resistance $\bar{K}^{PRO}$ is large, the flux can be greatest in FO mode. Interestingly, the two examples of flowback brine concentration and fertigation fall into this category. These applications therefore lie in the fortunate position of simultaneously minimising fouling and maximising flux when operating in FO mode.

Unfortunately, in hydration applications the draw solute diffusivity (typically that of sucrose or glucose) is smaller than that of solutes typically found in feeds (*e.g.*, sodium chloride and other mineral salts). Hydration applications thus face the fouling-flux dilemma when optimising the membrane orientation. In this case, Fig. 3-4 emphasises just how significant the trade-off in flux can be if a process is forced to operate in FO mode to avoid fouling. If membrane designs could minimise fouling in PRO mode, the time required for the generation of a hydrating drink could potentially be reduced by approximately half.

3.5 Conclusion

When seeking to maximise flux, a high draw-to-feed osmotic pressure ratio tends to favour the 'PRO' membrane orientation, while a high draw-to-feed diffusivity ratio tends to favour the FO mode. However, the relative resistance to water transport of the membrane support layer compared to the active layer ($\bar{K}^{PRO}$) also plays an important role. When $\bar{K}^{PRO}$ is small the optimal membrane orientation is primarily dictated by the osmotic pressure ratio, whereas when $\bar{K}^{PRO}$ is large the diffusivity ratio is more important. The relative resistance of the support layer in PRO

[e]Strictly speaking we should say when $\bar{K}^{PRO}/\bar{K}^{FO} > 1$

mode increases with the osmotic pressure of the feed. Thus, applications with low osmotic pressure feeds, such as the generation of personal hydration solutions, favour operation in the PRO mode. Applications with high osmotic pressure feeds and draw-to-feed diffusivity ratios above unity, such as the concentration of flowback waters or fertigation employing a seawater feed, favour operation in the FO mode. Thus, they constitute an interesting example of a case in which the FO mode of operation can maximise flux and minimise fouling.

3.A Determination of osmotic pressures, diffusivities and membrane parameters

3.A.1 Membrane parameters

Recent experimental measurements on Oasys Water forward osmosis membranes[17] were employed in selecting a membrane permeability of 1.13×10^{-6} m/s bar and a support layer structural parameter of 2.65×10^{-4} m.

3.A.2 Diffusivities

Experimental data was employed to determine the limiting diffusivities of solutes in aqueous solution[24] with the exception of $NH_4NH_2CO_2$, whose limiting diffusivity was simulated[25].

3.A.3 Osmotic Pressures

Osmotic pressures were computed via experimentally determined osmotic coefficients[24], ϕ, and the following relation:

$$\pi = RT\frac{\phi\nu m M_w}{V_{m,w}} \tag{3.9}$$

where R is the universal gas constant, T is the temperature, ν is the number of dissociated moles of ions per mole of solute, m is the molal concentration of the

Table 3.2 Osmotic pressures and limiting diffusivities employed in the generation of Fig. 3-3 and the determination of parameters in Table 3.1.

Application	Aqueous Feed	Aqueous Draw	Osmotic Pressure [bar]		Diffusivity [10^{-9}m^2/s]	
			π_D	π_F	D_D	D_F
Flowback	NaCl (7.5% wt)	NH_4-CO_2 6 M, N:C=2:1	350	65.2	1.76	1.61
Fertigation	NaCl (3.5% wt)	NH_4NO_3 (68% wt)	675	28.3	1.93	1.61
Hydration	NaCl (500 ppm)	Glucose (48% wt)	141	0.42	0.679	1.61

solution, M_w is the molecular weight of water, and $V_{m,w}$ is the molar volume of water. The saturation concentration of solutions (which influences the maximum osmotic pressure) was also determined using experimental data[24,26,27].

The exception to this procedure was the aqueous $NH_4NH_2CO_2$ solution, where the osmotic pressure at concentration of 6 M and a N:C ratio of 2:1 was simulated[25]. A summary of osmotic pressures and diffusivities employed in the generation of Table 3.1 is provided in Table 3.2.

3.B Optimal membrane orientation for reverse osmosis pre-dilution and post dilution

Reverse osmosis desalination systems have been proposed whereby forward osmosis is employed to pre-dilute the feed to a reverse osmosis process, to post-dilute reverse osmosis brine (Fig. 3-5), or to achieve a combination of the two[28]. The primary purpose of pre-dilution is to reduce the osmotic pressure of the reverse osmosis feed stream, thus saving energy, while the purpose of post-dilution is to reduce the salinity (and possibly temperature) of brine rejected to sea.

The main challenge faced by pre-dilution processes is competition with single or two-pass reverse osmosis systems that could directly provide a pure product from the impaired water stream. The direct reverse osmosis approach would benefit from treating a feed stream (the impaired stream) of lower osmotic pressure compared to diluted seawater emerging from an FO unit.

Where concentration of an impaired stream is the goal, the use of reverse osmosis

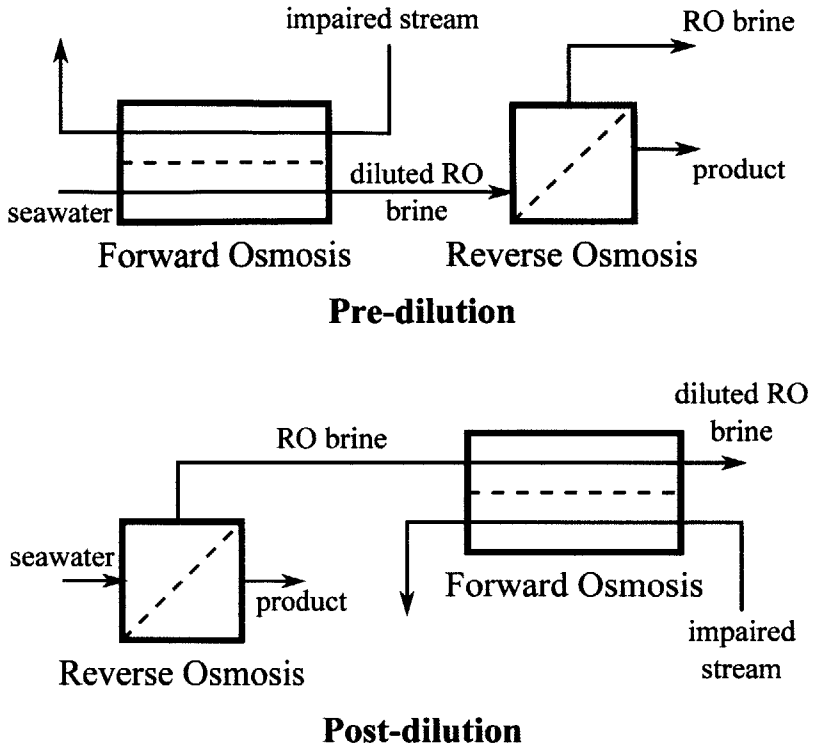

Figure 3-5 Reverse osmosis pre- and post-dilution processes (reverse osmosis pressure recovery not shown)

brine as an osmotic agent for post-dilution offers an energetic advantage over concentration with reverse osmosis. However, post-dilution processes employed to reduce the salinity of reject brine face competition from direct blending with further seawater, which would circumvent the need for membranes.

Setting commercial considerations aside, by considering representative values for the feed and draw salinities (Table 3.3), the optimal membrane orientation may be examined (Fig. 3-6). Since the diffusivity of solutes in the feed and draw are approximated as equal, operation in FO mode, where the support layer faces the solution of higher concentration, necessarily reduces flux relative to PRO mode. Thus, the optimal membrane orientation is likely to depend upon the rates of fouling present in each orientation; a finding that is in line with previous studies[9,10].

Table 3.3 Numerical values for the three dimensionless parameters influencing the role of membrane orientation upon flux in Fig. 3-6. Data are computed using osmotic coefficients[24], limiting diffusivities[24,25], and a representative membrane permeability and support layer structural parameter[17].

Application	**Aqueous Feed**	**Aqueous Draw**	**Osmotic Ratio** $(\Pi_D/\Pi_F)_{max}$	**Relative Resistivity** $\bar{K}^{PRO}$	**Resistivity Ratio** $\bar{K}^{PRO}/\bar{K}^{FO}$
Pre-dilution	NaCl (500 ppm)	NaCl (3.5% wt)	6.7×10^{1}	8×10^{-2}	1
Post-dilution	NaCl (500 ppm)	NaCl (7% wt)	1.4×10^{2}	8×10^{-2}	1

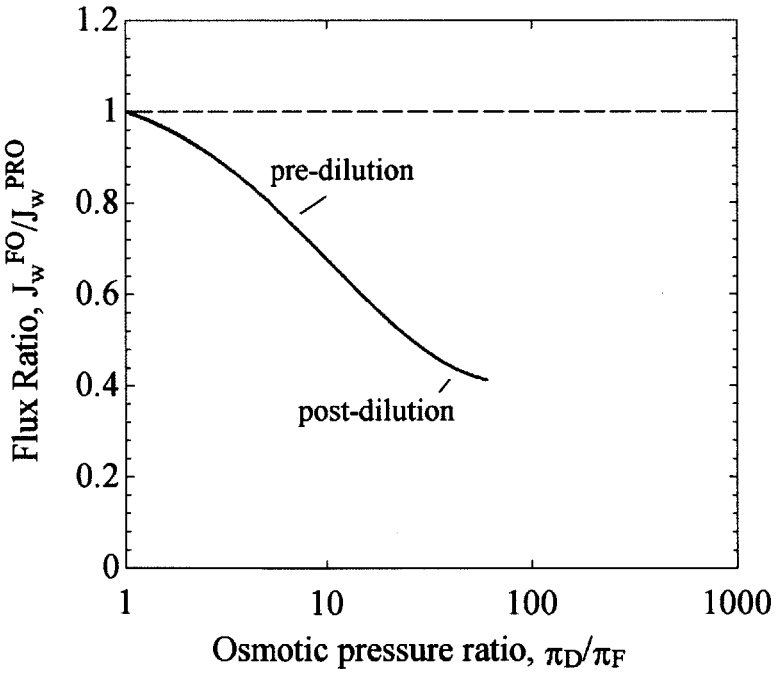

Figure 3-6 Role of the osmotic pressure ratio (abscissa) on influencing the optimal membrane orientation (ordinate) for reverse osmosis pre- and post-dilution

3.C The role of individual ions in determining solute diffusivity

The self-diffusion coefficient of a quasi-electroneutral dilute binary electrolyte is described by Eq. (3.10).

$$\frac{\frac{1}{|z_+|}+\frac{1}{|z_-|}}{D_s^0} = \frac{1}{|z_+|}\frac{1}{D_+^0} + \frac{1}{|z_-|}\frac{1}{D_-^0} \tag{3.10}$$

This self-diffusion coefficient is a"" harmonic mean of the limiting ionic diffusivities, weighted by the inverse of the ionic charges. We ask the question as to whether there is an inherent benefit in choosing multivalent over monovalent ions. To do this, let us consider all monovalent ions to have the same ionic diffusivity, D_1^0, and all divalent ions to have ionic diffusivity D_2^0. Considering Eq. (3.10), we find that binary monovalent (1:1) salts and binary divalent (2:2) salts would have the same solute diffusivity provided $D_1^0 = D_2^0$. We may also ask how an asymmetrically charged 2:1 or 1:2 electrolyte would compare to a 1:1 electrolyte. Equation 3.10 again reveals that, for equal solute diffusivity, we would require $D_1^0 = D_2^0$. Thus, ionic diffusivities being equal, no intrinsic benefit results from employing higher or lower valence ions. From a sensitivity standpoint, however, an increase in the diffusivity of one ion causes an increase in the overall solute diffusivity magnitudes that differ depending upon the ionic charge permutation. In the case of an asymetrically charged solute, incremental changes in the diffusivty of the lower charged ion will have a greater effect on solute diffusivity than changes to the higher charged ion, as can be proven using Eq. (3.10).

Fig. 3-7 illlustrates that the ions with the highest diffusivity are predominantly monovalent. Monovalent spherical ions demonstrate a clear trend in diffusivity with ion size, with a discernible maximum diffusivity present for monovalent cations and anions. For diffusion in dilute solutions, the chloride ion is close to the peak ionic diffusivity in Fig. 3-7a, leaving little room for improvement on anion diffusivity if our reference is an NaCl solution. The sodium ion, however, is below peak diffusivity in Fig. 3-7b, allowing for an improvement of approximately 40% in cation diffusivity by selecting K or NH_4^+. Returning to Eq. (3.10), this would allow for an improvement

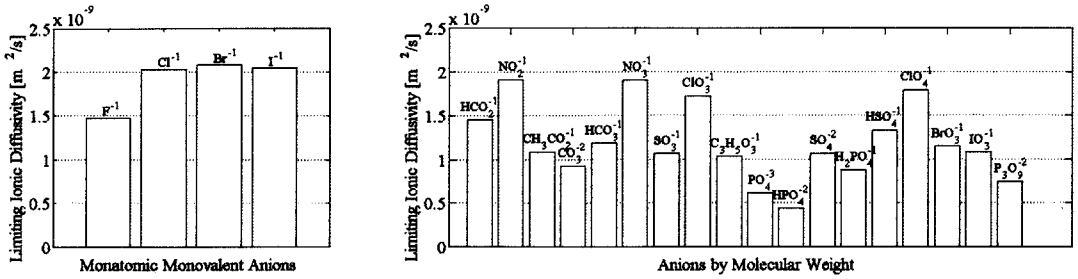

(a) Anions

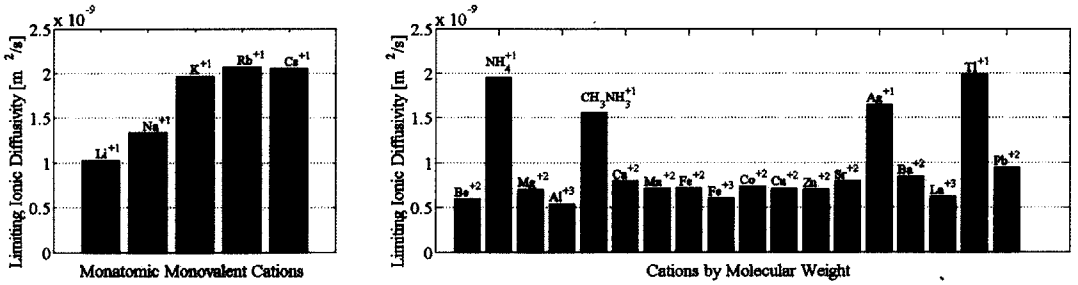

(b) Cations

Figure 3-7 Limiting ionic diffusivities at 25°C as calculated from the limiting ionic conductivity,[24,29,30]. The diffusivity maximum based on critical ionic size is seen very well in (a) and (b) where the ions are spherical. Other ionic radii, especially in molecules composed of multiple elements, follow a less predictable trend. Not included is the H^+ ion with a value of $9.3 \times 10^{-9} \frac{m^2}{s}$ [24], due to its natural affinity as an ion in water.

in solute diffusivity of approximately 25%. This brief analysis serves to show that at best we should expect $\bar{K}^{PRO}/\bar{K}^{FO}$ values of approximately 1.25 by tailoring the draw solution, if we assume an NaCl feed. Furthermore, we ascertain that NaCl, as a draw solution, already provides excellent diffusivity. Thus, when selecting other draw solutions over NaCl, it is important consider the implications upon membrane flux, particularly if the relative resistivity $\bar{K}^{FO}$ is greater than unity.

Nomenclature

Roman Symbols

A_m	Membrane permeability, m/s bar
D	Diffusivity, m^2/s
J_w	Water flux, m/s
K	Solute resistivity, s/m
m	molality, mol/kg solvent
M_w	Molar mass of water, kg/mol
R	Ideal gas constant, J/mol K
t'	Effective thickness, m
T	temperature, K
$V_{m,w}$	molar volume of water, m^3/mol
z	Charge number, -

Greek Symbols

ν	moles dissociated ions per mole of solute, -
π	Osmotic pressure, bar
Π	Osmotic pressure ratio, -
ϕ	Osmotic coefficient, -

Subscripts

A	Active layer
D	Draw
F	Feed
$+$	Positive charge
$-$	Negative charge
s	Salt
S	Support layer

Superscripts

D	Draw
FO	FO mode (draw-to-support)
F	Feed
PRO	PRO mode (feed-to-support)
0	dilute solution limit
$^-$	Dimensionless

Bibliography

[1] T. Y. Cath, A. E. Childress, M. Elimelech, Forward osmosis: Principles, applications, and recent developments, Journal of membrane science 281 (1) (2006) 70–87.

[2] K. Lee, R. Baker, H. Lonsdale, Membranes for power generation by pressure-retarded osmosis, Journal of Membrane Science 8 (2) (1981) 141–171.

[3] S. Loeb, L. Titelman, E. Korngold, J. Freiman, Effect of porous support fabric on osmosis through a Loeb-Sourirajan type asymmetric membrane, Journal of Membrane Science 129 (2) (1997) 243–249.

[4] J. McCutcheon, M. Elimelech, Influence of concentrative and dilutive internal concentration polarization on flux behavior in forward osmosis, Journal of Membrane Science 284 (1) (2006) 237–247.

[5] J. R. McCutcheon, M. Elimelech, Modeling water flux in forward osmosis: Implications for improved membrane design, AIChE Journal 53 (7) (2007) 1736–1744.

[6] G. D. Mehta, S. Loeb, Internal polarization in the porous substructure of a semipermeable membrane under pressure-retarded osmosis, Journal of Membrane Science 4 (1979) 261–265.

[7] G. T. Gray, J. R. McCutcheon, M. Elimelech, Internal concentration polarization in forward osmosis: role of membrane orientation, Desalination 197 (1) (2006) 1–8.

[8] C. Y. Tang, Q. She, W. C. Lay, R. Wang, A. G. Fane, Coupled effects of internal concentration polarization and fouling on flux behavior of forward osmosis membranes during humic acid filtration, Journal of Membrane Science 354 (1) (2010) 123–133.

[9] B. Mi, M. Elimelech, Chemical and physical aspects of organic fouling of forward osmosis membranes, Journal of Membrane Science 320 (1) (2008) 292–302.

[10] S. Zhao, L. Zou, D. Mulcahy, Effects of membrane orientation on process performance in forward osmosis applications, Journal of Membrane Science 382 (1) (2011) 308–315.

[11] B. Mi, M. Elimelech, Organic fouling of forward osmosis membranes: Fouling reversibility and cleaning without chemical reagents, Journal of Membrane Science 348 (1) (2010) 337–345.

[12] C. H. Tan, H. Y. Ng, Modified models to predict flux behavior in forward osmosis in consideration of external and internal concentration polarizations, Journal of Membrane Science 324 (1) (2008) 209–219.

[13] A. Achilli, T. Y. Cath, A. E. Childress, Selection of inorganic-based draw solutions for forward osmosis applications, Journal of Membrane Science 364 (1) (2010) 233–241.

[14] S. Phuntsho, H. K. Shon, S. Hong, S. Lee, S. Vigneswaran, A novel low energy fertilizer driven forward osmosis desalination for direct fertigation: Evaluating the performance of fertilizer draw solutions, Journal of Membrane Science 375 (1) (2011) 172–181.

[15] S. Loeb, Production of energy from concentrated brines by pressure-retarded osmosis: I. preliminary technical and economic correlations, Journal of Membrane Science 1 (1976) 49–63.

[16] S. A. Klein, Engineering Equation Solver, Academic Professional V9.438-3D (2013).

[17] N. T. Hancock, M. S. Nowosielski-Slepowron, L. S. Marchewka, Application of forward osmosis based membrane brine concentrators for produced water, The International Desalination Association World Congress on Desalination and Water Reuse 2013 / Tianjin, China.

[18] C. Moody, J. Kessler, Forward osmosis extractors, Desalination 18 (3) (1976) 283–295.

[19] C. D. Moody, Forward osmosis extractors: theory, feasibility and design optimization, Ph.D. thesis, The University of Arizona (1977).

[20] Hydration Technology Innovations, HydroPack, http://www.htiwater.com.

[21] R. K. McGovern, J. H. Lienhard V, On the potential of forward osmosis to energetically outperform reverse osmosis, Under review.

[22] J. R. McCutcheon, R. L. McGinnis, M. Elimelech, A novel ammonia carbon dioxide forward (direct) osmosis desalination process, Desalination 174 (1) (2005) 1–11.

[23] United States Department of Agriculture Economic Research Service, Table 1, U.S. consumption of nitrogen, phosphate, and potash, 1960-2011, Fertilizer Consumption and Use by Year. (2011).

[24] R. Robinson, R. Stokes, Electrolyte Solutions, 2nd Revised Edition, Dover Publications, Mineola, NY., 2002.

[25] OLI Systems, Inc., OLI Stream Analyser (2013).

[26] B. Wishaw, R. Stokes, The osmotic and activity coefficients of aqueous solutions of ammonium chloride and ammonium nitrate at 25°C, Transactions of the Faraday Society 49 (1953) 27–31.

[27] A. C. Ribeiro, O. Ortona, S. M. Simoes, C. I. Santos, P. M. Prazeres, A. J. Valente, V. M. Lobo, H. D. Burrows, Binary mutual diffusion coefficients of aqueous solutions of sucrose, lactose, glucose, and fructose in the temperature

range from 298.15 to 328.15 K, Journal of Chemical & Engineering Data 51 (5) (2006) 2836–1840.

[28] T. Cath, C. Lundin, J. Drewes, A dual-barrier and energy saving osmosis-assisted desalination process for drinking water augmentation, AwwaRF Project 4150 (2009) N/A.

[29] M. Flury, T. F. Gimmi, Chapter 6.2, solute diffusion, Methods of Soil Analysis: Part 4 Physical Methods (2002) 1323–1351.

[30] H. Sato, M. Yui, H. Yoshikawa, Ionic diffusion coefficients of Cs^{+}, Pb^{2+}, Sm^{3+}, Ni^{2+}, SeO_2^{4-} and TcO^{4-} in free water determined from conductivity measurements, Journal of Nuclear Science and Technology 33 (12) (1996) 950–955.

Chapter 4

The cost effectiveness of electrodialysis for diverse salinity applications

Abstract

We provide a thermoeconomic assessment of electrodialysis indicating that the technology is most productive and efficient for the partial desalination of feed streams at the higher end of the brackish range of salinities. After optimising the current density to minimise the sum of energy and equipment costs, we demonstrate that at low feed salinities the productivity, and hence equipment costs, of electrodialysis are hampered by the limiting current density. By contrast, at higher feed salinities both productivity and efficiency are hampered by the reduced chemical potential difference of salt in the diluate (low salinity) and concentrate (high salinity) streams. This analysis points indicates the promise of further developing electrodialysis for the treatment of waters from oil, gas and coal-bed methane as well as flue-gas de-sulphurisation, where the partial desalination of streams at the high-end of the brackish range can be beneficial.

Contributions

This chapter was co-authored by Adam Weiner, Lige Sun, Chester Chambers, Prof. Syed Zubair and Prof. John Lienhard V. The work received financial support from the Hugh Hampton Young Memorial Fund Fellowship and the King Fahd University of Petroleum and Minerals through the Center for Clean Water and Clean Energy at MIT and KFUPM under project number R15-CW-11.

4.1 Introduction

Electrodialysis involves the transfer of ions from a low salinity stream to a higher salinity stream — from diluate to concentrate. Together, the diluate salinity, the difference between diluate and concentrate salinity, and the ratio of concentrate-to-diluate salinity capture, via their effects on salt and water transport, the influence of salinity on cost. Our objective is to demonstrate that these three factors determine the influence of salinity on the cost-effectiveness of electrodialysis, and furthermore, that they have driven and will drive the selection of applications for which ED is worthy of development.

Recently, significant attention has been paid to the development of new electrical desalination methods[1–4], some of which report experimentally measured energy consumption close to reversible[2,4–6] and some of which report extraordinarily high salt removal rates per unit area[2,6]. Given the early stage of development of these technologies, there are interesting questions around their cost competitiveness at larger scales and, of interest in the present context, the range of salinities for which they are most economical. By analysing the effect of salinity upon the cost effectiveness of electrodialysis, a precedent is established allowing similar analyses to be conducted for emerging technologies as system models are developed.

No existing unified framework is available to explain, in a general sense, how diluate and concentrate salinities affect the cost of electrodialysis — though literature does provide certain distinct insights into the effects of salinity. At low diluate salinity, salt removal is restricted by the limiting current density and ohmic resistance is high. For brackish water desalination[7,8], and to a lesser extent salt production[9], the limiting current density effectively sets the size of equipment required. For the purification of higher salinity streams such as seawater[10] or produced water[11], currents are lowest (and, we surmise, capital costs highest) in the final stages of purification. High diluate resistance results in elevated energy consumption for brackish desalination, particularly due to the dominance of solution over membrane resistances. Indeed, the challenges posed by a low diluate salinity are largely responsible for the develop-

ment of narrow membrane channels[12], ion-conductive spacers within diluate channels (electrodeionisation)[13,14], hybrid designs combining ED with reverse osmosis[15–17], and theories to understand and possibly extend the operation of ED into the overlimiting current region[18].

With a large salinity difference between diluate and concentrate salinity, back diffusion of salt and water transport by osmosis degrade performance. In brackish desalination applications, this effect, coupled with the risk of scale formation at high concentrations, limits the recovery of feed water as a purified product. In concentrative applications, osmosis and diffusion serve to reduce the maximum concentration achievable in combination with the effect of water transport by electro-osmosis[19–22].

Our objective is to draw together the above insights and propose a unified framework explaining the influence of salinity upon the cost of electrodialysis. Rather than modelling, in detail, a variety of electrodialysis processes, our approach is to consider a short cell pair that can represent a portion of any electrodialysis process. By understanding how the performance and cost of this short cell pair depend upon diluate and concentrate salinity, we can understand how global systems will perform across different salinity ranges. Figure 4-1 illustrates how the process in a two stage brackish water desalination system may be represented on a salinity map, and furthermore, how a short cell pair at any point in the system is represented by a point along the process path. Our approach consists of mapping the cost of this short cell pair process over the entire range of diluate and concentrate salinities. The consequent map of cost then allows us to understand the cost effectiveness of diverse ED processes.

4.2 Methodology

To construct a map of cost we consider a numerical model of a short cell pair that allows us to parametrise diluate and concentrate salinity. We first establish a metric for the cost of separation. We then present a model for local salt transport, water transport and cell pair voltage. Finally, coupling these cost and cell pair models, and optimising for current density, we parametrise diluate and concentrate salinity

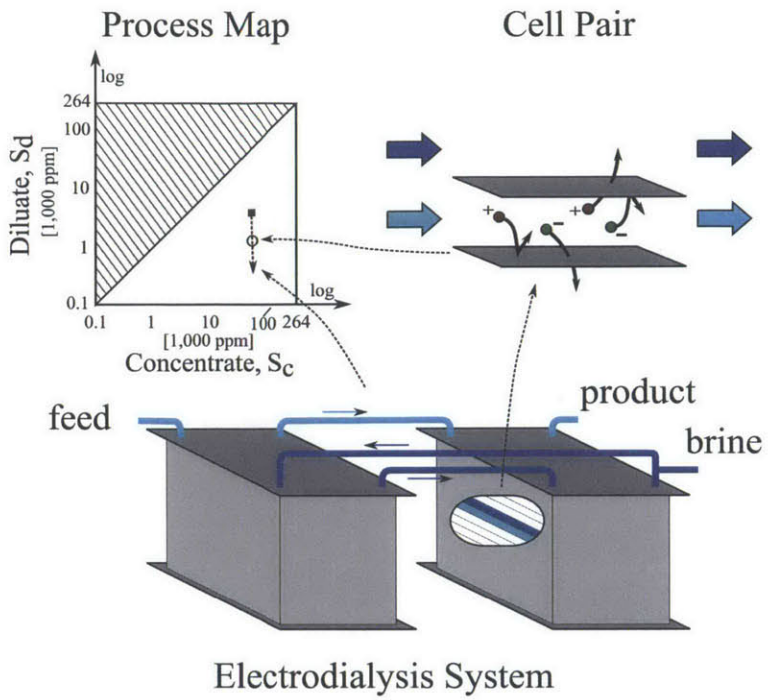

Figure 4-1 Illustration of the relationship between an ED cell pair, an ED system and an ED process (bleed stream from diluate to concentrate not shown)

to numerically investigate how they influence the 'Local Cost'.

4.2.1 The 'Local Cost' of separation

In a detailed analysis, costs associated with membrane replacement, chemical usage, the replacement of miscellaneous parts and pre-treatment might be considered[23]. In this analysis we focus upon equipment and energy costs and determine the cost per unit time of operating an incremental cell pair as follows:

$$\text{Cost per unit time} = \frac{K_Q \delta A^{cp}}{CAF} + K_E \delta P \tag{4.1}$$

Equipment costs are formulated as the product of a specific equipment cost per unit cell pair area K_Q and the incremental cell pair area δA^{cp}, together divided by the capital amortisation factor CAF — which allows for a return on the investment in

equipment:

$$CAF = \frac{1}{r}\left[1 - \left(\frac{1}{1+r}\right)^{\tau}\right] \tag{4.2}$$

Energy costs in Eq. (4.1) are formulated as the product of electricity price, K_E, and the incremental power consumption of the cell pair δP. Pumping power costs, typically smaller than stack power consumption in brackish[7] and salt production applications[9], are not considered as we focus on the trade-off between stack power and system size. Relative to stack power consumption, pumping power is most significant at low diluate salinity where the current density and hence the stack power density is small. That pumping power is a low fraction of total power at low salinity thus suggests that this should also be the case at higher salinities[7,24].

Setting pumping power aside power consumption in the cell pair is therefore given by the product of cell pair voltage, current density and incremental cell pair area:

$$\delta P = iV^{cp}\delta A^{cp} \tag{4.3}$$

Given the incremental cost of operating a cell pair we next establish a basis upon which this cost can be made specific. Rather than considering costs on the basis of water removal (*e.g.*, \$/m^3 of water) or salt removal (*e.g.*, \$/kg of salt), we consider costs on the basis of the rate of change in free energy of process streams. For a short (infinitesimal) cell pair, this rate of change is given by:

$$\delta G = \delta \dot{N}_s \Delta\mu_s + \delta \dot{N}_w \Delta\mu_w \tag{4.4}$$

where $\delta \dot{N}_s$ and $\delta \dot{N}_w$ are incremental molar flow rates of salt and water through the membranes, respectively, and μ denotes chemical potential, which takes the form of:

$$\mu_s - \mu_s^0 = RT\ln(\gamma m) \tag{4.5}$$

$$\mu_w - \mu_w^0 = RT\phi M_w \nu m \tag{4.6}$$

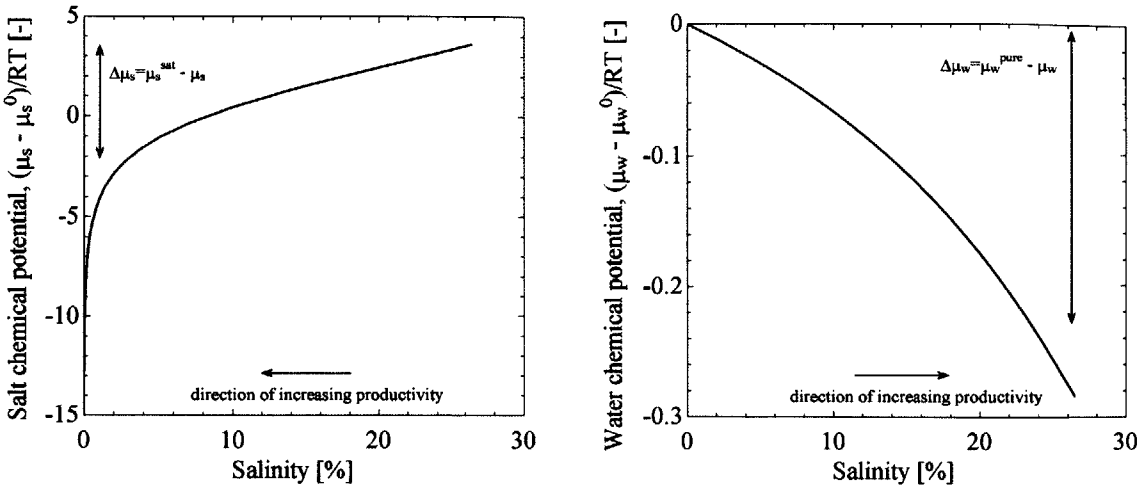

(a) Sodium chloride chemical potential **(b)** Water chemical potential

Figure 4-2 Chemical potentials of sodium chloride and water in an aqueous NaCl and water solution as a function of salinity. Osmotic coefficient and NaCl activity coefficient data from Robinson and Stokes[25]

for salt and water respectively, with R the universal gas constant, T the temperature, γ the mean molal salt activity coefficient, m the molal concentration of salt, ν the number of moles of dissociated ions per mole of salt (2 for NaCl), ϕ the osmotic coefficient, μ_s^0 the chemical potential of salt in its reference state and μ_w^0 the chemical potential of water in its reference state. The use of free energy is based on the thermodynamic consideration that the difficulty of salt (or water) removal depends upon salinity. The difficulty of salt removal, as measured by the change in chemical potential in Fig. 4-2a, is greater when salt is removed (say into a saturated solution) from a lower salinity stream. By contrast, the removal of water (in pure form) is more difficult from a higher salinity stream. Given the incremental cost of operating a cell pair and the incremental rate of change of free energy we define the specific 'Local Cost' of separation as follows:

$$SLCS = \frac{\frac{K_Q \delta A^{cp}}{CAF} + K_E \delta P}{\dot{N}_s \Delta\mu_s + \dot{N}_w \Delta\mu_w}. \tag{4.7}$$

Dividing across by K_E and defining the equipment-to-energy price ratio as:

$$R_p = \frac{K_Q}{CAF}\frac{1}{K_E} \tag{4.8}$$

we obtain a simple expression for the dimensionless 'Local Cost' of separation:

$$\begin{aligned} Local\ Cost = \frac{SLCS}{K_E} =& \frac{R_p \delta A^{cp}}{\dot{N}_s \Delta\mu_s + \dot{N}_w \Delta\mu_w} \\ &+ \frac{\delta P}{\dot{N}_s \Delta\mu_s + \dot{N}_w \Delta\mu_w} \end{aligned} \tag{4.9}$$

This expression, which for brevity we will term 'Local Cost', represents the comparison of the price of a unit change in free energy to the price of a unit of electricity. Further examination of Eq. (4.9) allows us to write the 'Local Cost' as:

$$Local\ Cost = \frac{SLCS}{K_E} = \frac{R_p}{\xi} + \frac{1}{\eta} \tag{4.10}$$

with productivity ξ defined as the incremental rate of change of free energy per unit system area (*e.g.*, cell pair area for ED):

$$\xi = \frac{\dot{N}_s \Delta\mu_s + \dot{N}_w \Delta\mu_w}{\delta A^{cp}} = J_s \Delta\mu_s + J_w \Delta\mu_w \tag{4.11}$$

and efficiency defined as the ratio of the productivity to the area normalised power input:

$$\eta = \frac{J_s \delta A^{cp} \Delta\mu_s + J_w \delta A^{cp} \Delta\mu_w}{i V^{cp} \delta A^{cp}} = \frac{\xi}{i V^{cp}}. \tag{4.12}$$

J denotes a transmembrane molar flux, i denotes current density and V^{cp} denotes cell pair voltage. Of particular importance, both for productivity and efficiency, are the changes in chemical potential of water and salt during transport. We can see, according to Fig. 4-2a, that the productivity of salt removal systems is poor when removing salt from low salinity solutions while, according to Fig. 4-2b, the productivity of water removal systems is poor when removing water from low salinity solutions. Further-

more we can see that water transport in electrodialysis (from diluate to concentrate) in electrodialysis and salt transport (from feed to product) in reverse osmosis reduces productivity. Thus, we establish that small changes in chemical potential of species during transport results in poor productivity and, if the denominator of Eq (4.12) were constant, poor efficiency.

4.2.2 The cell pair model

The key outputs of the cell pair model, required to determine 'Local Cost', are the salt flux, J_s, water flux, J_w, and the cell pair voltage, V^{cp}. Together these three quantities allow the determination of productivity and efficiency (Eqs. (4.11) and (4.12)), which in turn determine 'Local Cost' in Eq. (4.10).

Salt and water transport are modelled based upon the approach taken by Fidaleo and Moresi[20]. Salt transport is modelled by a combination of migration and diffusion:

$$J_s = \frac{T_s^{cp} i}{F} - L_s \left(C_{s,c,m} - C_{s,d,m} \right) \tag{4.13}$$

and water transport by a combination of migration (electro-osmosis) and osmosis:

$$J_w = \frac{T_w^{cp} i}{F} + L_w \left(\pi_{s,c,m} - \pi_{s,d,m} \right) \tag{4.14}$$

T_s^{cp} and T_w^{cp} are the overall salt and water transport numbers for the cell pair. L_s and L_w are the overall salt and water permeabilities of the cell pair. C denotes concentration in moles per unit volume and π osmotic pressure. The difference between bulk and membrane wall concentrations and osmotic pressures is accounted for by a convection-diffusion model of concentration polarisation[26]:

$$\Delta C = -\frac{\left(\bar{T}_{cu} - t_{cu} \right)}{D} \frac{i}{F} \frac{2h}{\mathrm{Sh}} \tag{4.15}$$

where t_{cu} is the counter-ion transport number in solutions and is approximated as 0.5 for both anions and cations. $\bar{T}_{cu}$ is the integral counter-ion transport number in the

membrane that accounts for both migration and diffusion.

$$\bar{T}_{cu} \approx \frac{T_s^{cp} + 1}{2}. \tag{4.16}$$

This expression would be exact were diffusion within the membrane to be negligible and the counter-ion transport number to be equal in anion and cation exchange membranes. The cell pair voltage, Fig. 4-3, is represented as the sum of ohmic terms, membrane potentials and junction potentials:

$$V^{cp} = i\left(\bar{r}_{am} + \bar{r}_{cm} + \bar{r}_d + \bar{r}_c\right) + E_{am} + E_{cm} + \sum E_j \tag{4.17}$$

Membrane surface resistances are considered to be independent of salinity. The surface resistances of the diluate and concentrate solutions are computed considering the channel height and the bulk solution conductivity:

$$\bar{r}_d + \bar{r}_d = \frac{h_d}{k_d} + \frac{h_c}{k_c} = \frac{h_d}{\Lambda_d C_d} + \frac{h_c}{\Lambda_c C_c} \tag{4.18}$$

where Λ is the molar conductivity, itself a function of concentration[27,28]. Concentration polarisation boundary layers are symmetric, since $\bar{T}_{cu}$ and t_{cu} are approximated as equal for anion and cation exchange membranes, and anions and cations, respectively. Thus, the junction potentials cancel within each channel. Finally, the sum of the anion and cation membrane potentials is computed considering quasi-equilibrium migration of salt and water across the membranes:

$$\begin{aligned} E_{am}+E_{cm} & \\ &= \frac{T_s^{cp}}{F}(\mu_{s,c,m} - \mu_{s,d,m}) + \frac{T_w^{cp}}{F}(\mu_{w,c,m} - \mu_{w,d,m}) \end{aligned} \tag{4.19}$$

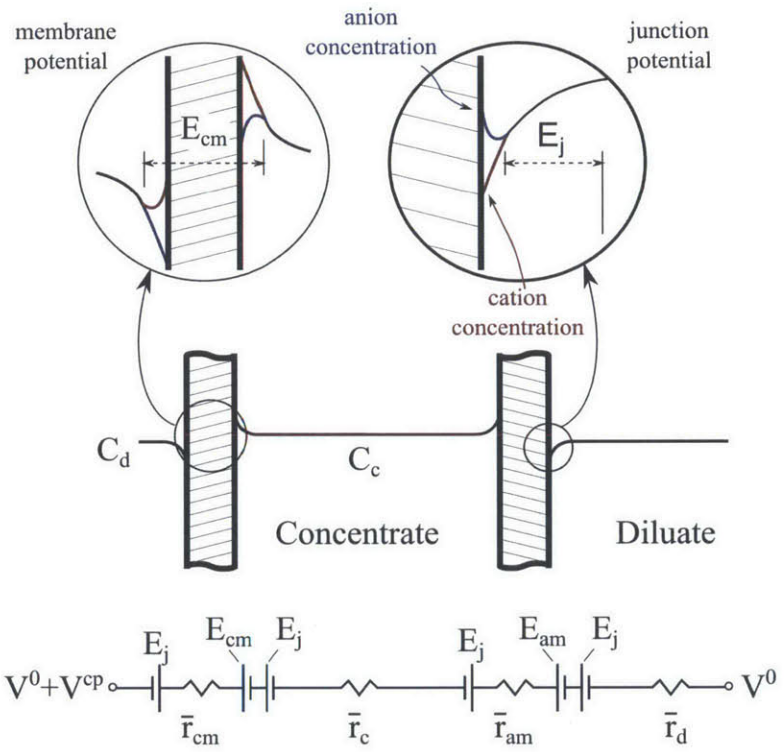

Figure 4-3 Representation of the voltage drop and concentration change across a single cell pair

Table 4.1 Membrane performance, solution and flow properties. For channel height, Lee et al.[7] suggest 0.65 mm, while Fidaleo et al.[29] employ 0.7 mm. For Reynolds number Lee et al.[7] suggest Re_{D_h} of approximately 100, while Fidaleo et al.[29] employ a Reynolds of approximately 25 to 50. Taken together with Fidaleo et al.'s Sherwood number correlation, $Sh = 0.37 \cdot Re_{D_h}^{1/2} Sc^{1/3}$, with $Sc \approx 620$, yields Sh in the range of 12-22.

Symbol	Value	Ref.
Membrane Performance Parameters		
T_s	0.97	29a
T_w	10	29
L_w	1.4×10^{-4} mol/bar-m^2-s	29
L_s	1.4×10^{-8} m/s	29
$\bar{r}_{am}$	2.8 Ω cm^2	29
$\bar{r}_{cm}$	2.8 Ω cm^2	29
Solution Properties		
D	1.61×10^{-9} m^2/s	25
t_{cu}	0.5	30
Flow Properties		
h	0.7 mm	7,29
Sh	20	7,29

Table 4.2 Cost model parameters

Symbol	Value	Ref.
K_{EQ}	300 \$/m^2 cell pair	7,8
τ	20 yr	-
r	5%	31
LCE	0.065 \$/kWh	32

4.2.3 The input parameters to the numerical model

To investigate the dependence of 'Local Cost' upon diluate and concentrate salinity, we select representative values from literature as inputs to the cell pair and cost models (Tables 4.1 and 4.2) respectively.

The salinity dependence of membrane performance parameters is membrane specific and data is not widely available for cell pairs[b]. No salinity dependence of membrane performance parameters is included, as a result of which, in particular due to the assumed high permselectivity of anion and cation membranes, this analysis provides a lower bound on cost at higher salinities. Flow conditions are taken as con-

[b]Data is available for cation exchange membranes[33,34]

stant, meaning viscous dissipation per unit cell pair area (relating to pumping power requirements) is unaffected[c] by diluate or concentrate salinity. The area normalised equipment cost is chosen in line with Lee et al.[7], and doubled to convert from m^2 membrane area to m^2 cell pair area. A cost of capital of 5% is considered, guided by the 4.78% interest rate paid to construction bondholders for the Carlsbad desalination plant[31]. Finally, the levelised cost of electricity cost is representative of the levelized cost of combined cycle natural gas-fired power plants, including tranmission investments, coming online in 2018[32].

4.3 Dependence of efficiency, productivity and cost upon current density for fixed salinities

There are two layers to the analysis of the 'Local Cost': the first is the optimisation of current density for fixed bulk salinities; the second, to be seen in Section 4.4, is the analysis of how diluate and concentrate salinity affect 'Local Cost'.

To illustrate the dependence of productivity and efficiency on current density we can combine Eqs. (4.13), (4.14) and (4.17) into Eqs. (4.11) and (4.12) to give:

$$\xi = C_{mig} i - C_{od} \tag{4.20}$$

$$\eta = \frac{C_{mig} i - C_{od}}{C_{mp} i + C_{oh} i^2} \tag{4.21}$$

where C_{mig}, C_{od}, C_{mp} and C_{oh} are pre-factors that relate to salt and water migration, osmosis and salt diffusion, membrane potentials and ohmic resistances respectively. C_{mig} and C_{oh} depend upon bulk salinities while C_{od} and C_{mp} depend upon salinities at membrane surfaces, and thus, via concentration polarisation, are implicit functions of current density:

$$S = \frac{M_s C}{\rho} \approx \frac{M_s m}{\rho} \tag{4.22}$$

[c]Strictly, salinity affects viscosity, resulting in a second order effect upon viscous dissipation

the approximate dependence of each pre-factor upon salinity is:

$$C_{mig} = \frac{1}{F}[t_s^{cp} \underbrace{(\mu_{s,c} - \mu_{s,d})}_{\sim \ln\left(\frac{S_c}{S_d}\right)} + t_w^{cp} \underbrace{(\mu_{w,c} - \mu_{w,d})}_{\sim -\ln\left(\frac{S_c}{S_d}\right)}] \tag{4.23}$$

$$C_{od} = L_w \underbrace{(\pi_{c,m} - \pi_{d,m})(\mu_{w,d} - \mu_{w,c})}_{\sim (S_{c,m} - S_{d,m})(S_c - S_d)} + L_s \underbrace{(C_{s,c,m} - C_{s,d,m})(\mu_{s,c} - \mu_{s,d})}_{\sim (S_{c,m} - S_{d,m}) \ln\left(\frac{S_c}{S_d}\right)} \tag{4.24}$$

$$C_{oh} = \bar{r}_{am} + \bar{r}_{cm} + \underbrace{\bar{r}_d}_{\sim \frac{1}{S_d}} + \underbrace{\bar{r}_c}_{\sim \frac{1}{S_c}} \tag{4.25}$$

$$C_{mp} = \frac{t_s^{cp}}{F} \underbrace{(\mu_{s,c,m} - \mu_{s,d,m})}_{\sim \ln\left(\frac{S_{c,m}}{S_{d,m}}\right)} + \frac{t_w^{cp}}{F} \underbrace{(\mu_{w,c,m} - \mu_{w,d,m})}_{\sim -(S_{c,m} - S_{d,m})} \tag{4.26}$$

To obtain the simplified expressions for each of the above pre-factors we have taken osmotic and salt activity coefficients as unity[d] and linearised the relationship between salinity and concentrations. In Section 4.4 we will analyse the dependence of these pre-factors upon diluate and concentrate salinity. At this point, we focus on how current density affects efficiency and productivity for constant diluate and concentrate salinities (Fig. 4-4a and 4-4b).

At low current densities both productivity and efficiency improve as the free energy change associated with migration increases relative to migration and diffusion. As a consequence, regardless of the price ratio R_p in Eq. (4.10), it would never be sensible, from a cost perspective, to operate at a current density below about 12 A/m^2. At higher current densities, up until the limiting current density of about 55 A/m^2, productivity increases while efficiency decreases with increasing current density. These trends give rise to an important trade-off, seen in Eq. (4.10), whereby an

[d]The osmotic coefficient of aqueous NaCl varies between a minimum of 0.92 and a maximum of 1.27, and the NaCl activity coefficient between 0.65 and 1.00, over the range from an infinitely dilute to a saturated solution[25].

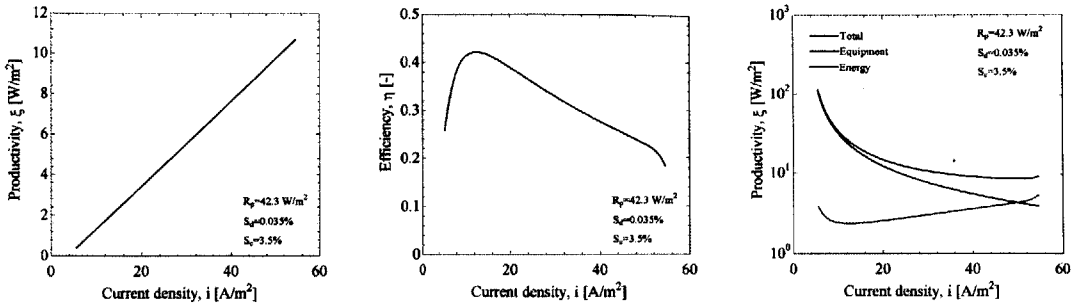

(a) Productivity (b) Efficiency (c) Cost

Figure 4-4 Influence of current density upon efficiency, productivity and cost

increase in capital cost results in a decrease in energy costs and vice versa, and ultimately, the optimal current density will depend upon the price ratio R_p. At a value of $R_p = 42.3$ W/m^2 the need to minimise capital costs drives the optimal current density (about 50 A/m^2) very close to the limiting current density. Interestingly this finding is consistent with industrial practice in brackish water desalination where the current density is set close to its limiting value[7].

4.4 Dependence of productivity, efficiency and cost upon salinities at the optimal current density

From here on, in analysing the effect of diluate and concentrate salinities, we consider only the value of current density that minimises the 'Local Cost' for a given diluate-concentrate salinity pair. The 'Local Cost' for each diluate-concentrate salinity pair is thus given, combining Eqs. (4.10), (4.20) and (4.21), by:

$$Local\ Cost^* = \min_i \frac{R_p}{C_{mig} i - C_{od}} + \frac{C_{mp} i + C_{oh} i^2}{C_{mig} i - C_{od}}. \tag{4.27}$$

Fig. 4-5 illustrates the effect of both diluate and concentrate salinities upon the optimal productivity, efficiency, Local Cost and current density, solved for numerically, in each case, using a quadratic approximations method in Engineering Equation Solver[35]. There are four important trends to observe, which we will explain in the

following subsections:

1. For any value of diluate salinity, there exists a value of concentrate salinity that minimises 'Local Cost' — since both productivity and efficiency exibit maxima at lower diluate salinities and efficiency exhibits a maximum for any diluate salinity. Furthermore, that the optimal concentrate salinity decreases as the diluate salinity decreases supports the logic of operating electrodialysis stacks with the diluate and concentrate in counterflow[36].

2. There exists a diluate-concentrate pair that minimises the 'Local Cost' — roughly because efficiency falls at higher diluate salinities and productivity rises at lower salinities.

3. For fixed diluate salinity, the optimal current density increases with increasing concentrate salinity.

4. For fixed concentrate salinity, the optimal current density increases with increasing diluate salinity at low diluate salinities but decreases at high diluate salinities.

4.4.1 Influence of salinities upon productivity, efficiency and 'Local Cost'

To understand why there is an optimal concentrate salinity for each diluate salinity and why there is an overall optimal diluate-concentrate salinity pair we examine the influence of salinity upon productivity (Eq. (4.20)), efficiency (Eq. (4.21)) and Local Cost (Eq. (4.27)). To do this we return to Eqs. (4.23), (4.24), (4.25) and (4.26). Fig. 4-6 provides a graphical illustration of these equations to further help understand the relationships between the four pre-factors and the diluate and concentrate salinity. It is arrived at by considering that:

(A) C_{mig} becomes low when the salinity ratio S_c/S_d becomes low. This is qualitatively represented in Fig. 4-6 by a line of constant salinity ratio above which the change in free energy associated with migration is low.

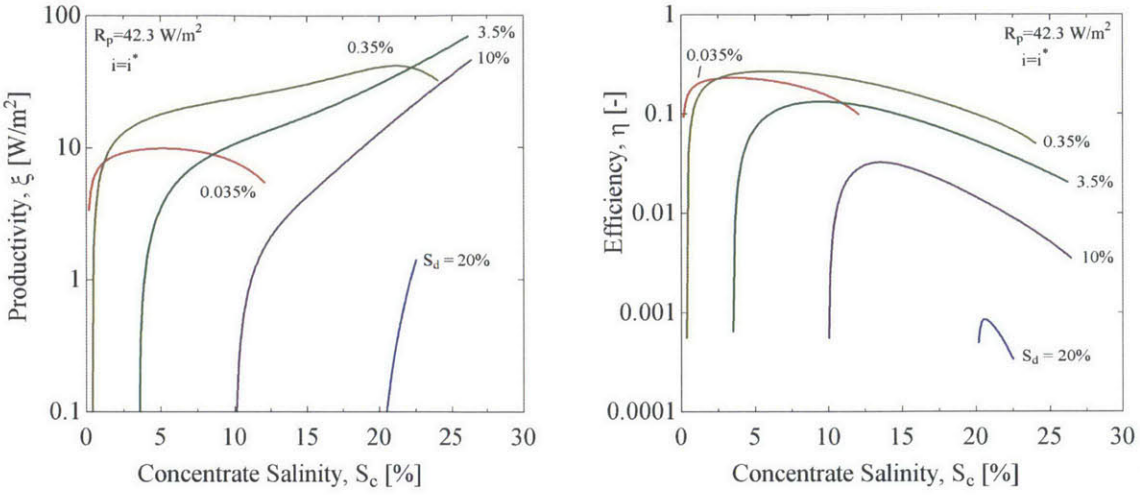

(a) Productivity

(b) Efficiency

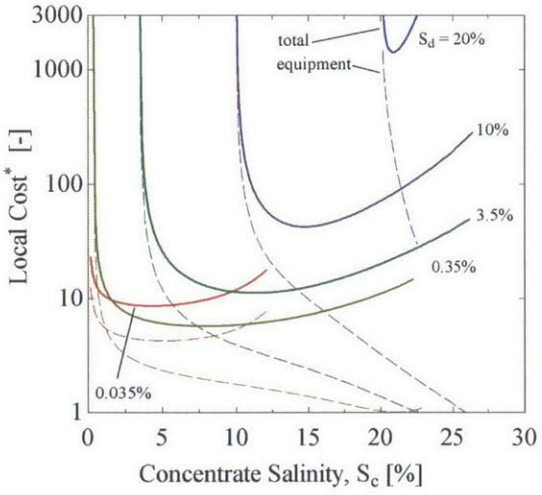

(c) Dimensionless local specific cost

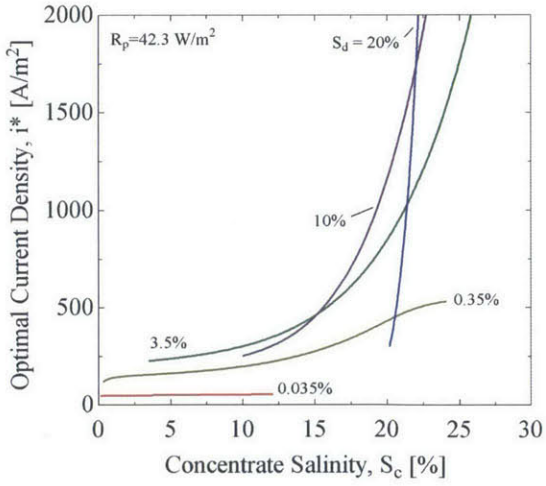

(d) Optimal current density

Figure 4-5 Influence of diluate and concentrate salinity upon efficiency, productivity, 'Local Cost' and optimal current density

(B) C_{od} becomes high when there is significant separation between diluate and concentrate salinity. This is represented in Fig. 4-6 by a line of constant salinity difference to the right of and below which the effects of osmosis and diffusion are strong.

(C) C_{oh} becomes high at low diluate salinity. This is represented in Fig. 4-6 by a line of constant diluate salinity below which ohmic resistance is high.

(D) C_{mp} has a similar dependence upon salinities as C_{mig} but differs in that its value must always be greater due to concentration polarisation. This difference is primarily important at low diluate salinity where the salinity difference $\Delta S = S_d - S_{d,m}$ has a strong effect upon the denominator of the first term on the right hand side of Eq. (4.26). Thus, the region where C_{mp}/C_{mig} is high is represented in Fig. 4-6 by illustrating a horizontal line of constant diluate salinity (the same line as for C_{oh}), below which concentration polarisation results in a deviation of C_{mp} above C_{mig}[e].

Given this understanding we can return to (4.10), Eqs. (4.20) and (4.21) to see how, for a fixed diluate salinity, low concentrate salinities result in low C_{mig} (low salinity ratios) and consequently reduce efficiency, productivity and 'Local Cost', while high concentrate salinities result in high values of C_{od} (high salinity differences) and consequently also reduce efficiency, productivity and 'Local Cost'. Hence, for fixed diluate salinity, intermediate values of concentrate salinity lead to minimum 'Local Cost'.

Secondly, we can understand how low values of diluate salinity lead to high C_{oh} and high C_{mp}/C_{mig} while high values of diluate salinity make high salinity ratios, and hence high C_{mig} unachievable. This explains the existence of a single diluate-concentrate pair that minimises the 'Local Cost'. In summary, there are three primary drivers of high 'Local Cost' for electrodialysis:

[e]Note also that while osmosis, diffusion and electro-osmosis serve to reduce productivity (4.11), electro-osmosis acts in two opposing ways that mitigate its effect upon efficiency; as electro-osmosis increases C_{mig} in Eq. (4.23) decreases, decreasing efficiency, but C_{mp} in Eq. (4.26) also decreases, increasing efficiency. Thus the practical implications of electro-osmosis are to limit the maximum concentrate concentration and to reduce productivity but not to significantly affect efficiency.

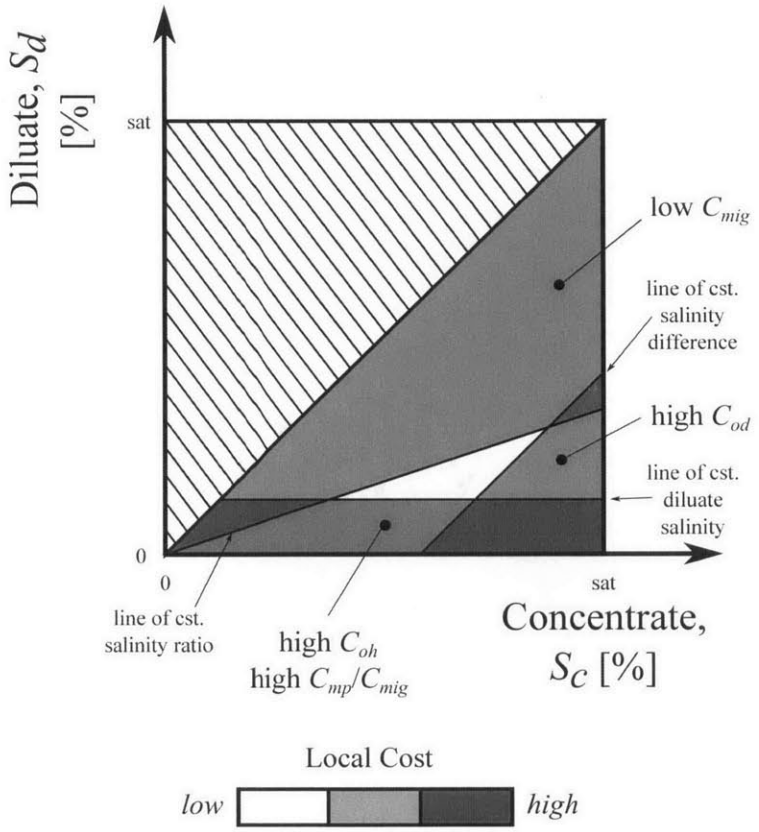

Figure 4-6 Dimensionless local specific cost

1. A low salinity ratio — resulting in poor productivity

2. A large difference between diluate and concentrate salinity — resulting in high diffusion and osmosis

3. A low diluate salinity — resulting in significant ohmic resistance and concentration polarisation

4.4.2 Influence of salinities on optimal current density

To understand trends in the optimal current density with diluate and concentrate salinity we analyse the solution to Equation (4.27), which makes apparent the dependence of 'Local Cost' upon current density. C_{mp} and, to a lesser extent, C_{od}, are functions of current density since they depend upon concentrations at membrane surfaces. This makes it impossible to obtain an exact analytical solution for the optimal current density. However, considering cases where concentration polarisation is negligible, and thus $C_{mp} \approx C_{mig}$, the optimal current density is given analytically by:

$$i^* = \frac{C_{od}}{C_{mig}} + \sqrt{\left(\frac{C_{od}}{C_{mig}}\right)^2 + \frac{C_{od}}{C_{oh}} + \frac{R_p}{C_{oh}}}. \tag{4.28}$$

This reveals the dependence of optimal current density upon three trade-offs:

1. $\frac{C_{od}}{C_{mig}}$, the trade-off between osmosis and diffusion effects, and migration effects — with higher osmosis and diffusion driving higher current density to enhance productivity, ξ.

2. $\frac{C_{od}}{C_{oh}}$, the trade-off between osmosis and diffusion, and ohmic resistance — with higher ohmic resistance driving lower current density to enhance efficiency, η.

3. $\frac{R_p}{C_{oh}}$, the trade-off between the equipment-to-energy cost ratio and ohmic resistance — with higher specific equipment costs driving higher current density to reduce overall equipment costs

Fig. 4-7 provides a graphical illustration of Eq. (4.28) equations to further help understand the relationships between the three ratios above and the optimal current

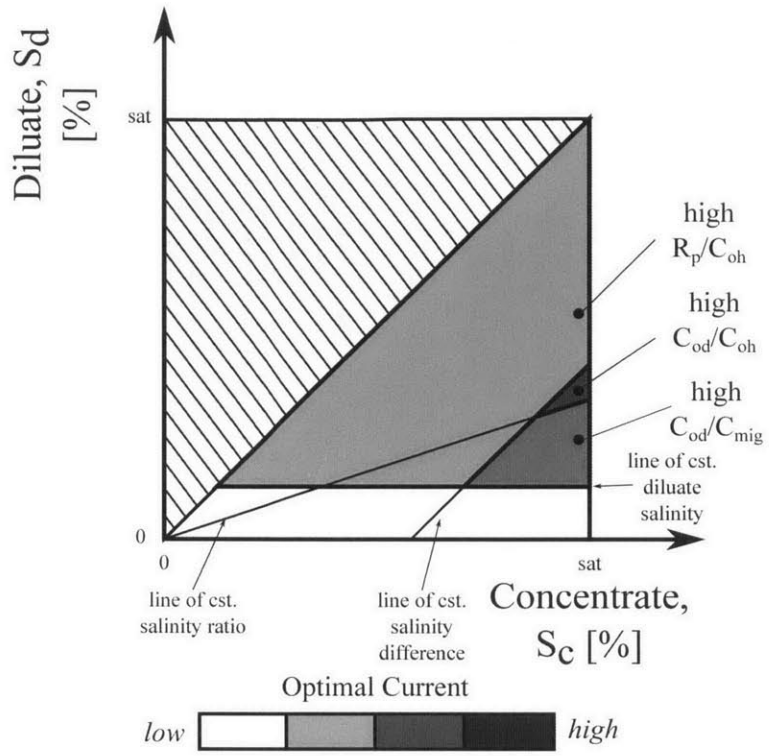

Figure 4-7 Optimal current density

density. It is arrived at by considering the dependence of the four pre-factors C_{mig}, C_{od}, C_{mp} and C_{oh} in Fig. 4-6.

Considering Fig. 4-7 in combination with Eq. (4.28) we can see how, for fixed diluate salinity, high concentrate salinity leads to a higher optimal current density, as in Fig. 4-5d. Furthermore, we can see how, in particular at high concentrate salinity, the optimal current density increases with diluate salinity at low diluate salinity but decreases again at high diluate salinity.

4.4.3 Implications for the cost of ED systems

Knowing the dependence of 'Local Cost' upon salinity allows us to examine the cost of diverse ED systems. Figure 4-8 depicts four electrodialysis processes overlaid as pathlines on a (logarithmic) graph of local cost. From this figure we can draw the following conclusions:

- Brackish desalination is cost effective in its initial stage as the limiting current density remains reasonably high while the high salinity ratio lends itself to high productivity. By contrast, the final stages of salt removal are expensive as productivity is restricted by the limiting current density.

- The major difficultly faced in seawater desalination with electrodialysis is the low salinity ratio that persists during the majority of the process. This results in low productivity and efficiency.

- The ratio of concentrate-to-diluate salinity in brine concentration applications is low, resulting in low productivity and efficiency. Furthermore, depending on the concentrate concentration desired osmosis and diffusion can further hamper performance particularly in the final stages of desalination (low diluate salinity).

- Of all processes, the most cost effective is partial brackish desalination, where a high-end brackish salinity stream is partially desalted. In such cases, both a high salinity ratio and a high diluate salinity can be maintained, allowing excellent productivity and efficiency. Such a process is of particular interest where a high purity product is not a requirement or where a polishing process such as reverse osmosis follows ED treatment. Examples of suitable applications might include the treatment of waters from coal-bed methane extraction[23], flue-gas desulphurisation or the treatment of low salinity produced waters in the oil and gas industry.

4.5 Conclusion

We show that electrodialysis processes are most productive and energy efficient when removing salt from a diluate stream that is in the high end of the brackish range (*e.g.* circa 1,000 ppm to 20,000 ppm). At higher diluate salinities both productivity and efficiency are compromised due to the small difference in chemical potential of salt in the diluate and concentrate streams. At lower diluate salinities productivity is

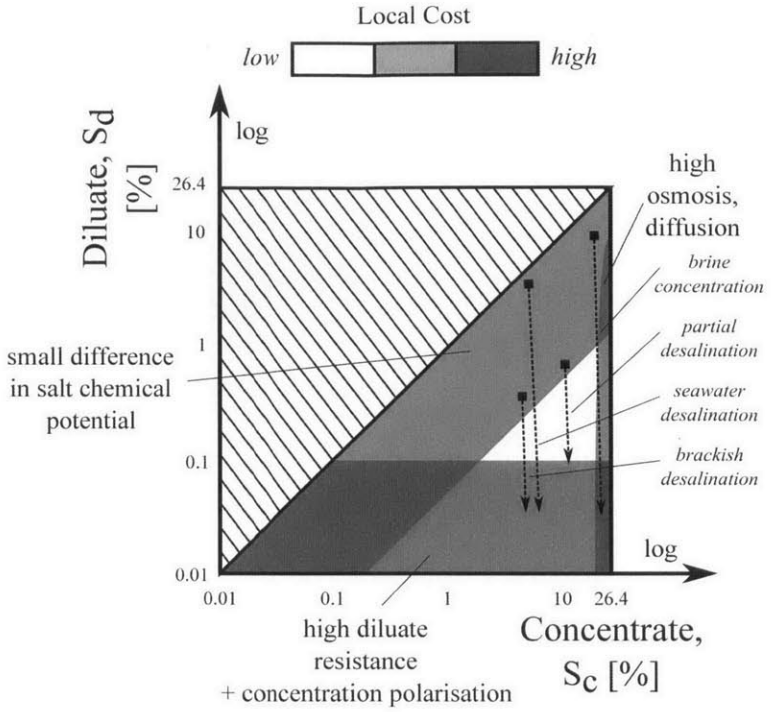

Figure 4-8 Graphical depiction of four electrodialysis processes

compromised by low values of limiting current density. These results suggest there is promise in further developing electrodialysis for the treatment of waters from coal-bed methane, oil and gas extraction as well as flue-gas desulphurisation, where high-end brackish salinity streams are partially desalted.

Nomenclature

Roman Symbols

a	activity, -
A_m	membrane permeability, l/m^2-h-bar
c	molar concentration, mol/litre
C	concentration, mol/m^3
C_{cap}	production normalised equipment cost,\$/(m^3/day)
D	diffusion coefficient, m^2/s

E	potential, V
F	Faraday's constant, C/mol
G	Gibb's free energy, J
h	channel height, m
h_{fg}	latent heat of vaporisation, J/kg
i	current density, A/m^2
J	transmembrane molar flux, $mol/m^2 \cdot s$
K_Q	specific cost of equipment, $\$/m^2$
L_w	permeability to water, $mol/m^2 \cdot s \cdot bar$
m	molal concentration, mol/kg solvent
MW	molecular weight, kg/mol
p	power density, W/m^2
P	pressure, bar
r	rate of return on capital, -
$\bar{r}$	area resistance, Ωm^2
R	universal gas constant, $J/mol \cdot K$
R_p	price ratio, -
S	salinity, kg salt/kg solution
Sh	Sherwood number, -
T	temperature, K
t	solution transport number, -
T_s	membrane salt transport number, -
T_w	membrane water transport number, -
$\bar{T}$	integral ion transport number, -
V	voltage, V
$\bar{v}$	molar volume, m^3/mol

Greek Symbols

γ	molal activity coefficient, -
Δ	difference

η	efficiency, -
Λ	molar conductivity, Sm^2/mol
μ	chemical potential, J/mol
ν_s	number of moles of dissociated ions per mole of salt, -
ξ	productivity, W/m^2
Ξ	dimensionless cost, -
π	osmotic pressure, bar
ρ	density, kg/m^3
τ	time, years
ϕ	osmotic coefficient, -

Subscripts

am	anion exchange membrane
app	apparent
b	bulk
c	concentrate
cm	cation exchange membrane
cond	condensation
cp	cell pair
cu	counter ion
d	diluate
ev	evaporation
F	feed
lim	limiting
m	at membrane surface
mig	migration
i	counting index
j	junction
mp	membrane potential
oh	ohmic

os	osmotic
p	pump
$pure$	pure
s	salt
v	volumetric
w	water
0	reference value

Superscripts

am	anion exchange membrane
cm	cation exchange membrane
eo	electo-osmosis
o	osmosis
sw	seawater
$1, 2$	thermodynamic states
$\cdot$	rate

Acronyms

CAF	capital amortization factor
LCE	levelised cost of energy
MCS	marginal cost of separation

Bibliography

[1] J.-B. Lee, K.-K. Park, H.-M. Eum, C.-W. Lee, Desalination of a thermal power plant wastewater by membrane capacitive deionization, Desalination 196 (1) (2006) 125–134.

[2] S. J. Kim, S. H. Ko, K. H. Kang, J. Han, Direct seawater desalination by ion concentration polarization, Nature Nanotechnology 5 (4) (2010) 297–301.

[3] A. Mani, M. Z. Bazant, Deionization shocks in microstructures, Physical Review E 84 (6) (2011) 061504.

[4] M. Pasta, C. D. Wessells, Y. Cui, F. La Mantia, A desalination battery, Nano letters 12 (2) (2012) 839–843.

[5] S. Porada, B. Sales, H. Hamelers, P. Biesheuvel, Water desalination with wires, The Journal of Physical Chemistry Letters 3 (12) (2012) 1613–1618.

[6] K. N. Knust, D. Hlushkou, R. K. Anand, U. Tallarek, R. M. Crooks, Electrochemically mediated seawater desalination, Angewandte Chemie International Edition.

[7] H.-J. Lee, F. Sarfert, H. Strathmann, S.-H. Moon, Designing of an electrodialysis desalination plant, Desalination 142 (3) (2002) 267–286.

[8] P. Tsiakis, L. G. Papageorgiou, Optimal design of an electrodialysis brackish water desalination plant, Desalination 173 (2) (2005) 173–186.

[9] R. Yamane, M. Ichikawa, Y. Mizutani, Y. Onoue, Concentrated brine production from sea water by electrodialysis using exchange membranes, Industrial & Engineering Chemistry Process Design and Development 8 (2) (1969) 159–165.

[10] T. Seto, L. Ehara, R. Komori, A. Yamaguchi, T. Miwa, Seawater desalination by electrodialysis, Desalination 25 (1) (1978) 1–7.

[11] T. Sirivedhin, J. McCue, L. Dallbauman, Reclaiming produced water for beneficial use: salt removal by electrodialysis, Journal of membrane science 243 (1) (2004) 335–343.

[12] V. Nikonenko, A. Istoshin, M. K. Urtenov, V. Zabolotsky, C. Larchet, J. Benzaria, Analysis of electrodialysis water desalination costs by convective-diffusion model, Desalination 126 (1) (1999) 207–211.

[13] J. Wood, J. Gifford, J. Arba, M. Shaw, Production of ultrapure water by continuous electrodeionization, Desalination 250 (3) (2010) 973–976.

[14] G. Ganzi, Electrodeionization for high purity water production, in: AIChE Symposium series, Vol. 84, 1988.

[15] E. R. Reahl, Reclaiming reverse osmosis blowdown with electrodialysis reversal, Desalination 78 (1) (1990) 77–89.

[16] Y. Oren, E. Korngold, N. Daltrophe, R. Messalem, Y. Volkman, L. Aronov, M. Weismann, N. Bouriakov, P. Glueckstern, J. Gilron, Pilot studies on high recovery BWRO-EDR for near zero liquid discharge approach, Desalination 261 (3) (2010) 321–330.

[17] S. Thampy, G. R. Desale, V. K. Shahi, B. S. Makwana, P. K. Ghosh, Development of hybrid electrodialysis-reverse osmosis domestic desalination unit for high recovery of product water, Desalination 282 (SI) (2011) 104–108.

[18] M. Urtenov, A. Uzdenova, A. Kovalenko, V. Nikonenko, N. Pismenskaya, V. Vasil'eva, P. Sistat, G. Pourcelly, Basic mathematical model of overlimiting

transfer enhanced by electroconvection in flow-through electrodialysis membrane cells, Journal of Membrane Science 447 (2013) 190 – 202.

[19] M. Turek, Dual-purpose desalination-salt production electrodialysis, Desalination 153 (1) (2003) 377–381.

[20] M. Fidaleo, M. Moresi, Optimal strategy to model the electrodialytic recovery of a strong electrolyte, Journal of Membrane Science 260 (1) (2005) 90–111.

[21] V. Zabolotskii, K. Protasov, M. Sharafan, Sodium chloride concentration by electrodialysis with hybrid organic-inorganic ion-exchange membranes: An investigation of the process, Russian Journal of Electrochemistry 46 (9) (Sept. 2010) 979 – 986.

[22] S. Koter, A. Cuciureanu, M. Kultys, J. Michałek, Concentration of sodium hydroxide solutions by electrodialysis, Separation Science and Technology 47 (9) (2012) 1405–1412.

[23] E. T. Sajtar, D. M. Bagley, Electrodialysis reversal: Process and cost approximations for treating coal-bed methane waters, Desalination and Water Treatment 2 (1-3) (2009) 284–294.

[24] R. K. McGovern, S. M. Zubair, J. H. Lienhard V, The benefits of hybridising electrodialysis with reverse osmosis. Under review.

[25] R. Robinson, R. Stokes, Electrolyte Solutions, Courier Dover Publications, 2002.

[26] K. Kontturi, L. Murtomaki, J. A. Manzanares, Ionic Transport Processes In Electrochemistry and Membrane Science, Oxford Press, 2008.

[27] T. Shedlovsky, The electrolytic conductivity of some uni-univalent electrolytes in water at 25 C, Journal of the American Chemical Society 54 (4) (1932) 1411–1428.

[28] J. Chambers, J. M. Stokes, R. Stokes, Conductances of concentrated aqueous sodium and potassium chloride solutions at 25 C, The Journal of Physical Chemistry 60 (7) (1956) 985–986.

[29] M. Fidaleo, M. Moresi, Electrodialytic desalting of model concentrated nacl brines as such or enriched with a non-electrolyte osmotic component, Journal of Membrane Science 367 (1) (2011) 220–232.

[30] A. Sonin, R. Probstein, A hydrodynamic theory of desalination by electrodialysis, Desalination 5 (3) (1968) 293–329.

[31] San Diego County Water Authority, Carlsbad desalination project (2012).

[32] U.S. Energy Information Administration, Annual energy outlook 2013, Tech. rep. (2013).

[33] A. Narebska, S. Koter, W. Kujawski, Ions and water transport across charged nafion membranes. irreversible thermodynamics approach, Desalination 51 (1).

[34] A. Narebska, S. Koter, W. Kujawski, Irreversible thermodynamics of transport across charged membranes. Part I. macroscopic resistance coefficients for a system with nafion 120 membrane., Journal of membrane Science 25 (2) (1985) 153–170.

[35] S. Klein, F. Alvarado, Engineering equation solver, F-Chart Software.

[36] B. Batchelder, W. W. Carson, L. Zhang, Electrodialysis system and process, uS Patent 8,142,633 (March 2012).

Chapter 5

A hybrid electrodialysis-reverse osmosis system and its optimization for the treatment of highly saline brines

Abstract

The demand is rising for desalination technologies to treat highly saline brines arising from hydraulic fracturing processes and inland desalination. Interest is growing in the use of electrical desalination technologies for this application. The hybridization of electrodialysis (ED) with reverse osmosis (RO) allows high salinities (beyond the range of RO alone) to be reached while avoiding the operation of ED with a low conductivity diluate stream. Such hybrid systems have been experimentally investigated for concentrates from brackish and seawater desalination. However, progress is required in the modelling and optimization of hybrid systems at higher concentrations. A novel hybrid arrangement of counterflow ED systems with reverse osmosis is presented to concentrate a saline feed at 120 ppt. The system is considered from the perspective of efficiency, membrane productivity and the levelised cost of water, with emphasis on the optimisation of current density. In contrast to brackish ED systems, membrane resistances are found to dominate diluate and concentrate resistances at high salinity. The current density found to minimise LCW (levelised cost of water) is significantly greater than the current density found to maximise efficiency, indicating the high current capital cost of ED per unit membrane area and poor membrane transport properties relative to RO. Finally, performance at high recoveries is found to be limited by high stream-to-stream concentration differences, increasing water

transport via osmosis, decreasing efficiency and increasing the LCW.

Contributions

This chapter was co-authored by Prof. Syed Zubair and Prof. John Lienhard V. The work received financial support from the US Department of State via the Fulbright Science and Technology Program, the International Desalination Association's Channabasappa Memorial Scholarship, the MIT Martin Fellowship for Sustainability and the King Fahd University of Petroleum and Minerals through the Center for Clean Water and Clean Energy at MIT and KFUPM under project number R15-CW-11.

5.1 Introduction

5.1.1 Motivation

Reverse osmosis (RO) has demonstrated great success in the desalination of seawater over the past decade, accounting for over 80% of total contracted capacity in 2010 and 2011[1]. However, its ability to treat waters of higher salinity is limited by the hydraulic pressure allowable within pressure vessels. Meanwhile, the volume of highly saline brines produced in the world is increasing rapidly. Disposal of concentrated brines from inland desalination and produced water in the oil and gas industry is a growing issue[2,3]. Energy efficient, low cost technologies to recover water and salts from concentrated streams are needed.

5.1.2 Literature review

Korngold et al.[4] investigated a batch electrodialysis (ED) system for volume reduction of a brackish water reverse osmosis concentrate stream (containing silica and gypsum). Concentrate of 15,000 ppm salinity was fed to the ED system and concentrated to approximately 100,000 ppm. Gypsum was precipitated from the concentrate stream in an adjacent precipitation unit. Oren et al.[4] operated a continuous ED-RO process whereby the concentrated stream from a 2nd stage RO unit was fed to the diluate side of the ED unit and recirculated to the feed side of the first RO stage. TDS of 10,000 ppm was achieved within the continuously circulated ED concentrate side while simultaneously crystalizing solids within a side loop crystallizer.

Thampy et al.[6] evaluated a continuous ED process with the ED diluate stream flowing for final treatment to an RO unit and the RO concentrate being recirculated to the ED feed. The concentrate concentrations achieved by the ED unit were lower than that of Oren et al. due to the once-through flow path on the concentrate side of the ED unit. Casas et al.[7] investigated batch concentration of RO concentrate, finding the concentration of sodium chloride achievable to be limited by back diffusion and electro-osmotic transport. As remarked by Casas et al.[7], further analysis of energy

consumption and process optimization is required for hybrid ED-RO systems. This is the gap this research aims to address.

5.1.3 Goals

By hybridizing electrodialysis with reverse osmosis, higher salinity feeds may be treated than with RO alone, while the use of RO avoids operation of ED with streams of low conductivity. This study outlines the design of a desalination system consisting of counterflow ED units hybridised with RO. In particular, the following tasks are the focus of this work:

1. Modelling of the efficiency, membrane productivity and levelised cost of water (LCW) of this hybrid system

2. Determination of the current density maximising the LCW and the efficiency.

The design of the ED systems rather than the RO system is emphasised. An RO system design typical of a single stage single pass seawater RO (SWRO) is assumed. Furthermore, to limit the scope of this work, the design and optimisation of ED pumping systems is overlooked, though important in eventually determining and optimizing overall system costs.

5.2 Design considerations for ED at high salinity

The design of electrodialysis systems for the desalination of high concentration solutions is notably different than brackish water electrodialysis or indeed electrodeionisation. In particular, the limiting current density and concentration polarization are no longer limiting at higher concentrations. Instead the balance between ohmic losses and losses due to water transport via electro-osmosis and osmosis becomes central in design.

5.2.1 Relative importance of ohmic losses in solutions and membranes

In brackish water ED, ohmic losses within the diluate stream are very significant due to low conductivity. It is useful to compare the ohmic resistance of the diluate stream, Eq. 1, and the ohmic resistance of typical cation and anion exchange membranes. Neosepta anion and cation exchange membranes are considered with surface resistances of 2.4 and 3 Ω cm^2 respectively[17].

$$\bar{r}_d = \frac{h_d}{\Lambda_d C_d} \tag{5.1}$$

Here, $\bar{r}_d$ is the surface resistance of the diluate in Ω m^2, h_d is the diluate channel spacing in m, Λ_d is the molar conductivity of the diluate stream in Sm^2/mol, and C_d is the diluate concentration in mol/m^3. Figure 1 illustrates the ohmic resistance of the diluate stream relative to the ohmic resistance of the membranes. Experimental data relating conductivity and NaCl concentration is interpolated to calculate the molar conductivity[11] of the diluate stream in Eq. 1. For diluate channel spacings even up to 2.5 mm, membrane resistances dominate at concentrations above approximately 1 mol/L. Overall ohmic resistance of the stack is significantly less sensitive to changes in concentration of the diluate and concentrate streams for high salinity ED applications. For desalination to concentrations that meet drinking water standards (less than 500 ppm), however, the benefit of hybridization with RO is to avoid high stack resistances encountered at low concentrations.

5.2.2 Limiting current density and concentration polarization

In low salinity applications, the limiting current density hinders the quantity of salt that may be removed per unit of membrane area. In essence, this limit upon the rate of ion removal occurs as ion diffusion towards the membrane surface becomes insufficient to replenish the concentration of salt at membrane-solution interfaces.

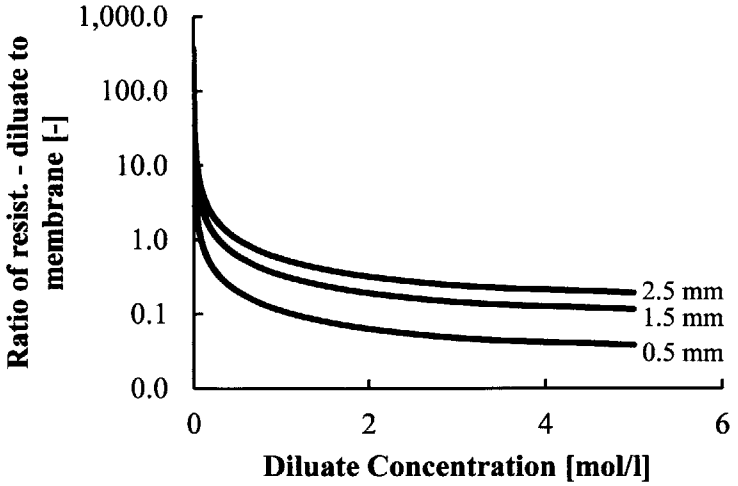

Figure 5-1 Ratio of diluate to membrane channel resistance for three values of channel spacing

The physics observed in this regime of operation is complex and analysed in detail in literature[8,9].

In high salinity applications, the concentration of salt in the diluate and concentrate streams is large enough for the depletion of ions at the membrane-solution interface to occur only at very high current densities. Furthermore, the impact of concentration polarization is relative to a much larger difference in concentration between the diluate and concentrate streams, i.e. higher levels of concentration polarization may be tolerated. Considering a balance between convection and diffusion within a film adjacent to a membrane, the extent of concentration polarization on the diluate side of each membrane may be estimated employing Eq. 2[10].

$$\frac{\Delta C}{\Delta x} \approx -\frac{i(T_i^d - t_i^m)}{z_i F D_s} \tag{5.2}$$

Here, i denotes the current density, F Faradays constant, T_i^d the transport number of ion i in the diluate and t_i^m the apparent transport number of ion i in the membrane. Although D_s, the electrolyte diffusivity, is affected by the current density and by solution concentration, we may approximate a lower bound on its value by considering the self-diffusion coefficient of a dilute NaCl solution at zero current density[11]. The

Table 5.1 Concentration polarization estimation

Symbol	Value	Ref.
D_s	$1.61\times10^{-9}\mathrm{m}^2/\mathrm{s}$	[11]
T_i^d	1	Assumed
t_{Na}^m	0.396	Calculated[a]
ν	$8.9\times10^{-7}\mathrm{m}^2/\mathrm{s}$	[12]
$Sc \equiv \nu/D_s$	580	Calculated
Re	25	[13]

value of the effective transport number of the co-ion in a membrane is typically close to one. For the desalination of NaCl solutions, concentration polarization is higher at the cation exchange surface according to Eq. 2, since the transport number of sodium in solution is lower than chloride (sodium has a larger hydration shell causing greater drag). The transport number for sodium in solution is estimated from the diffusivity and viscosity of pure water, Table 1.

To estimate the gradient of concentration in Eq. 2, a relation for flow within a meshed channel is required, and it is provided by Eqs. 3 and 4, valid for $10\leq\mathrm{Re}\leq25$ [13].

$$\frac{\Delta C}{\Delta x} = \frac{\Delta C}{D_h}\mathrm{Sh} \tag{5.3}$$

$$\mathrm{Sh} = 0.53\mathrm{Re}^{1/2}\mathrm{Sc}^{1/3} \tag{5.4}$$

Here, D_h is the hydraulic diameter of the channel spacing, Sh is the Sherwood number, Re is the Reynolds number, and Sc is the Schmidt number, the ratio of momentum diffusivity, ν, to mass diffusivity, D_s. Figure 2 illustrates the degree of concentration polarization at the diluate side surface of a cation exchange membrane in contact with an NaCl solution. For a small membrane spacing the concentration polarization can be small relative to stream-to-stream concentration differences. For larger membrane spacings concentration polarization is a significant effect beyond current densities of approximately 500 $\mathrm{A/m}^2$. Importantly, the conclusions drawn are all contingent upon the Reynolds number and the diluate channel gap. Although not within the scope of this work, the optimization of these parameters in accordance with the trade-off between polarization effects and pumping power requirements is important.

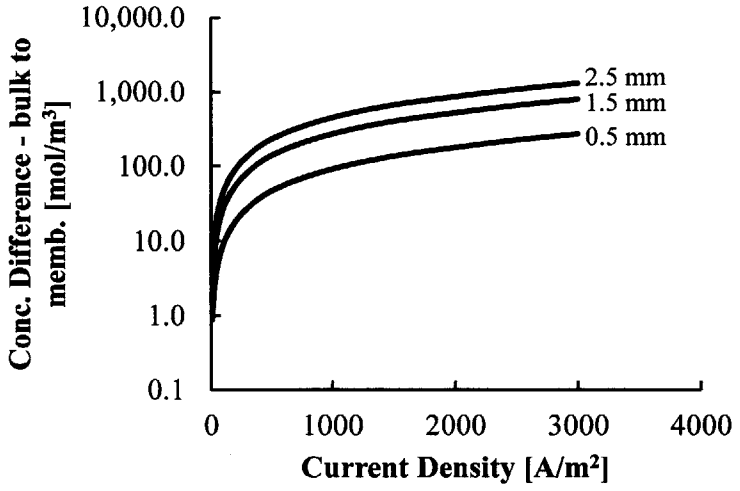

Figure 5-2 Concentration difference due to concentration polarization at a Reynolds of 25

Concentration polarization affects ED performance in three significant ways, which are only briefly described here:

1. Solution resistance increases within diluate stream boundary layers, although the impact upon overall resistance is less significant in high concentration ED systems.

2. Concentrations at the solution-membrane interface are decreased in the diluate and increased in the concentrate, causing an increase in the minimum potential required for desalination.

3. Potential differences, known as junction potentials[14], occur across the concentration polarization layers as a result of concentration gradients.

5.2.3 Maximum concentration achievable in electrodialysis

The ability of electrodialysis to produce a high concentration concentrate is limited by electro-osmotic transport from the diluate to the concentrated stream. This transport of water results from ions passing from the diluate to the concentrate and dragging a quantity of water with them, through the membrane. The ratio of the number of moles of water transported to the number of moles of ions is denoted the water transport

number. Thus, the maximum concentration achievable, cmax, in concentrating a sodium chloride solution depends upon the water transport numbers of the sodium and chloride ions in the cation and anion exchange membranes respectively[13]:

$$c_{max} = \frac{1}{(1 + t_{w,Na} + t_{w,Cl})\bar{v}_{sol}} \tag{5.5}$$

Here, $\bar{v}_{sol}$ is the molar volume of the solution. In low salinity applications, the effective concentration of a volume containing an ion with water transported remains significantly above the concentration of the concentrated stream. However, where the salinity of the concentrate is high, the effective concentration of this volume transported can be similar in value. The modelling of electro-osmotic transport through membranes is complex and depends upon the degree of crosslinking of the membrane (related to pore and channel size and distributions) and also the concentration of the diluate and concentrated solutions[15]. To some extent, in particular at high concentrations, the water transport number is related to the hydration number of the ion in a concentrated solution[15].

For large differences between concentrate and diluate concentrations, water transport due to osmosis becomes very significant. More specifically, the loss in Gibbs free energy due to the osmotic transport of water from the diluate to the concentrate stream becomes large relative to the increase in free energy achieved in moving salt from the diluate to the concentrated stream. Losses due to osmosis may be reduced relative to the desirable change of free energy associated with desalination by increasing the current density. However, increases in current density come at the expense of increased ohmic losses. Consequently, there exists a balance between losses due to osmosis and losses due to ohmic resistances (see results).

With improved models for water transport, it would be possible, during system design, to consider the trade-offs between electro-osmotic losses and other losses within the system. Furthermore, it should be possible to develop membranes with properties that optimize system performance. For now, we only recognize that electro-osmosis limits the maximum concentration achievable with ED and consider values obtained

experimentally in system testing of ED concentration.

5.2.4 Summary of high salinity ED

ED desalination at high salinity exhibits three distinctive characteristics:

1. The overall ohmic resistance of the stack is insensitive to changes in diluate or concentrate concentration. Membrane resistances dominate.

2. For small channel spacings, the degree of concentration polarization can be small relative to stream-to-stream concentration differences. The true impact of concentration polarization can only be clarified in the context of an optimization of the pumping system, channel width and Reynolds number.

3. The maximum concentration achievable is limited by electro-osmotic transport of water but also by transport via osmosis. As shall be seen in Sect. VI, the trade-off between membrane ohmic losses and losses associated with water transport is central in optimizing efficiency and the levelised cost of water (LCW).

5.3 System description and modelling

Figure 3 illustrates the hybrid ED-RO system configuration. The purpose of ED system A is to concentrate a portion of feed water to the desired concentrate concentration whilst diluting the remainder towards the concentration of the feed to the RO unit. The feed salinity at the inlet to the RO unit may thereby be reduced to a level whereby its osmotic pressure is not prohibitively high. ED system B serves the purpose of diluting concentrate from the RO system (along with the diluate of ED system A) to a concentration amenable to treatment with RO. ED system B also produces a concentrate at the same concentration as the feed water, allowing it to be recycled and treated by ED system A.

Both ED systems are envisioned to operate in a counter-flow arrangement. Such an arrangement allows a significant difference in concentration to be maintained between

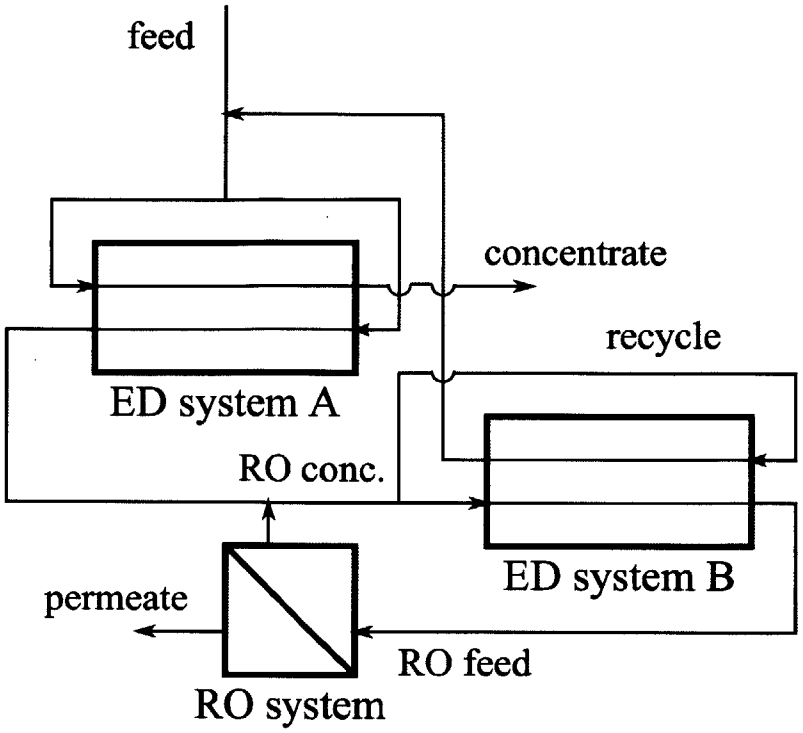

Figure 5-3 Schematic diagram of the hybrid ED RO system

the diluate and concentrate streams. This is in contrast to a co-flow arrangement where streams would necessarily be at the same concentration in the inlet to system A. The maintenance of such a difference in concentration is important to ensure that each unit of membrane area achieves a significant rise in the free energy of salt (the desirable result of the desalination process). Were concentrations to be close, energy is expended while moving salt between streams of very similar concentration.

In the present analysis, the design of an RO unit is chosen to be typical of a SWRO unit, taking a feed of 35 ppt and producing a concentrate at 70 ppt (constituting a recovery ratio for the unit of 50%).

The following key assumptions are involved in the analysis:

- Focus is maintained upon the efficiency of the system and the membrane area required. Though important, the optimization of the pumping system is outside of the analysis scope.

- Channel spacings are assumed to be sufficiently small for the effects of concen-

tration polarization to be negligible.

- In practice, ED systems A and B would consist of multiple stages. Here, they are each modelled as single stages.

- Electrode potentials are neglected relative to the voltage drop across cell pairs.

5.3.1 Evaluation of Donnan potentials

On the surface of each membrane, a thin region, orders of magnitude thinner than concentration polarization layers, and known as the electrical double layer, is present, within which electro-neutrality is not satisfied. An electrical potential exists across these double layers to compensate for the difference in chemical potential between species in the electro-neutral solution and within the membrane. Due to the differences in chemical potential of species in the bulk solution on either side of a membrane (associated with concentration differences) the overall effect of the Donnan potentials on either side of the membrane is to cause a net electrical potential across the membrane, denoted with for membrane potential. For a membrane with ideal counter-ion permselectivity the membrane potential is given by:

$$E_m = \frac{RT}{z_- F} \ln\left(\frac{a_{NaCl,c}}{a_{NaCl,c}}\right) \tag{5.6}$$

Here, a denotes the activity of a species (in this case NaCl), R is the ideal gas constant, T is ambient temperature, and z_- denotes the anion charge number. For non-ideal membranes in which the current is not solely carried by the counter ion (i.e. where the counter-ion transport number is less than unity), the membrane potential is lower than the ideal value. The convection of water via osmosis and electro-osmosis, and the diffusion of ions within the membrane influence the membrane potential to a lesser extent. A review of such effects is provided by Helfferich[16]. Here, we shall satisfy ourselves with the first order accuracy provided by Eq. 6.

Table 5.2 ED Membrane Properties

Symbol	Value	Ref.
$\bar{r}_{am}$	$2.4\times10^{-4}\Omega m^2$	17
$\bar{r}_{am}$	$3\times10^{-4}\Omega m^2$	17
t_w	10.08	18
L_w[b]	7.09×10^{-6}m/s	18
L_s	1.38×10^{-8}m/s	18

5.3.2 Evaluation of solution resistances

Both the diluate and concentrate solutions flow through a mesh spacer within their respective channels. For the purpose of modeling, these solutions are considered to be well mixed with a uniform conductivity throughout the channel. The ohmic resistances of these solutions, based upon unit area (i.e. Ωm^2) is given by Eq. 7:

$$\bar{r}_l = \frac{h_l}{\Lambda_l c_l} \tag{5.7}$$

where Λ_l is the molar conductivity of the concentrate or diluate solution and is a function of salinity[11], and cl is the concentrate or diluate concentration in mol/m^3 A channel width of 0.5 mm is assumed in the subsequent calculations.

5.3.3 Membrane properties

A summary of experimental measurements of membrane resistances, water permeability, salt permeability and overall water transport number from the literature are provided in Table 2.

Of importance is the relevant magnitude of the salt diffusion coefficient and permeability of the membrane to water. It is unsurprising that the diffusion coefficient for salt should be lower since co-ions are strongly rejected by the membrane. As a consequence of electro-neutrality, the diffusion of ions is rendered difficult. As a simplifying assumption, salt transport via diffusion is neglected as losses associated with water transport through osmosis dominate.

5.3.4 ED system modelling

ED systems A and B are modelled via finite difference equations for a single cell pair, allowing the voltage and hence the power consumption in each finite difference to be evaluated. Conservation of salt and of total mass within each finite difference is employed for the concentrate and diluate streams within each unit. Salt and water transport from the diluate to the concentrate channel are described by Eqs. 8 and 9:

$$j_s = i/F \tag{5.8}$$

$$j_w = t_w j_s + L_w(C_c - C_d) \tag{5.9}$$

Here j indicates a molar flux in mol/m^2 s and L_w the water permeability in m/s. The overall voltage across a differential element of one cell pair during each time step is given by a sum of the membrane and solution surface resistances along with the membrane potential:

$$\Delta V_{cp}[k] = i(\bar{r}_{ma} + \bar{r}_{mc} + \bar{r}_d[k] + \bar{r}_c[k]) + \Delta E_m[k]] \tag{5.10}$$

Here, and indicate the membrane surface resistance of the anion and cation exchange membranes, in Ωm^2. k is an index in space for the elements Instantaneous power consumption is computed via the product of cell pair voltage, current and the area of the differential cell pair element area:

$$P[k] = \Delta V_{cp}[k] i \delta A_m \tag{5.11}$$

where δA_m is the area of a cell pair increment. Summing over the index k, the total power (for all cell increments) may be computed. A simple RO model is employed with membranes producing an average permeate flux of 13 L/m^2 h [19]. The RO membrane is assumed to have perfect salt rejection and a permeability of 0.31 L/(m^2 h bar) [19]. Pressure drop due to viscous effects in the feed channel and concentration polarization are both neglected. A finite difference model (with 20 finite differences)

is employed to model permeate flux along membrane pressure vessels. Salinity at the inlet to each finite difference is calculated via the conservation of salt in the concentrate stream:

$$S_{c,RO}[k]\dot{m}_{c,RO}[k] = S_{c,RO}[k+1]\dot{m}_{c,RO}[k+1] \tag{5.12}$$

Here, is a mass flow rate in kg/s. Osmotic pressure, Π, in bar, in each cell is calculated at the cells inlet salinity using Eq. 13.

$$\Pi[k] = \frac{RT}{\bar{v}}\nu_{NaCl}m_{RO,c}(S_{RO,c})\phi(S_{RO,c}) \tag{5.13}$$

Here, ϕ is the osmotic coefficient and m is the solute molality in mol solute/kg solvent. The 1-dimensional finite difference model solves the following equation in each cell, with A_m the membrane permeability and j_w the water flux:

$$j_{w,RO}[k] = A_m(P - \Pi[k]) \tag{5.14}$$

These equations are solved iteratively in combination with equations describing the ED system to evaluate the inlet hydraulic pressure to the RO unit and the membrane area required. In computing power consumption the pump efficiency, η_p, is assumed to be 75% and no pressure recovery device is employed. Work per unit of permeate is thus described by Eq. 15:

$$w_{RO} = \frac{p\dot{m}_{f,RO}}{\eta_p\rho_{f,RO}\dot{m}_{p,RO}} \tag{5.15}$$

Here, w_{RO} denotes work done in J per kg of RO permeate, p is the pressure in Pa of the feed and $\rho_{f,RO}$ is the feed density in kg/m^3.

5.3.5 Physical properties

The salt considered is sodium chloride. Data relating the osmotic coefficient, salt activity coefficient and electrolyte conductivity were taken from Robinson and Stokes[11]

while density was taken from Busey[20].

5.3.6 Solution of hybrid system equations

In addition to parameters described in Sect. 3.4 and 3.5, the following constraints are applied in solving the coupled systems of equations for the ED systems and the RO system.

- Feed salinity to the entire system is set at 120 ppt.
- The volume flow rate of permeate from the entire system is set at 100 m3/day.
- The relative mass flow rate at the inlet to the diluate and concentrate compartments in system A is set such that the stream-to-stream concentration differences at either end of the unit are equal. This condition is also imposed in system B. This is to promote a constant current density within the stages of systems A and B.
- The current densities within units A and B are chosen in accordance with the optimization to be described in Section 4.
- Mass conservation equations are employed at nodes of intersection of streams in Fig. 3.
- For clarity and ease of comparison, all energetic quantities are calculated on the basis of unit permeate production of the RO unit. Each of ED system A, system B and the RO unit can be seen as contributing to the total energy required to produce each unit of permeate.

Solving the entire system of equations yields the power consumption of each unit, the membrane area of each unit, the concentrate stream concentration and the overall recovery ratio of the system.

5.4 Minimization of the levelized cost of water

Minimization of the levelized cost of water requires an understanding of how energy requirements and system size scale with current density. In this simplified analysis, energy is costed on the basis of \$/kWh, K_E, and capital equipment is costed on the basis of \$/m^2 cell pair area, K_C. For a defined process of desalination, where mass flow rates and salinities of the feed, concentrate and product are fixed, the required change in Gibbs free energy of the streams, known as the reversible work, may be determined. Knowing the Second Law efficiency of the system, η, the total work required may be computed by dividing the reversible work by the efficiency, Eq. 17. Likewise, knowing the average membrane productivity of the system, ξ, defined as rate of reversible work per unit of membrane area, the total membrane area may be computed by dividing the reversible work by the membrane productivity, Eq. 18.

$$\eta = \frac{\frac{RT}{F}\left[i \ln\left(\frac{a_{NaCl,c}}{a_{NaCl,d}}\right) - it_w \ln\left(\frac{a_{w,c}}{a_{w,d}}\right) - L_w(C_c - C_d)\ln\left(\frac{a_{w,c}}{a_{w,d}}\right)\right]}{iV_{cp}} \tag{5.16}$$

$$\xi = \frac{RT}{F}\left[i \ln\left(\frac{a_{NaCl,c}}{a_{NaCl,d}}\right) - it_w \ln\left(\frac{a_{w,c}}{a_{w,d}}\right) - L_w(C_c - C_d)\ln\left(\frac{a_{w,c}}{a_{w,d}}\right)\right] \tag{5.17}$$

Second Law efficiency is defined as the rate of change of free energy to the rate of work input, both per unit of membrane area. The rate of change of free energy is equal to the rate of increase of free energy of the salt when transported from the diluate to the concentrate minus the rate of change of free energy associated with water transport from the diluate to the concentrated stream. The rate of work input is simply the product of the current density times the cell pair voltage. The membrane productivity is the net change in free energy per unit of membrane area, i.e. the numerator of the efficiency. The contribution of each system, i, to the levelised cost of water is calculated by combining the amortised capital costs of the system with the cost of energy, Eq. 19.

Table 5.3 Cost Modelling Parameters

Symbol	Value
R	10%
T	20 years
CF	0.9
K_C	\$1000/m^{25}
K_E	\$0.15/kWh
S_c^A	143 ppt
S_d^A	95 ppt
S_d^B	85 ppt
S_d^B	53 ppt

$$LWC_i \left[\frac{2}{m^3 \text{ product}}\right] = \frac{r}{1-\left(\frac{1}{1+r}\right)^T} + \frac{w_i^{rev}}{\eta_i} \frac{K_E}{3.6 \times 10^6 \frac{\text{kWh}}{\text{J}}} \tag{5.18}$$

where r is the return on capital invested, T is the system life in years, CF is the capacity factor and w^{rev}, in J/m^3, is defined as the reversible work done in system i per unit of product produced by the entire hybrid system. w^{rev} is calculated considering the mass flow rates and concentrations of streams entering and exiting units A and B. This must be done via an iterative process specifying the current density in Systems A and B to estimate w^{rev} and then updating the current density based on cost considerations. Choosing representative values for the concentrate and diluate concentrations in ED systems A and B, Eq. 17, Eq. 18 and consequently Eq. 19 become functions of the current density, thus allowing us to perform single variable optimization.

5.5 Results

In this section, the effect of current density upon the levelised cost of water, the efficiency and the membrane productivity of the hybrid system is presented. Table 3 provides the range of input values required for Eq. 19, allowing these values to be computed.

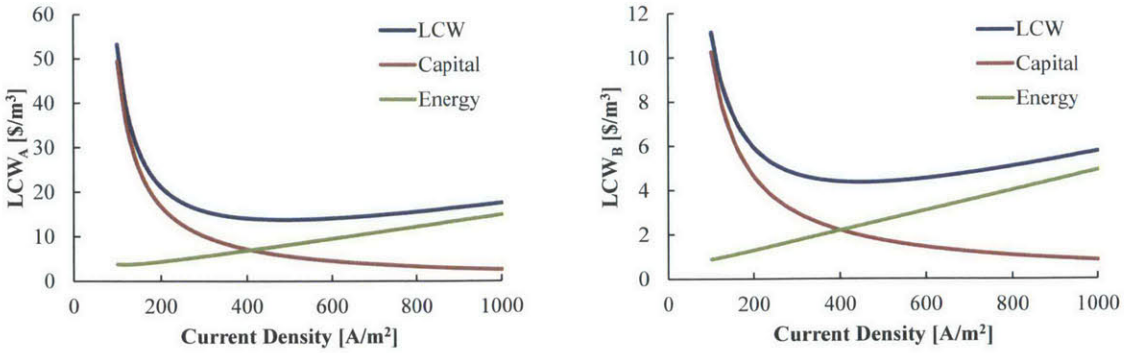

(a) ED System A

(b) ED System B

Figure 5-4 Impact of current density upon the levelised cost of water

The return on capital should be selected in accordance with similar electrodialysis projects, of which there are few, if any, for high salinity hybrid ED-RO desalination. A moderate value of 10% is selected[c]. A moderate to high cost of electricity is selected to reflect poor grid connectivity if operated in remote locations. The capital cost per unit of cell pair area is approximated by quotations obtained by Oren et al.[5]. The mean concentrate and diluate salinities in ED systems A and B are computed via iteration over the current density between the hybrid system model and the cost model. Considering Eq. 19, increases in the return on capital or the capital cost per unit area would drive systems to higher optimal current densities, while increases in system lifetime, capacity factor and cost of energy would do the opposite.

Figs. 4A and 4B illustrate how the contribution of ED system A to the levelised cost of water (from the overall hybrid system) depends upon the current density. Of course, the total system cost should include the costs of systems A, B and the RO system. Figs. 5A and 5B illustrate the dependence of efficiency and membrane productivity upon current density. For both systems A and B, the LCW is minimised at a current density of approximately 500 A/m^2. Capital costs are high at low current density due to low membrane productivity little change in free energy of the streams is achieved per unit of membrane area. Conversely, at high current density the costs

[c]More rigorously, according to a capital asset pricing model, the rate of return should be consistent with the covariance of the projects cash flows with the returns of the overall financial markets. As a benchmark, as of 31st Jan 2013 3-year annualized returns on the S&P500 index were 14.14%[21]

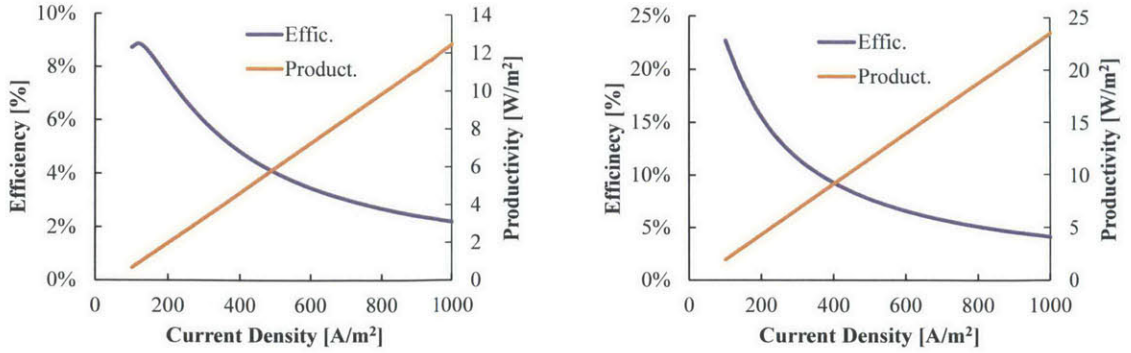

(a) ED System A **(b)** ED System B

Figure 5-5 Impact of current density upon efficiency and membrane productivity

of energy dominate as efficiency decreases, due almost solely to the increased ohmic losses. The effects of efficiency and membrane productivity are easily visualised in Fig. 5.

In Fig. 5A, it is seen that at low current there is a value of current density that maximises efficiency (though not the LCW). This optimum is explained by a balance of losses due to osmosis and ohmic resistance. At very low current density (below 100 A/m^2 in Fig. 5A), water transport via osmosis occurs rapidly relative to salt transport. By increasing the current density the relative effect of osmosis weakens. However, there is a competing trend whereby ohmic losses increase with current density hence the presence of an optimum[d].

Comparing Fig. 5A and Fig. 5B, it is noticeable that for the same current density the efficiency of system B is higher. This is explained by the lower average stream-to-stream concentration difference in unit B compared to unit A. In unit B, the effect of water transport via osmosis is less than in unit A. As a consequence, higher efficiencies are achievable in unit B and also the current density that maximises efficiency is smaller (and therefore not visible in Fig. 5B) than in unit A.

Of further interest is the fact that the current density maximising the LCW of

[d]Though efficiency exhibits an optimum, membrane productivity is monotonic in current density in this model as there is no competing factor reducing productivity at higher current density. Concentration polarization would constitute such a competing factor and its effect would be seen at high current densities, see Fig. 2.

Table 5.4 Optimised system performance

Symbol	Value
$\dot{V}_p$	100 m^3/day
RR_{RO}	50%
RR_{RO+EDB}	29.5%
$RR_{hyb-sys}$	29%
S_f	120 ppt
S_c	167 ppt
S_p	0 ppt

Table 5.5 Optimised system membrane areas and power consumption

	ED A	ED B	RO
Membrane Area [e] [m^2]	240	100	90
Power Consumption [kWh/m^3]	43	21	6.1
LCW	\$13/m^3	\$4.3/m^3	

units A and B is far above the current density maximising efficiency. Only with significant decreases in capital costs per unit membrane area, or significant increases in membrane properties such as conductivity (or decreases in water permeability) would the current density that maximises the LCW be driven towards the current density that maximises efficiency. This is in contrast to RO, which operates at a higher efficiency, indicating that the combination of capital costs per unit membrane area and membrane properties is superior to that in ED.

In the optimized embodiment of the hybrid system, current densities are selected for systems A and B that minimize the contributions of those systems to the levelised cost of water. Tables 4 and 5 summarise key system characteristics. Of note is the finding that ED system A exhibits higher energy consumption and requires higher membrane area than ED system B. This is attributable to two factors. The reversible work done by system A is greater than that of B (on the basis of unit RO permeate production). This is due to the larger range of salinity covered by A compared with B. Secondly, the greater stream-to-stream concentration difference within A compared to B results in lower Second Law efficiency, due to a greater rate of water transport via osmosis. The power consumption of the RO unit, though lower than the ED systems is high by SWRO standards, due to the absence of pressure recovery. Finally, the

recovery ratio of the overall system is low, at 23%. It is possible to increase recoveries within system A by altering the relative mass flow rates of the unit. However, an increase in the stream-to-stream salinity difference would further decrease energy efficiency, membrane productivity and hence increase the LCW.

5.6 Conclusions

A hybrid arrangement of counterflow ED systems with reverse osmosis is presented. The premise of such an arrangement is to exploit ED for its ability to reach high osmotic pressures and exploit RO at low salinities where ohmic resistances are large in ED. The following specific conclusions are drawn:

- Contrary to brackish ED systems, membrane resistances dominate diluate and concentrate resistances in high salinity ED desalination.
- The dominant factors influencing process efficiency and productivity are ohmic losses within membranes and losses of free energy due to water transport, each being relative to changes in free energy achieved in transporting salt from the diluate to the concentrated stream.
- At low current density capital costs dominate the LCW while energy costs dominate at high current density. The current density that minimises LCW is significantly greater than the current density that maximises efficiency, indicating the high current capital cost of ED per unit membrane area and poor membrane transport properties relative to RO.
- The efficiency of operation of an ED system depends significantly upon the stream-to-stream concentration with high values thereof increasing water transport via osmosis, decreasing efficiency and increasing the LCW. Consequently, the performance of ED systems achieving higher recoveries is significantly compromised.

In addition, the following areas meriting further analysis are exposed by the current work:

- The present analysis indicates that concentration polarization is not a significant factor given the low value of current densities minimising LCW. Consequently, larger membrane spacings appear achievable than in brackish water desalination, thus allowing significant reductions in the required pumping power. However, beyond the scope of the present contributions, an optimisation of ED pump systems is required to understand the trade-off between pumping power and concentration polarisation.

- There are few, if any, examples of counterflow ED systems for desalination at high salinity. Such a design allows the distinct advantage of maintaining a constant stream-to-stream concentration difference within stacks, thus maintaining a more constant current density and also rate of water transport. However, design issues such as the presence of trans-membrane pressures and leaking must be analysed carefully.

Bibliography

[1] Analysis, 2012. desaldata.com

[2] Waters growing role in oil and gas, 2011. Global Water Intelligence. URL: http://www.globalwaterintel.com/archive/12/3/market-profile/waters-growing-role-oil-and-gas.html

[3] The desal revolution in a box, 2012. Global Water Intelligence. URL: http://www.globalwaterintel.com/archive/13/3/market-profile/desal-revolution-box.html

[4] Korngold, E., L. Aronov, and N. Daltrophe. "Electrodialysis of brine solutions discharged from an RO plant." Desalination 242.1 (2009): 215-227.

[5] Oren, Y., Korngold, E., Daltrophe, N., Messalem, R., Volkman, Y., Aronov, L., Weismanna, M., Bouriakova, N., Glueckstern, P. & Gilron, J. "Pilot studies on high recovery BWRO-EDR for near zero liquid discharge approach." Desalination 261.3 (2010): 321-330.

[6] Thampy, S., Desale, G. R., Shahi, V. K., Makwana, B. S., & Ghosh, P. K. "Development of hybrid electrodialysis-reverse osmosis domestic desalination unit for high recovery of product water." Desalination 282 (2011): 104-108.

[7] Casas, S., Bonet, N., Aladjem, C., Cortina, J. L., Larrotcha, E., & Cremades, L. V. Modeling Sodium Chloride Concentration from Seawater Reverse Osmosis Brine by Electrodialysis: Preliminary Results. Solvent Extraction and Ion Exchange 29.3 (2011): 488-508.

[8] Kwak, R.; Guan, G.; Peng, W. & Han, J. Microscale electrodialysis: Concentration profiling and vortex visualization, Desalination 308 (2012): 138-146.

[9] Bazant, M.; Kilic, M.; Storey, B. & Ajdari, A., Towards an understanding of induced-charge electrokinetics at large applied voltages in concentrated solutions, Advances in colloid and interface science. 152.1 (2009): 48–88.

[10] Nikonenko, V., Yaroslavtsev, A. B. and Pourcelly, P. Structure, Properties and Theory. Ion transfer in and through charged membranes (2011).

[11] Robinson, R. A. and Stokes, R. H., 2002. Electrolyte solutions. Second Revised Edition. Mineola, NY: Dover Publications.

[12] Kestin, J.; Khalifa, H. & Correia, R. Tables of the dynamic and kinematic viscosity of aqueous NaCl solutions in the temperature range 20-150 C and the pressure range 0.1-35 MPa, (1981): American Chemical Society and the American Institute of Physics for the National Bureau of Standards.

[13] Fidaleo, M. & Moresi, M., Optimal strategy to model the electrodialytic recovery of a strong electrolyte, Journal of membrane science 260.1, (2005): 90–111.

[14] Prentice, G. Electrochemical engineering principles, 1991. Vol. 1. Englewood Cliffs, New Jersey: Prentice Hall.

[15] Berezina, N.; Gnusin, N.; Dyomina, O. & Timofeyev, S., Water electrotransport in membrane systems. Experiment and model description, Journal of membrane science 86.3, (1994): 207–229.

[16] Helfferich, F., 1995. Ion exchange. New York: Dover Publications Inc.

[17] Neosepta. ASTOM Corporation. URL: http://www.astom-corp.jp/en/en-main2-neosepta.html, [accessed 2013.15.02].

[18] Fidaleo, Marcello, and Mauro Moresi. Electrodialytic desalting of model concentrated NaCl brines as such or enriched with a non-electrolyte osmotic component. Journal of Membrane Science 367.1 (2011): 220-232.

[19] Wilf, Mark, and Leon Awerbuch. The guidebook to membrane desalination technology. L'Aquila, Italy: Balaban Desalination Publications, (2007).

[20] Busey, R. H. Thermodynamic Properties of Aqueous-Sodium Chloride Solutions. J. Phys. Chem. Ref. Data 13.1 (1984).

[21] Standard and Poor. S&P 500 Performance Data. URL: http://www.standardandpoors.com/indices/sp-500/en/us/?indexId=spusa-500-usduf–p-us-l– [accessed 2013.02.19]

Chapter 6

On the cost of electrodialysis for the desalination of high salinity feeds

Abstract

We propose the use of electrodialysis to desalinate produced waters from shale formations in order to facilitate water reuse in subsequent hydraulic fracturing processes. We focus on establishing the energy and equipment size required for the desalination of feed waters containing total dissolved solids of up to 192,000 ppm, and we do this by experimentally replicating the performance of a 10-stage electrodialysis system. We find that energy requirements are lower than current vapour compression desalination processes, and we project water costs to be similar or even lower than vapour compression. We also find that the cost per unit salt removed is significantly lower when removed from a high salinity stream as opposed to a low salinity stream, pointing towards the potential of ED to operate as a partial desalination process for high salinity waters. We then develop a numerical model for the system, validate it against experimental results and use this model to minimise salt removal costs by optimising the stack voltage. We find that the higher the salinity of the water from which salt is removed the smaller should be the ratio of the electrical current to its limiting value. We conclude, on the basis of energy and equipment costs, that electrodialysis processes show promise for the desalination of high salinity waters and merit further investigation under field conditions.

Contributions

This chapter was co-authored by Prof. Syed Zubair and Prof. John Lienhard V. The work received financial support from the US Department of State via the Fulbright Science and Technology Program, the Hugh Hampton Young Memorial Fund Fellowship, the International Desalination Association's Channabasappa Memorial Scholarship, the MIT Martin Fellowship for Sustainability and the King Fahd University of Petroleum and Minerals through the Center for Clean Water and Clean Energy at MIT and KFUPM under project number R15-CW-11.

6.1 Introduction

We have experimentally investigated factors affecting the cost of electrodialysis (ED) for the desalination of high salinity feeds, focusing on the dependence of the cost of salt removal upon diluate salinity. We have also developed a numerical model for the system, validated it against the experimental results and identified a strategy to optimise the stack voltage such that the sum of equipment and energy costs are minimised. Our motivation for this investigation was the desalination of produced waters in unconventional oil and gas extraction where, amongst other factors, the presence of high levels of total dissolved solids can disincentivise water reuse. Water reuse in hydraulic fracturing is of great interest both from an environmental perspective, as it reduces water use and minimises disposal through deep-well injection, but also from an economic perspective as water management costs can account for between 5 and 15% of drilling costs[1].

For the purpose of this investigation, we were most interested in flows of water during the life-cycle of a well, which are depicted in Fig. 6-1. For reuse to be economical, the savings in the sourcing, disposal and transport of water must outweigh any increased costs of treatment or of chemicals in the formulation of the fracturing fluid. This means that regional differences in recycling rates are strongly influenced by regional differences in sourcing, disposal and transport costs. For example, reuse rates are currently greatest in the Marcellus shales[3] (reused water makes up 10-15% of water needed to fracture a well) where transport and disposal costs can reach \$15-18/bbl (\$94-113/m^3)[4]. The initial rate at which produced water flows to the surface (e.g. within the first 10 days) also influences the viability of reuse as low initial produced water volume flow rates making the logistics of reuse more difficult[3,5].

Moving to the costs of reuse, and setting aside the expense associated with logistics, the costs come primarily in the form of: increased water treatment costs; increased chemical costs in the formulation of the hydraulic fracturing fluid to mitigate undesirable feed water properties; and/or reduced oil or gas production from the well. By and large, the increase in treatment costs is highest, and the increase

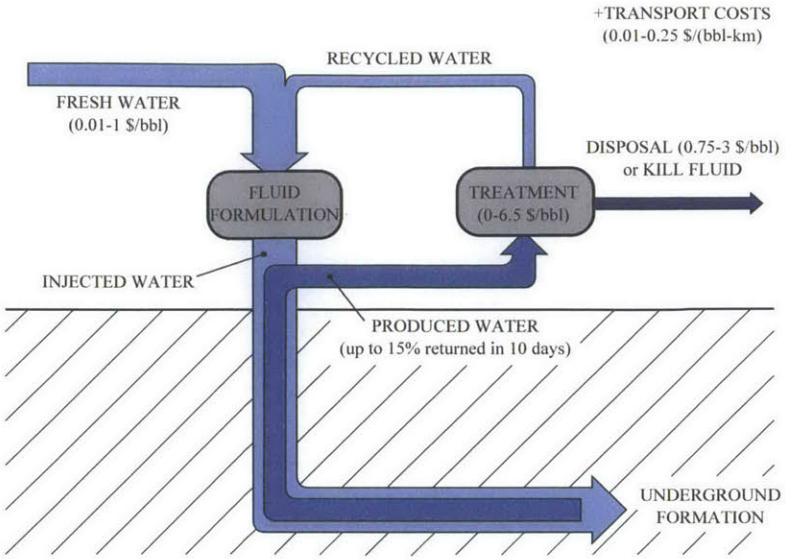

Figure 6-1 Fresh water[1] is mixed with recycled water and chemicals are added, that may include acids, friction reducers, gelling agents and proppant (sand)[2] to form the hydraulic fracturing fluid. The fluid is then injected into the well at high pressure to create fractures in the underlying shale formation. A portion of this fluid[3], perhaps in addition to fluid originally contained in the formations, subsequently returns to the surface, at a rate that generally decreases with time, and is known as produced water. The produced water may be: subjected to levels of treatment that vary from suspended solids removal to complete desalination[1] and recycling; sent to a disposal well; and/or employed elsewhere as a kill fluid (a fluid used to close off a well after production is complete) or as a salt based drilling fluid[1].

in chemical costs lowest, when produced water is treated with mechanical vapour compression. This comes at a cost of circa 3.50-6.25 $/bbl ($22-39/m^3) of distillate[1] but provides a high purity feed for the formulation of the hydraulic fracturing fluid. By contrast, direct reuse, whereby produced water is directly blended with freshwater before formulation of the fracturing fluid, results, by and large, in the lowest treatment costs but greater chemical costs for fluid formulation and perhaps a decline in the well's production. Increased costs associated with reuse, depending on the degree of treatment employed, can come in the form of: increased friction reducer and scale inhibitor demand with high chloride contents; increased scaling within the shale formation with the presence of divalent ions; increased corrosion of pipes; increased sulphate reducing bacteria resulting in the production of H_2S gas[6]; and a reduction in the performance of coagulation/flocculation, flotation, gravity settling and plate

and frame dewatering equipment due to residual unbroken polymer gel[7].

Many of the challenges faced in reuse can be dealt with through primary treatment that removes suspended solids, oil, iron, unbroken polymers and bacteria[7], generally at a cost much below complete desalination (circa \$1/bbl (\$6.3/m^3) compared to \$3.50-6.25/bbl (\$22-39/m^3) for complete desalination[1]). The need for the removal of all solids, suspended and dissolved, is less clear. Opinions vary as to the level of total dissolved solids (TDS) that can be tolerated[8] and a complete understanding of issues of chemical compatibility remains elusive[2]. There is evidence that, with improved chemical formulations, high salinity produced waters may be reused without desalination, particularly in the formulation of fluids for slickwater processes[9–14] (involving high volume flow rates to avoid the settling of sand, which serves to maintain fractures propped open) and to some extent for cross-linked gel fracturing processes[15] (lower volume flow rate processes employing low molecular weight guar gum based gels to ensure proppant remains suspended). However, the increase in chemical costs associated with such formulations not evident. Depending on the fracturing fluid desired, chemical use can be significant. Fedotov et al.[7] indicated that the use of drag reducing agents in slickwater fracturing processes, can reach approximately 1,000 ppm (2 lbs per 1,000 gallons), while for cross-linked gel fracturing processes chemical use can be much higher and reach 15,000 ppm (30 lbs/1,000 gallons).

In place of a distillation process, we propose the use of electrodialysis desalination to partially desalt produced water. The objective is to achieve a configuration that can reduce water treatment costs relative to distillation, by avoiding complete desalination, but can provide the benefit of reduced total dissolved solids relative to a direct reuse configuration. At present, a clear illustration of the dependence of ED salt removal costs on feed salinity is not present in literature, particularly for feed salinities above brackish. Lee et al.[16] consider the effect of feed salinity upon the cost of water from a continuous, as opposed to batch, electrodialysis system for brackish feed waters. Few studies exist that do the same for higher salinity feeds[17]. Batch studies of low salinity produced waters report energy consumption figures of 1.1 kWh/m^3 for 90% TDS removal and 0.36 kWh/m^3 for 50% TDS removal from a

3,000 ppm TDS stream[18]. A study at higher feed water salinity reports energy consumption of 12.4 kWh/m^3 for 80,000 ppm TDS[19]. A number of experimental studies, with desalination occurring in a batch mode, report the process times required to achieve a final target purity as increasing with the feed salinity[20,21] but leave unclear how process times translate into equipment costs. Furthermore, energy consumption in batch processes is often reported as an average kWh/kg salt removed for an entire process without focusing on how this value varies depending upon the diluate, and to a lesser extent the concentrate, salinity.

In this work, we conduct multiple stages of batch desalination on an experimental electrodialysis setup such that each stage replicates closely a stage within a continuous process. Furthermore, we relate batch process times and energy consumptions to the production rate and specific energy consumption that would be achieved from an equivalent continuous system. Coupled with a simple financial model, these metrics allow us to investigate and optimise the dependence of cost upon the feed salinity to a continuous electrodialysis system.

6.2 Methods

6.2.1 Experimental

We performed an experiment to replicate the performance of a ten stage continuous flow electrodialysis system capable of desalinating a feed stream from 224 mS/cm (195,000 ppm TDS NaCl) down to 0.5 mS/cm (240 ppm TDS NaCl). To do this, we ran ten batch experiments, each representing a single stage in a continuous process. We chose the diluate conductivities at the start of each stage such that the diluate conductivity was halved in each stage and the salt removal was approximately 50% per stage[16] (see Fig. 6-2). We chose the concentrate concentration in each stage to replicate the concentration that would prevail if the concentrate salinity were to be determined solely by the rates of salt and water transport across the membranes (see 6.A.1). We held the stack voltage constant at 8 V in all stages and chose this

value such that the current density at the end of the final stage would be 50% of its limiting value (see 6.A.2).

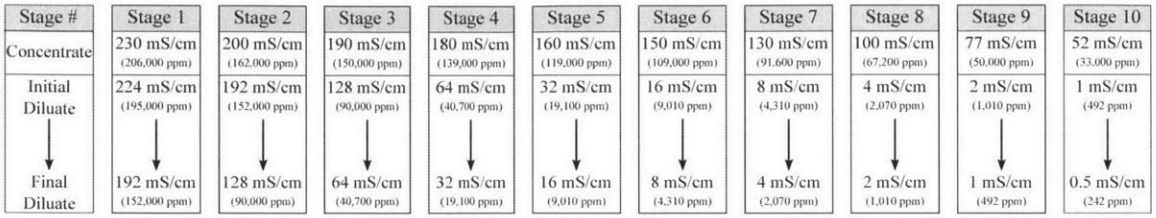

Figure 6-2 We designed each of the ten stages such that the diluate conductivity was halved in each successive stage, with the exception of the first two stages. We reduced the salt removal in the first two stages to avoid the depletion of water in the diluate beaker before the end of a trial. We chose concentrate conductivities based on the rates of salt and water transport across the membranes (see 6.A.1).

The experimental apparatus, illustrated in Fig. 6-3 involved an ED200 stack[22] with 17 cell pairs consisting of seventeen Neosepta AMS-SB, eighteen CMS-SB membranes, thirty-four 0.5 mm spacers and two 1 mm end spacers. We employed a GW Instek GPR-60600 and an Extech 382275 power supply to provide current in the ranges of 0-5 A and 5-20 amps respectively. We measured conductivity on a Jenco 3250 conductivity meter interfacing with model 106L (cell constant, K=1) and model 107N (cell constant, K=10) probes. We performed experiments in constant voltage mode, with current measured by an Extech EX542 multimeter. We determined initial diluate and concentrate volumes by summing initial fluid volumes contained within the beakers (diluate and concentrate beaker volumes of 1 litre and 3 litres for all tests) and determined internal diluate and concentrate circuit volumes by a conductivity-based method, see 6.A.3. We determined changes in diluate mass by tracking the conductivity and the mass of the diluate within the beaker with time and measured the diluat mass using an Ohaus Scout Pro balance with a range of 0-2 kg.

To quantify performance we considered certain key performance metrics. The first metrics are specific process times, based on stage salt removal, τ_i^s, and final

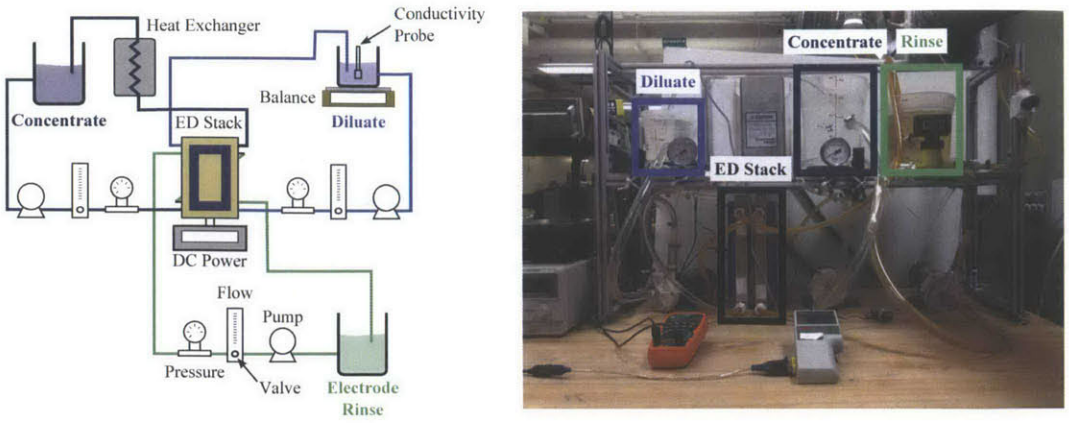

Figure 6-3 The electrodialysis setup consisted of a diluate, concentrate, and rinse circuit feeding an ED200 stack. We employed a heat exchanger to regulate the temperature of the concentrate, with the stack effectively operating as a second heat exchanger to regulate the diluate temperature. We employed valved-rotameters to regulate the flow rates in each circuit.

stage diluate volume, τ_i^w:

$$\tau_i^s = \frac{t_i}{\left(V_i^{in,d} C_i^{in,d} - V_i^{f,d} C_i^{f,d}\right)} \tag{6.1}$$

$$\tau_i^w = \frac{t_i}{V_i^{f,d}} \tag{6.2}$$

where t_i is the process time for stage i, $V_i^{in,d}$ and $V_i^{f,d}$ are the initial and final stage volumes, and $C_i^{in,d}$ and $C_i^{f,d}$ are the initial and final stage concentrations. The second metrics are specific energy consumption, based on stage salt removal, E_i^s, and final stage diluate volume, E_i^w:

$$E_i^s = \frac{\sum_j I_{i,j} V_{i,j} \Delta t_{i,j}}{\left(V_i^{in,d} C_i^{in,d} - V_i^{f,d} C_i^{f,d}\right)} \tag{6.3}$$

$$E_i^w = \frac{\sum_j I_{i,j} V_{i,j} \Delta t_{i,j}}{V_i^{f,d}} \tag{6.4}$$

where $I_{i,j}$ and $V_{i,j}$ are the stack current and voltage of stage i in time period j of the process. $\Delta t_{i,j}$ refers to time increment j of the process within stage i.

We used the above performance metrics to compute cost metrics, employing the following simplifying assumptions:

1. We set aside pre-treatment, post-treatment, maintenance and replacement costs, focusing solely on the energy cost and upfront cost of electrodialysis equipment.

2. We neglect pumping power costs (see 6.B for justification).

3. We assumed electricity to be priced at K_E = \$0.15/kWh (a conservative estimate of gas powered distributed generation[23]).

4. We assumed equipment costs to scale with membrane area and computed these costs by considering an equipment cost per unit membrane area of K_Q = 150 \$/m^2 [16,24].

5. We assumed the total installed cost of the equipment to equal three times the estimated equipment costs[25].

6. We amortised equipment costs over a twenty-year life, $T = 20$ years, assuming an annualised cost of capital of $r = 10\%$.

Given these assumptions, we defined the specific cost of salt removal, in \$/lb salt (or \$/kg salt) and the specific cost of product water \$/bbl (or \$/m^3) from each stage:

$$\Xi_i^s = K_E E_i^s + \frac{K_Q A_m}{\frac{1}{r}\left[1 - \left(\frac{1}{1+r}\right)^T\right]} \tau_i^s \tag{6.5}$$

$$\Xi_i^w = K_E E_i^w + \frac{K_Q A_m}{\frac{1}{r}\left[1 - \left(\frac{1}{1+r}\right)^T\right]} \tau_i^w \tag{6.6}$$

where A_m is the total membrane area in the stack.

6.2.2 Model

To minimise the cost of salt removal, through optimisation of the stack voltage, we constructed a semi-empirical model for the electrodialysis system, which we validated with experimental results. The process time, energy consumption, and cost of salt removal from each stage were computed using a numerical model that broke each stage into twenty time periods, with an equal change in diluate salinity in each period.

During each of these periods the stack voltage and rates of salt and water transport were approximated as constant and used, in conjunction with molar conservation equations, to determine the conditions at the start of the next period. Within each stage, the number of moles of salt and water present in the diluate at the start and the end of each time step j are related to the molar fluxes of salt and water, $J_{s,j}$ and $J_{w,j}$ and the total cell pair area, A_m:

$$N_{s,j+1} - N_{s,j} = -A_m J_{s,j} \tag{6.7}$$

$$N_{w,j+1} - N_{w,j} = -A_m J_{w,j} \tag{6.8}$$

with N_{j+1} and N_j the number of moles of salt, s, or water, w, at the end or start of each time step, A_m the total cell pair area of the stack and J_j the average flux across the membrane area, s, or water, w, at time step j. The concentrate conductivity was approximated as constant in time for each stage and equal to the value employed in experiments. At each instant in time the diluate concentration is approximated as uniform across the membrane area. This is because the time taken for fluid to travel the length of the membrane (¡8 s) is much less than the stage processing time (¿120 s for all stages).

Salt, water, and charge transport were modelled based upon the approach taken in previous work[26,27]. Salt transport was modelled by a combination of migration and diffusion:

$$J_s = N_{cp}\left[\frac{T_s^{cp} i}{F} - L_s\left(C_{s,c,m} - C_{s,d,m}\right)\right] \tag{6.9}$$

and water transport by a combination of migration (electro-osmosis) and osmosis:

$$J_w = N_{cp}\left[\frac{T_w^{cp} i}{F} - L_w\left(\pi_{s,c,m} - \pi_{s,d,m}\right)\right]. \tag{6.10}$$

In Eq. (6.10), N_{cp} is the number of cell pairs, T_s^{cp} and T_w^{cp} are the overall salt and water transport numbers for the cell pair, L_s and L_w are the overall salt and water permeabilities of the cell pair, C denotes concentration in moles per unit volume, and

π denotes osmotic pressure (calculated employing osmotic coefficients for aqueous NaCl from Robinson and Stokes[28]). The difference between membrane surface concentrations, $C_{s,c,m}$ and $C_{s,d,m}$, and bulk concentrations, $C_{s,c}$ and $C_{s,d}$, was computed via a convection-diffusion based model for concentration polarisation (see 6.C.1).

The stack voltage was represented as the sum of ohmic terms and membrane potentials:

$$V_{stack} = N_{cp}\left(\bar{r}_{am} + \bar{r}_{cm} + \frac{h_d}{\sigma\Lambda_d C_d} + \frac{h_c}{\sigma\Lambda_c C_c}\right) i$$
$$+\bar{r}_{cm} i + \frac{2h_r}{\sigma k_r} i + N_{cp}\left(E_{am} + E_{cm}\right) + V_{el} \qquad (6.11)$$

where Λ is the molar conductivity, itself taken to be a function of concentration[29,30] and h denotes channel height. k denotes electrical conductivity, the subscript r denotes the rinse solution, σ denotes the spacer shadow factor, $\bar{r}$ denotes the membrane surface resistance of the anion or cation exchange membrane and V_{el} denotes the sum of the anode and cathode electrode potentials. Junction potentials associated with concentration differences across boundary layers were neglected while membrane potentials E_{am} and E_{cm} were computed assuming quasi-equilibrium salt and water migration through the membranes (see 6.C.2).

A series of calibration tests was conducted to establish the values of T_s^{cp}, T_w^{cp}, L_s, L_w, r_m, σ, V_el and the Sherwood number Sh (see 6.D). Each test was repeated three times to ensure repeatability. Bias errors arising from the determination of the diluate circuit volume (6.A.3) and of leakage rates from diluate to concentrate were propagated through the equations defining these nine parameters and combined with the random error [Eq. (6.12)] that was determined from the sample standard deviation of results computed from the three tests. Errors are computed at a 68% confidence level.

$$\epsilon_{tot}^2 = \epsilon_{bias}^2 + \epsilon_{random}^2 \qquad (6.12)$$

Salt and water transport numbers, T_s^{cp} and T_w^{cp}, were determined via constant current

migration tests where the diluate and concentrate conductivities were close to one another. Salt and water permeabilities, L_s and L_w, were determined via diffusion tests with zero current and initial diluate concentrations close to zero. Membrane resistance, r_m, the spacer shadow factor, σ, the electrode potential, V_{el}, and the Sherwood number, Sh, were determined from voltage-current tests at constant diluate and concentrate salinity.

6.3 Results: Process time, energy consumption and costs

The process time, energy and cost requirements of electrodialysis treatment are shown on a unit salt removal basis in Figs. 6-4, 6-5 and 6-6 and on a unit product water basis in Figs. 6-7, 6-8 and 6-9, in each case illustrating agreement, within error, between the model and the experiment. The deviation between the model and experiment is greatest in the final stages, where the modelled values of energy consumption and process time are highly sensitive to the electrode potential. This is because the driving force for salt transport is the difference between the stack voltage and the sum of the electrode potentials and membrane potentials ($V^{stack} - N_{cp}\left(E_{am} + E_{cm}\right) - V_{el}$). The sum of membrane potentials, $E_{am} + E_{cm}$, scales with the natural logarithm of the salinity ratio (concentrate to diluate)[27] and therefore, in the final stage where the diluate salinity is lowest, the sum of the membrane potentials is greatest — accounting for over 50% of the 8 V applied across the stack. This remaining voltage driving salt transport is therefore highly sensitive to the modelled value of the electrode potential (V_{el}=2.13±0.3 V). This sensitivity further posed a difficulty in modelling desalination, within the final stage, down to 0.5 mS/cm (242 ppm TDS). The modelled value of the electrode potential (in combination with the modelled values of other fitted parameters, see 6.D) was such that the back diffusion of salt outweighed salt removal via migration before a conductivity of 0.5 mS/cm was reached. For this reason, the model of the final stage is for an final diluate conductivity of 0.55 mS/cm rather than

0.5 mS/cm.

The trends in process time, energy and cost are most easily explained by considering these quantities on the basis of salt removal. Here we provide scaling estimates that describe the first order variation in process time, energy and cost with stage number. The process time τ for any given stage scales with the change in salinity in that stage ΔS and the inverse of the current I, which describes the number of moles of salt removed per coulomb of charge:

$$\tau \sim \frac{\Delta S}{I} \tag{6.13}$$

Meanwhile, the current scales approximately with the quotient of the stack voltage over the stack resistance:

$$I \sim \frac{V_{st}}{R_{st}}. \tag{6.14}$$

The stack resistance scales with the sum of the membrane, concentrate and diluate resistances:

$$R_{st} \sim \left(2r_m + \frac{h}{\sigma k_c} + \frac{h}{\sigma k_d}\right) \tag{6.15}$$

where σ is the spacer shadow factor, h is the diluate and concentrate channel height, k is the solution conductivity of the diluate d or the concentrate c, and r_m is the anion or cation exchange membrane surface resistance. The process time therefore scales approximately as:

$$\tau \sim \frac{\Delta S}{V}\left(2r_m + \frac{h}{\sigma k_c} + \frac{h}{\sigma k_d}\right). \tag{6.16}$$

At high diluate conductivity (lower number stages in Fig. 6-2) the membrane resistance dominates the stack resistance and thus the diluate and concentrate conductivities have a weak effect on process time. At low diluate conductivity (high number stages) the diluate resistance dominates the stack resistance and the process time per

unit salt removed scales roughly with the inverse of the diluate conductivity. The stack resistance roughly doubles in moving from one stage to the next and so too does the specific process time.

The energy consumption per unit salt removed, E^s, for any given stage scales with the product of voltage, the current and the process time divided by the change in salinity:

$$E^s \sim \frac{VI\tau^s}{\Delta S}. \tag{6.17}$$

Considering how process time scales in Eq. (6.13) it is clear that the energy consumption per unit salt removed scales with the quotient of the voltage over the salt transport number:

$$E^s \sim V. \tag{6.18}$$

Thus, while process time varies significantly with stage number (note the $\log_2$ scale in Fig. 6-4) specific energy consumption (plotted on a linear scale in Fig. 6-5) remains relatively constant.

Given the above explanations for the trends in process time and energy, on the basis of unit salt removal, it is clear that the cost per unit of salt removal must remain relatively constant at low stage numbers (high diluate salinities) but will rise rapidly due to increasing equipment costs at higher number stages (lower salinities) as seen in Fig. 6-6.

Combining these insights on Fig. 6-4, 6-5 and 6-6 with the fact that salt removal is approximately halved in each stage moving from stage 3 to stage 10 we can easily explain the trends on a basis of stage product water, seen in Fig. 6-4, 6-5 and 6-6. Specific process time on the basis of water produced falls with an increasing stage number because the processing time per unit of salt removed (Fig. 6-4) rises more slowly than the quantity of salt removed per stage (see Fig. 6-2). Specific energy consumption, on the basis of product water, falls because energy consumption per unit of salt removed is approximately constant(see Fig. 6-4) and the quantity of salt

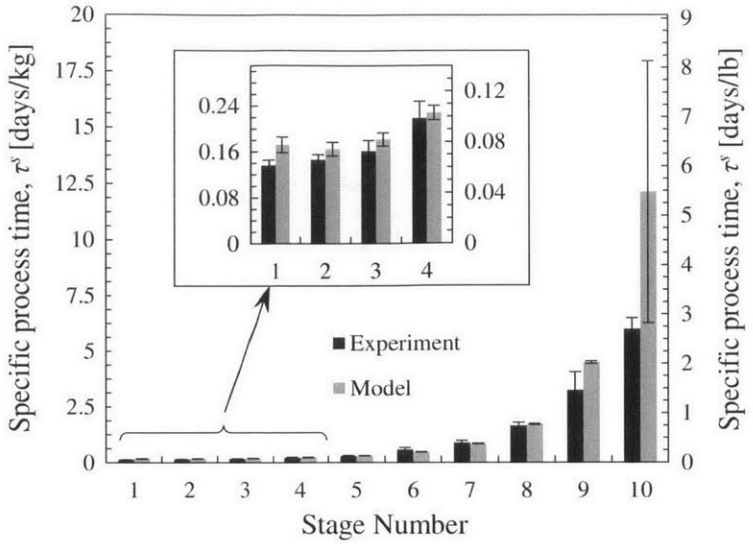

Figure 6-4 Stage process time per unit of salt removed.

removed per stage falls rapidly (see Fig. 6-2). As a consequence of falling τ^w and E^w with increasing stage number, the specific cost of water also falls in moving to higher stage numbers, primarily because the quantity of salt removed per stage is falling rapidly.

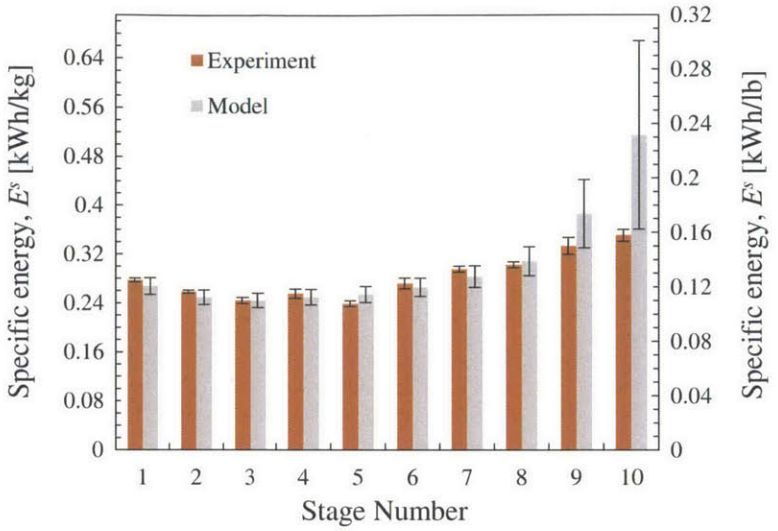

Figure 6-5 Stage energy consumption per unit of salt removed.

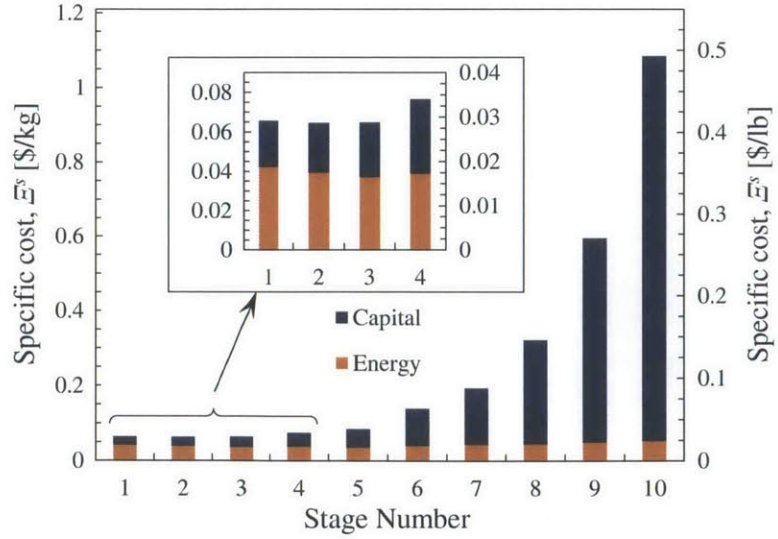

Figure 6-6 Stage cost per unit of salt removed (based on experimental results).

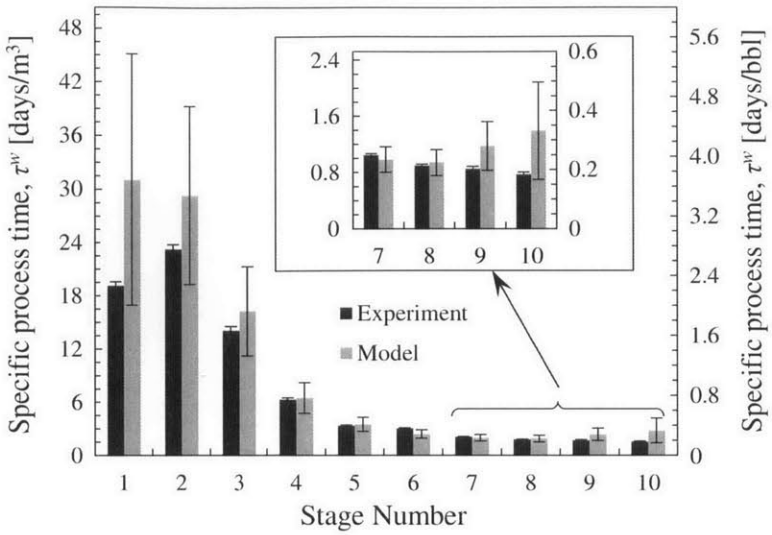

Figure 6-7 Stage process time per unit of product water.

6.3.1 Discussion

The specific energy requirements and specific costs on a unit water basis (Fig. 6-5 and 6-9) suggest that ED may achieve significant changes in salinity with lower energy consumption and lower cost than evaporative systems. Considering electrodialysis costs on the basis of salt removal (Fig. 6-6), it is interesting that costs fall significantly at higher salinity (*e.g.* in lower number stages). This points to the potential of electrodialysis for the partial desalination of high salinity feed streams.

Not included in the computation of energy in Fig. 6-5 or Fig. 6-8 is energy required for pumping, shown in Fig. 6-10. These values for pumping power are computed via experimental measurements of the pressure drop across the stack and assuming 100% pump efficiency (see 6.B for detailed calculations). Comparing these values to those for stack energy consumption in Fig. 6-8, it is clear that pumping power accounts for a significant portion of total power consumption only at low diluate salinity (e.g. stages 10, 9 and 8 where salt removal rates are lowest). Importantly, these values of pumping power for a laboratory scale system are unlikely to be representative of pumping power consumption in a large scale system. This is because the processing length of the system investigated is only 20 cm, meaning that entrance and exit head loss has a disproportionately large effect on the pumping power relative to frictional

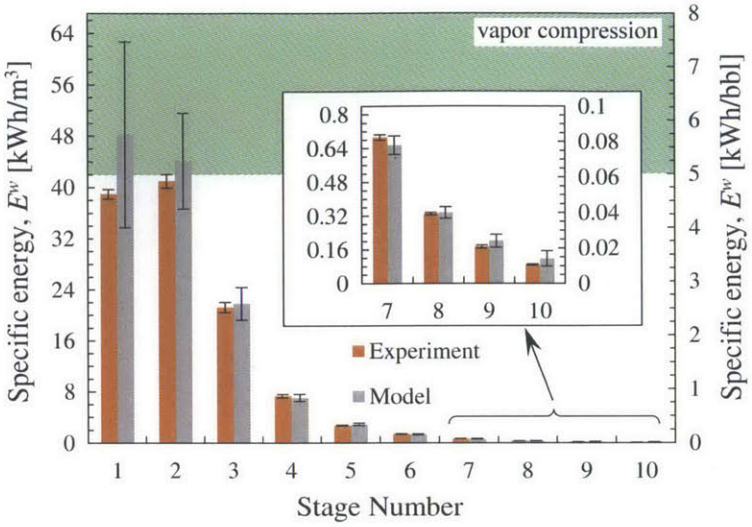

Figure 6-8 Stage energy per unit of product water. The range of energy consumption for vapour compression is taken from Hayes and Severin[31].

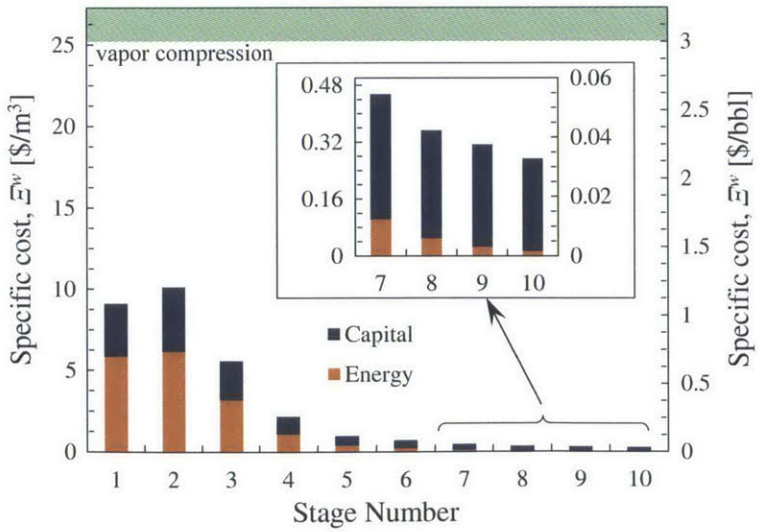

Figure 6-9 Stage cost per unit of product water (based on expermental results). The range of water costs for vapour compression is taken from Slutz et al.[1].

pressure drop within the membranes, which would be expected to dominate in large scale systems with larger processing lengths.

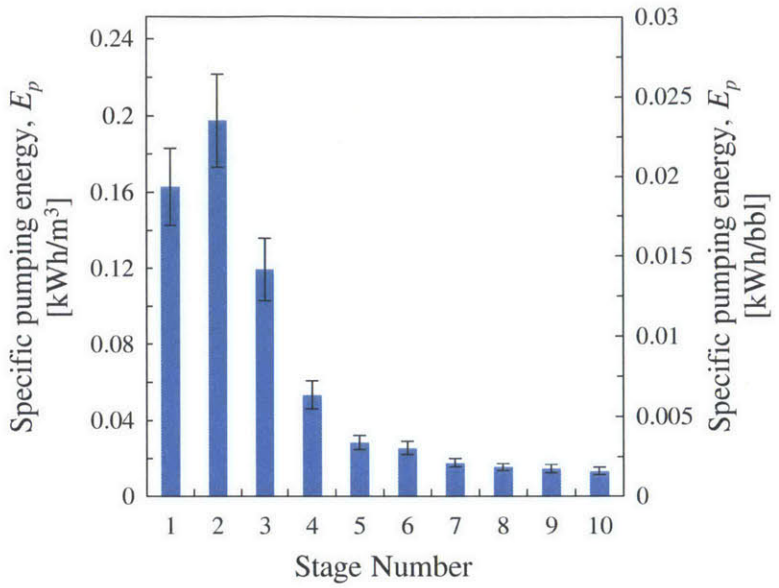

Figure 6-10 Energy consumption associated with pumping power.

6.4 Voltage optimisation

Having validated a numerical model for the system we may next optimise the voltage in each stage to minimise the costs of salt removal. In Fig. 6-11, we compare three distinct strategies that are shown in Fig. 6-12:

1. a constant voltage strategy where the voltage is set such that the current density is 80% of its limiting value at the end of stage 10 ($V_{stack,i}$= 16 V, see Fig. 6-13);

2. a constant voltage strategy where the voltage is set such that the current density is 50% of its limiting value at the end of stage 10 ($V_{stack,i}$= 8 V, see Fig. 6-13); and

3. an optimised strategy where the total costs per stage (equipment and energy) are numerically minimised using a quadratic method[32] to identify an optimal voltage $V^*_{stack,i}$).

Figure 6-11 reveals that in higher number stages (lower diluate salinities) the strategy of setting the voltage such that the current is just below its limiting value (*e.g.*, 80%) is a good one as this greatly reduces equipment costs. However, at higher salinities (lower stage numbers), it is best to operate with a lower stack voltage that allows for reduced energy consumption. Of course, depending on the relative price of equipment to energy the optimal stack voltage for each stage will differ. Higher electricity prices will drive lower optimal stack voltages and vice-versa. Nevertheless, it is clear that the brackish water strategy of setting the current close to its limiting value[16] is not necessarily optimal for the treatment of higher salinity waters.

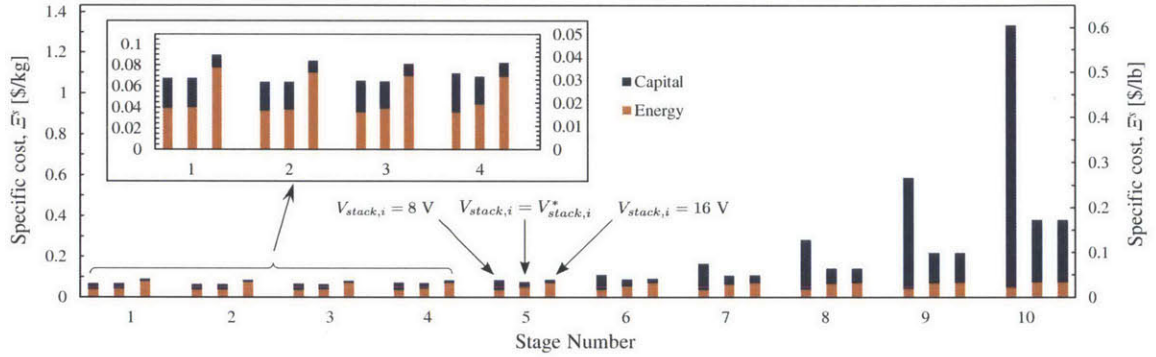

Figure 6-11 Effect of voltage strategy upon the cost of salt removal.

6.5 Conclusions

Our experimental and economic assessment of electrodialysis at salinities up to 192,000 ppm NaCl indicates good potential for the process at high salinities, such as those seen in produced waters from hydraulically fractured shales. The energy requirements are lower than those of commercial vapour compression processes. Furthermore, our projections indicate combined equipment and energy costs to be similar, if not lower, than those of vapour compression. If partial, as opposed to complete, desalination of a feed water is required, the prospects for ED are even greater as the cost per unit of salt removed is much lower at high diluate salinities. For example, salt removal from a stream of 500 ppm TDS might cost up to four times that of salt removal from a

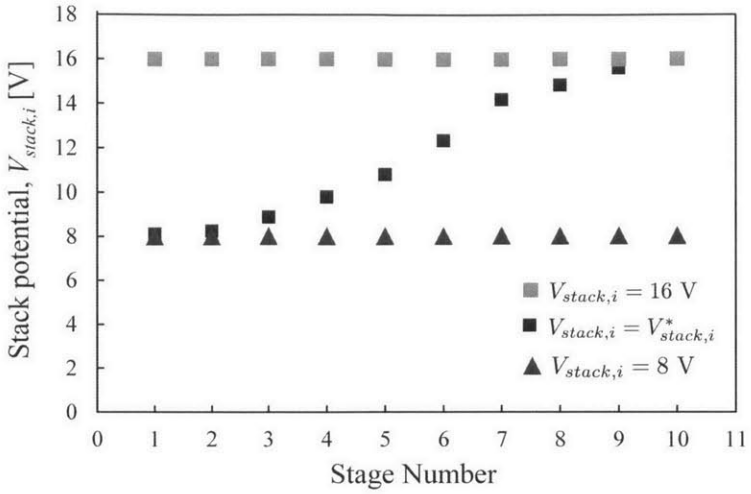

Figure 6-12 Effect of voltage strategy upon the optimal voltage. At low stage numbers the $V_{stack,i}$= 8 V strategy is close to optimal while at high stage numbers the $V_{stack,i}$= 16 V is closest to optimal.

stream at 192,000 ppm TDS per unit of salt removed.

Beyond our experimental assessment of electrodialysis at high salinities, we have developed and validated a numerical model covering a range of diluate salinities from 250 ppm up to 192,000 ppm NaCl. This model reveals the importance of optimising the stack voltage to minimise salt removal costs. For the set of equipment and energy prices examined, we found that brackish water desalination costs are minimised by operating close to the limiting current density, while for salt removal from higher salinity streams lower stack voltages can allow cost reductions of up to 30%.

This analysis addresses two major considerations affecting the viability of ED for the desalination of high salinity produced waters, namely the energy and equipment requirements. Given that ED compares favourably with vapour compression on these metrics a more detailed analysis of an ED system under field conditions is warranted. This might include studies of system fouling and scaling when treating more complex feed waters and an analysis of feedwater pre-treatment requirements and costs to ensure robust operation.

6.A Determination of experimental conditions

6.A.1 Determination of the concentrate salinity in each stage

A key benefit of multi-staging the ED process at high salinities is the possibility of selecting a different concentrate salinity in each stage. If the concentrate salinity were to be the same in all stages it would necessarily be greater than the diluate salinity in the first stage. This would result in very strong salt diffusion from concentrate to diluate and water osmosis from diluate to concentrate in the final stages where the diluate salinity would be much lower than the concentrate. In our experiment we therefore choose higher concentrate salinities in stages with higher diluate salinities and vice versa. In each stage we set the concentrate salinity equal to the steady state salinity that would be dictated by the relative rates of salt and water transport across the membranes:

$$x_{s,c} = \frac{J_s}{J_s + J_w} \tag{6.19}$$

where $x_{s,c}$ is the mole fraction of salt in the concentrate at steady state. To compute each steady-state concentrate value we modelled salt and water transport using the methods of Section 6.4. Rather than modelling the steady state concentrate salinity for each stage we approximated its value by considering the molar fluxes of salt and water at the very end of each stage.

Since the fitted parameters required for the model were not known a priori, we considered values from the literature for similar ED experiments (Table 6.1). Furthermore, in practice an ED system operator may choose to run the stacks with a lower concentrate salinity than could be reached in steady state, perhaps to avoid scale formation. The concentrate salinities chosen for a given application may not exactly match the present study. Nonetheless, the results obtained remain significant as stack performance is primarily affected by the diluate conductivity and membrane resistance rather than concentrate salinity, as explained in Section 6.3.

Table 6.1 Key parameters used to model salt and water transport across membranes in the electrodialysis stack in order to determine steady-state concentrate salinities for each stage

Symbol	Value	Ref.
Membrane Performance Parameters		
T_s	0.97	33
T_w	10	33
L_w	8.12×10^{-5} mol/bar-m^2-s	33
L_s	5.02×10^{-8} m/s	33
$\bar{r}_{am}, \bar{r}_{cm}$	6.0 Ω cm^2	33
σ	0.69	26
Solution Properties		
D	1.61×10^{-9} m^2/s	28
t_{cu}	0.5	34
Flow Properties/Geometry		
h	0.7 mm	-
A_m	271 cm^2	-
n_{cp}	17	-
V_{circ}	0.5367 L	-
Sh	20	33
Operational Conditions		
V	8 V	-
V_{el}	2 V	33

6.A.2 Selection of the stack voltage

We selected a constant operating voltage of 8 V, which ensured that we never exceeded 50% of the limiting current density during any stage test. We determined the operating voltage from a voltage vs. current test performed at the lowest diluate conductivity (0.5 mS/cm), shown in Fig. 6-13.

6.A.3 Determination of diluate circuit volume

We determined the diluate circuit volume by measuring the change in salinity (via conductivity) of the diluate solution following the addition of a known amount of salt.

We initially filled the diluate beaker to the 1 L mark with deionised water. We then added a small, known mass of salt, w_s, to the beaker and turned the pumps on. We measured the steady-state conductivity to determine the concentration, C_d

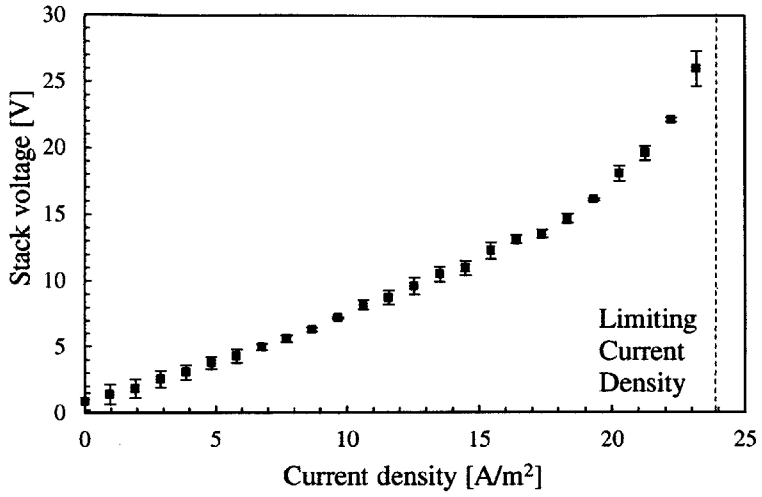

Figure 6-13 Voltage vs current test with diluate and concentrate conductivities of 0.5 mS/cm.

in mol/L, of the diluate circuit:

$$C_d = \frac{k_d}{\lambda_d} \tag{6.20}$$

where k_d is the diluate conductivity in S/m and λ_d is the conductance in m^2/Ω equiv. We then converted this concentration to molality, $m_{s,d}$, and solved for the volume of the circuit, V_{circ}:

$$V_{circ} = \frac{w_s}{M_s \rho_w m_{s,d}} \tag{6.21}$$

where M_s is the molar mass of salt (kg/mol) and ρ_w is the density of distilled water at 25°C. After repeating the measurement three times, we obtained a diluate circuit volume of 0.54±0.02 L.

6.B Assessment of pumping power

We calculated the required pumping power by measuring the pressure drop in the diluate circuit, ΔP, and multiplying by the diluate flow rate, $\dot{V}$, held at 76 L/hr for each stage. To compute the total pumping power, we assumed the pressure drops in

the diluate and concentrate circuits to be equal and multiplied by a factor of two. We discounted the pumping power to drive the rinse circuit since in a large scale system the number of cell pairs per stack is large and hence the ratios of diluate and concentrate flow rates to the rinse flow rate would be small.

We made pressure measurements after flushing the stack with distilled water and operating with diluate, concentrate, and rinse feeds below 500 ppm. Thus we neglected the effect of salinity on density and viscosity. Multiplying by the specific process time of each stage, τ_i, we computed and plotted the specific pumping energy (See Figure 6-10):

$$E_{p,i}^{w} = 2\dot{V}\Delta P\tau_i^{w} \tag{6.22}$$

For the high salinity stages (numbers 5 and below), the specific pumping energy makes up less than 5% of the total specific energy consumed and the contribution to the total specific cost of energy is negligible. In the low salinity stages, the specific pumping energy makes up as much as 40% of the total specific energy consumed. However, this number is largely a characteristic of the small process length of the laboratory scale system used. The relative contribution of stack entrance and exit effects to pressure drop is large relative to frictional pressure drop through the passages between the membranes.

6.C Electrodialysis model

6.C.1 Concentration polarisation

The difference between bulk and membrane wall concentrations and osmotic pressures is accounted for by a convection-diffusion model of concentration polarisation:

$$\Delta C = -\frac{\left(\bar{T}_{cu} - t_{cu}\right)}{D}\frac{i}{F}\frac{2h}{\mathrm{Sh}} \tag{6.23}$$

where D is the solute diffusivity, F is Faraday's constant, h is the channel height and t_{cu} is the counter-ion transport number in the diluate and concentrate solutions and

is approximated as 0.5 for both anions and cations. $\bar{T}_{cu}$ is the integral counter-ion transport number in the membrane that accounts for both migration and diffusion. It is assumed to be equal in the anion and cation exchange membranes and approximated as:

$$\bar{T}_{cu} \approx \frac{T_s^{cp} + 1}{2}. \tag{6.24}$$

For the a priori calculations of concentrate salinities in 6.A.1, the Sherwood number is computed using the correlation obtained by Kuroda et al.[35] for spacer A in their analysis:

$$\mathrm{Sh} = 0.5\mathrm{Re}^{1/2}\mathrm{Sc}^{1/3} \tag{6.25}$$

where Sc is the Schmidt number, calculated using the limiting diffusivity of NaCl in water[28] and the kinematic viscosity of pure water ν[36], both at 25°C. Re is the Reynolds number defined as:

$$Re = \frac{2hV}{\nu} \tag{6.26}$$

where V is the mass averaged velocity in the channel.

6.C.2 Junction and membrane potentials

Junction potentials associated with concentration polarisation are neglected (which is compatible with taking the transport number of both Na and Cl in solution as 0.5), while the sum of the anion and cation membrane potentials $E_{am} + E_{cm}$ is computed considering quasi-equilibrium migration of salt and water across the membranes:

$$E_{am}+E_{cm} = \frac{T_s^{cp}}{F}(\mu_{s,c,m} - \mu_{s,d,m}) + \frac{T_w^{cp}}{F}(\mu_{w,c,m} - \mu_{w,d,m}) \tag{6.27}$$

where μ_s denotes the chemical potential of salt and μ_w the chemical potential of water; both calculated employing osmotic coefficients and NaCl activity coefficient

data from Robinson and Stokes[28]. The subscripts c and d denote the concentrate and diluate while the subscript m denotes a concentration at the membrane surface.

6.D Determination of fitted parameters

6.D.1 Sherwood number

The Sherwood number was determined via the limiting current density. A current-voltage test was repeated three times for diluate and concentrate conductivities of 0.5 mS/cm, the results of which are shown in Fig. 6-13. The Sherwood number was then determined by considering the following relationship between it and the limiting current density:

$$i_{lim} = \frac{D_{NaCl} F C_d \mathrm{Sh}}{2h\left(\frac{T_s+1}{2} - t_{cu}\right)}. \tag{6.28}$$

with D_{NaCl} the diffusivity of sodium chloride in solution, F Faraday's constant, C_d the diluate concentration, h the concentrate and diluate channel heights and T_s the salt transport number. The Sherwood number was found to equal 18±1 (68% confidence).

6.D.2 Spacer shadow factor

The spacer shadow factor, σ, quantifies the conductance of the diluate and concentrate channels relative to what the conductance would be were there to be no spacer. When the diluate and concentrate solutions are of high conductivity the stack voltage is insensitive to the spacer shadow factor, since the membrane resistance dominates. Therefore, in determining σ we considered tests where the diluate and concentrate conductivities were low (0.5, 1.5, 2.5 and 7.5 mS/cm). We also considered low values of current density (9.7, 19.3 and 29 A/m^2) where the voltage-current relationship was only weakly affected by concentration polarisation.

The stack voltage data was first corrected (from V_{stack} to V_{corr}) to remove the effects of concentration polarisation, employing the Sherwood number from 6.D.1

and the model described in 6.C.1. This allowed the voltage current relationship to be represented by:

$$V_{corr} = (2n_{cp} + 1)i\bar{r}_m + \frac{2Nih}{\sigma k} + \frac{2ih_r}{\sigma k_r} + V_{el} \tag{6.29}$$

where the terms on the right hand side represent voltage drops across the membranes, the diluate and concentrate (both at the same conductivity), the rinse solutions and the electrodes, respectively. Plotting V_{corr} versus the inverse conductivity of the solution in Fig. 6-1 allowed σ to be determined from the slope. Considering:

$$m = \frac{2Nih}{\sigma}, \tag{6.30}$$

where m is the slope of each of the lines in Fig. 6-1, we determined the spacer shadow effect at the three different current densities. Since σ should be independent of current density we computed its value as the average of these three values, giving $\sigma = 0.64 \pm 0.03$.

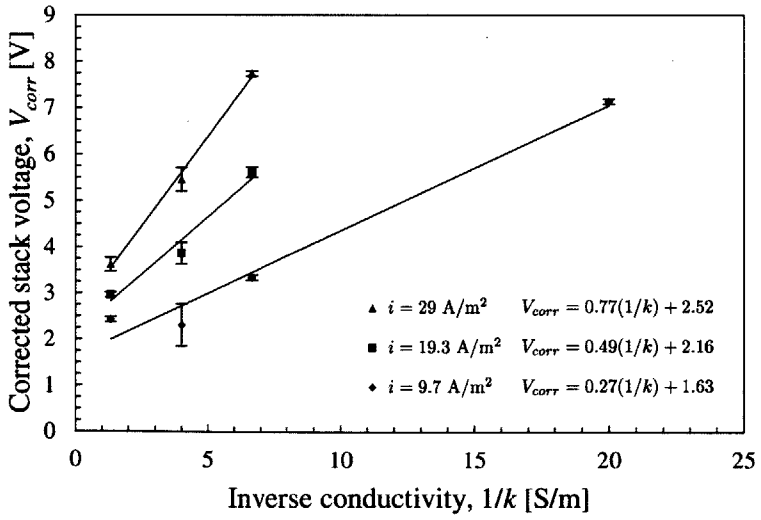

Figure 6-1 Determination of spacer shadow effect and electrode potential at low voltage. The markers represent experimental values while the solid lines represent the fitted equations.

6.D.3 Electrode potential

At low current densities the electrode potential was computed considering the intercept c of each of the lines in Fig. 6-1:

$$V_{el} = c - (2N+1)i\bar{r}_m + \frac{2ih_r}{\sigma k_r}. \tag{6.31}$$

At low current densities, the determination of V_{el} is relatively insensitive to the voltage drop across the membranes and the rinse solutions since both are small. Therefore, even though $\bar{r}_m$ is not known a priori, it is reasonable to assume $\bar{r}_m = 3 \times 10^{-4}\ \Omega\ \mathrm{m}^2$, in line with the membrane resistance quoted by the manufacturer[37]. The values of V_{el} found at 9.7, 19.3 and 29 A/m^2 were 2.4±0.1, 1.9±0.3 and 2.2±0.3, respectively.

To determine the electrode potential at higher current densities, current-voltage tests were carried out with diluate and concentrate conductivities of 25 mS/cm, 75 mS/cm and 150 mS/cm (Fig. 6-2). The linearity of these plots at high current densities (above approximately 240 A/m^2) illustrates that neither membrane resistance nor electrode potential is a strong function of current density at high current densities. Furthermore, for these three conductivities, the range of current densities illustrated is far below the limiting current density and the voltage correction for concentration polarisation is thus negligible ($i.e. V_{stack} \approx V_{corr}$). The electrode potentials, calculated considering the intercept of the linear fits shown in Fig. 6-2 (see Eq. 6.29), for data taken at 25 mS/cm, 75 mS/cm and 150 mS/cm were found to be 1.5±0.5, 2.4±0.25 and 2.3±0.4 V, respectively. On the basis of electrode potentials thus being similar at low and high current density, a value of V_{el}=2.13±0.4 V was considered for the model over the entire range of current densities.

6.D.4 Membrane resistance

At low diluate and concentrate conductivities the stack voltage is insensitive to the membrane resistance. Thus, we determined the membrane resistance from the high conductivity data of Fig. 6-2. The membrane resistance at each value of conductivity

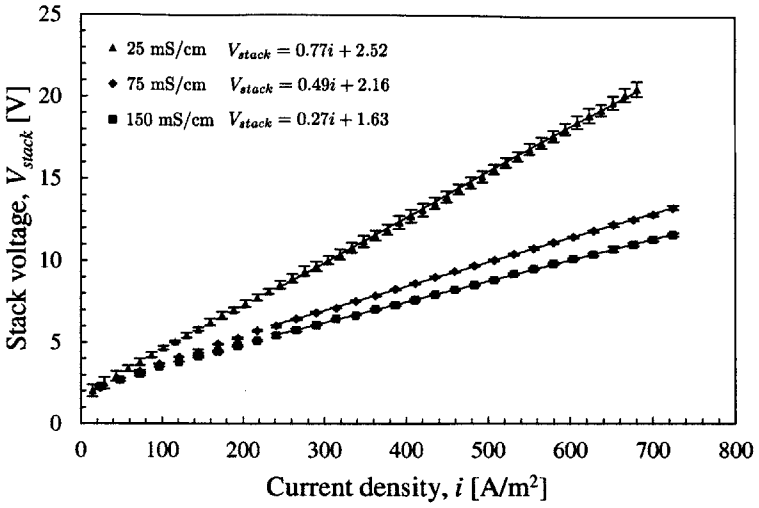

Figure 6-2 Determination of membrane resistances and electrode potentials from high conductivity data. The markers represent experimental values while the solid lines represent the fitted equations.

was determined using the slope of a linear fit,

$$m = (2N + 1)\bar{r}_m + \frac{2Nh}{\sigma k} + \frac{2h_r}{\sigma k_r}, \tag{6.32}$$

knowing already the value of σ from 6.D.2. The values of membrane resistance found for solution conductivities of 25 mS/cm, 75 mS/cm and 150 mS/cm were $4.5\times10^{-4} \pm 5 \times 10^{-5}$, $2.8\times10^{-4} \pm 3 \times 10^{-5}$ and $3.0\times10^{-4} \pm 5 \times 10^{-5}$ Ω m^2. Thus, the membrane resistance was modelled as $3.5 \times 10^{-4} \pm 1 \times 10^{-4}$ Ω m^2 over the entire range of diluate and concentrate salinities.

6.D.5 Salt and water transport numbers

Salt and water transport numbers at solution conductivities of 7.5 mS/cm, 75 mS/cm, 150 mS/cm and 225 mS/cm were determined by running tests at constant current and measuring the mass of salt and water transported across the membranes in a fixed amount of time. Three tests were performed at each set of conditions to ensure repeatability. During these tests, an approximately constant concentrate conductivity was maintained by selecting an initial concentrate solution volume that was three

times that of the diluate. The concentrate beaker was filled with NaCl solution of the desired conductivity and the diluate beaker was filled with NaCl solution that was 1.5, 5, 15 and 15 mS/cm higher than the concentrate conductivity for the 7.5, 25, 75 and 150 mS/cm cases, respectively. The pumps were turned on and a constant current was applied across the stack. The diluate mass and conductivity were recorded until the diluate conductivity reached a value 1.5, 5, 15 and 15 mS/cm below that of the concentrate for the 7.5, 25, 75 and 150 mS/cm cases, respectively. The salt and mass transport numbers were then determined by Eq. (6.33) and Eq. (6.34):

$$T_s^{cp} = \frac{\Delta w_{s,d} F}{n_{cp} I \Delta t M_s} \tag{6.33}$$

$$T_w^{cp} = \frac{\Delta w_{w,d} F}{n_{cp} I \Delta t M_w T_s}. \tag{6.34}$$

Here, $\Delta w_{s,d}$ and $\Delta w_{w,d}$ were the changes in the diluate mass for salt and water respectively, F Faraday's constant, I the applied current across the membrane (10 A), N_{cp} the number of cell pairs, and Δt the process run time. The temperature was held constant at 25°C and the diluate mass was corrected for leakage from diluate to concentrate (determined through leakage tests performed at zero current with deionised water in the concentrate and diluate chambers). Bias errors arising from determining the diluate circuit volume (6.A.3) and leakage were propagated through Eqs. (6.34) and (6.33) and combined with the random error [Eq. (6.12)] that was determined from the sample standard deviation of results from the three tests run at the same conditions. As shown in figure 6-3, the salt transport numbers are decreasing with increasing conductivities due to the falling charge density of membranes relative to the solutions[38]. Figure 6-4 shows that the water transport numbers are also decreasing with increasing conductivities because of falling water activity, which reduces the membranes' capacity to hydrate[39].

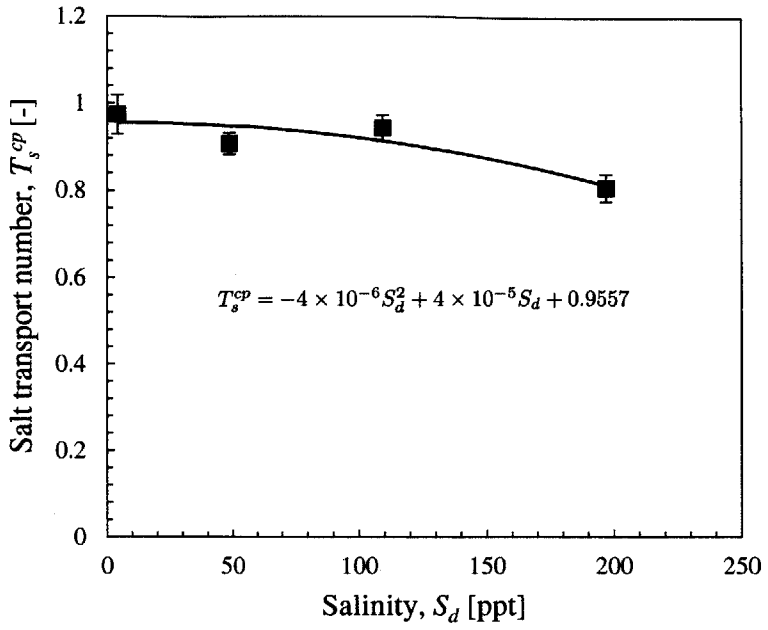

Figure 6-3 Salt transport number. The markers represent experimental values while the solid lines represent the fitted equations

6.D.6 Salt and water permeability

The permeabilities of the membranes to salt and water at solution conductivities of 7.5 mS/cm, 75 mS/cm 150 mS/cm and 225 mS/cm were determined by running tests at zero current with de-ionised water flowing in the diluate compartment. Three tests were performed at each value of concentrate conductivity to ensure repeatability. During these tests, an approximately constant concentrate conductivity was maintained by selecting an initial concentrate solution volume that was three times that of the diluate. The pumps were turned on and data for diluate conductivity and mass were recorded versus time. Throughout the tests, the temperature was held constant at 25°C. The tests were stopped after the diluate concentration reached conductivities of 200 μS/cm, 900 μS/cm, 900 μS/cm and 3,200 μS/cm for the four values of concentrate conductivity respectively. The salt and water permeability coefficients

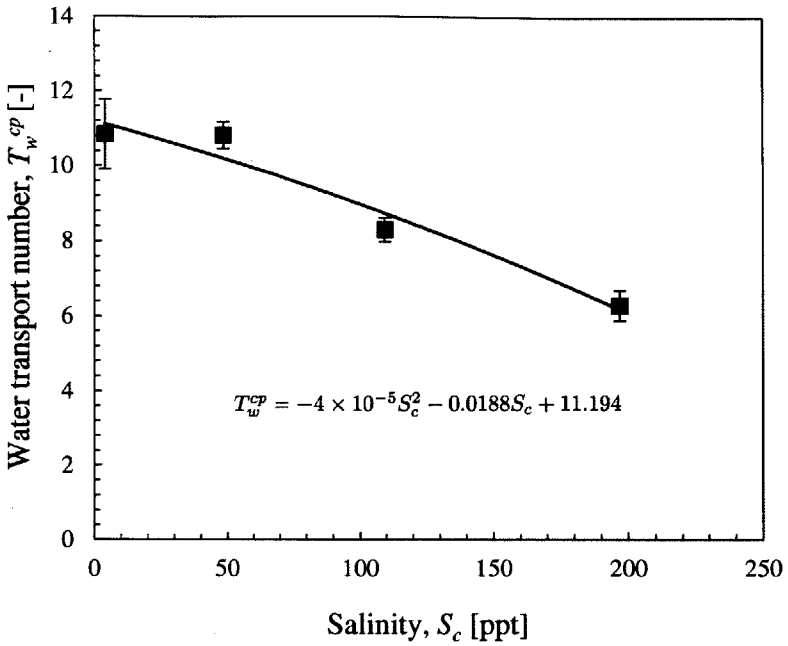

Figure 6-4 Water transport number. The markers represent experimental values while the solid lines represent the fitted equations

were determined employing Eqns. (6.35) and (6.36)

$$L_s^{cp} = \frac{J_s}{(C_c - \frac{\Delta C_d}{2}) A_m N_{cp}} \tag{6.35}$$

$$L_w^{cp} = \frac{J_w}{\Delta \pi A_m N_{cp}} \tag{6.36}$$

with A_m the active membrane area and N_{cp} the number of cell pairs in the stack. A second order polynomial fit was applied to the salt permeabilities and a power-law fit was applied to the water permeabilities. Bias errors arising from determining the diluate circuit volume (6.A.3) and leakage were propagated through Eqs. (6.34) and (6.33) and combined with the random error [Eq. (6.12)] arising from the sample standard deviation of results from the three tests run at the same conditions.

6.D.7 Summary of model parameters

A summary of the model parameters and equations is provided in Table 6.2. Membrane salt transport, water transport, salt permeability and water permeability are

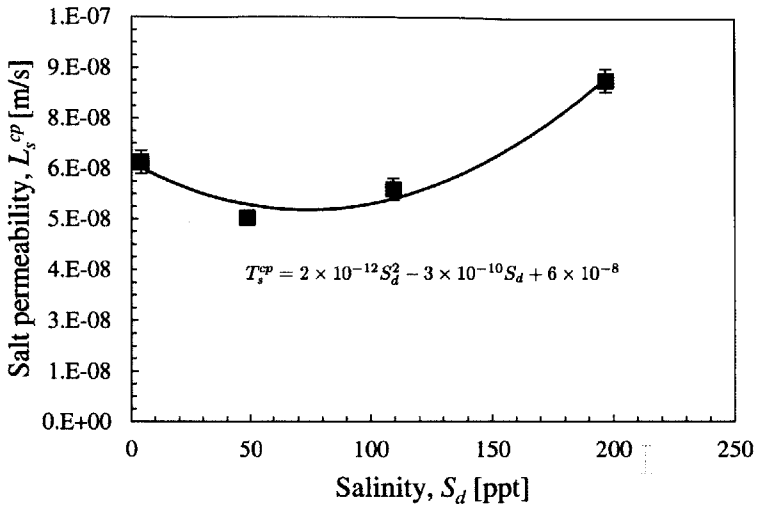

Figure 6-5 Salt permeability. The markers represent experimental values while the solid lines represent the fitted equations

modelled as:

$$T_s^{cp} = -4 \times 10^{-6} S_d^2 + 4 \times 10^{-5} S_d + 0.96 \pm 0.04 \tag{6.37}$$

$$T_w^{cp} = -4 \times 10^{-5} S_c^2 - 1.9 \times 10^{-2} S_c + 11.2 \pm 0.6 \tag{6.38}$$

$$\begin{aligned} L_s^{cp} = \min(&2 \times 10^{-12} S_d^2 - 3 \times 10^{-10} S_d + 6 \times 10^{-8}, \\ &2 \times 10^{-12} S_c^2 - 3 \times 10^{-10} S_c + 6 \times 10^{-8}) \\ &\pm 6 \times 10^{-9} [\text{m/s}] \end{aligned} \tag{6.39}$$

$$L_w^{cp} = 5 S_c^{-0.416} \pm 2 \times 10^{-5} [\text{mol/m}^2\text{s bar}] \tag{6.40}$$

Nomenclature

Roman Symbols

A_m	membrane area, m^2
C	concentration, mol/m^3
D	diffusivity, m^2/s
E^s	specific energy of salt removal, kWh/lb or kWh/kg

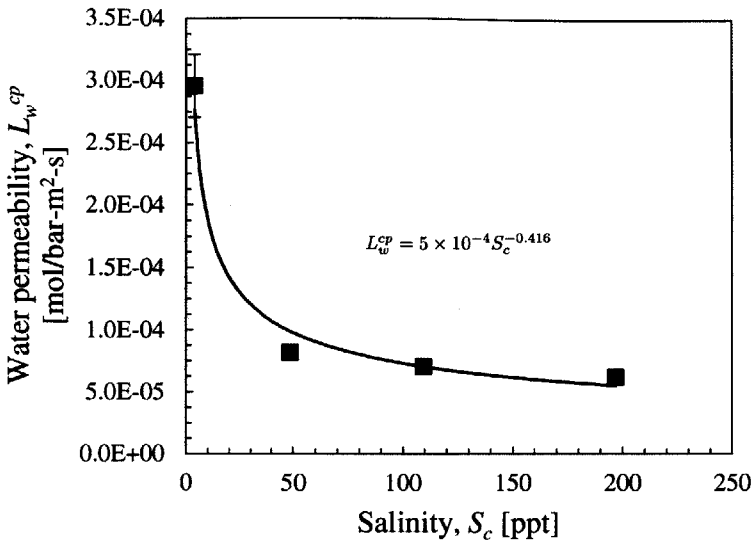

Figure 6-6 Water permeability. The markers represent experimental values while the solid lines represent the fitted equations

E^w	specific energy of water produced, kWh/bbl or kWh/m^3
h	channel height, m
i	current density, A/m^2
I	current, A
k	conductivity, S/m
K_E	energy price, \$/kWh
K_Q	area normalised equipment price, \$/m^2 membrane
L_s	membrane salt permeability, m^2/s
L_w	membrane water permeability, mol/m^2 s bar
m	slope
M	molar mass, kg/mol
m_s	molal concentration, mol/kg w
N	number of moles, mol
n_{cp}	number of cell pairs, -
$\bar{r}$	membrane surface resistance, $\Omega\ m^2$
R	universal gas constant, J/mol K
Re	Reynolds number

Table 6.2 Electrodialysis Model Parameters

Symbol	Value	Ref.
Solution Properties		
D	1.61×10^{-9} m^2/s	[28]
t_{cu}	0.5	[34]
ν	8.9×10^{-7} m^2/s	[36]
Flow Properties/Geometry		
h	0.5 mm	-
n_{cp}	17	-
Sh	18	-
Membrane Parameters		
σ	0.64 ± 0.03	-
$\bar{r}_m$	$3.5\times10^{-4}\pm1\times10^{-4}$ Ω m^2	-
T_s^{cp}	Eq. (6.37)	-
T_w^{cp}	Eq. (6.38)	-
L_s^{cp}	Eq. (6.39)	-
L_w^{cp}	Eq. (6.40)	-
Stack Parameters		
V^{cp}	8 V	-
V_{el}	2.1 ± 0.4 V	-

Sc Schmidt number

Sh Sherwood number

t process time, s

T system life, years

$\bar{T}_{cu}$ integral membrane counterion transport number, -

t_{cu} solution counter-ion transport number, -

T_s^{cp} cell pair salt transport number, -

T_w^{cp} cell pair water transport number, -

V_{corr} stack voltage corrected for concentration polarisation, V

V_{stack} stack voltage, V

V volume, m^3

$\dot{V}$ volume flow rate, m^3/s

w mass, lbs or kg

x concentration, mol s/mol w

Greek Symbols

Δ	change
ϵ	error
Λ	molar conductivity, S m^2/mol
μ	chemical potential, J/mol
ν	viscosity, m^2/s
Ξ^s	specific cost of salt, \$/lb or \$/kg
Ξ^w	specific cost of water, \$/bbl or \$/m^3
π	osmotic pressure, bar
ρ	density, kg/m^3
σ	spacer shadow factor, -
τ^s	specific process time, days/lb or days/kg
τ^w	specific process time, days/bbl or days/m^3

Subscripts

am	anion exchange membrane
c	concentrate
$circ$	circuit
cm	cation exchange membrane
d	diluate
el	electrode
i	stage number
j	time period
m	membrane surface
p	pump
r	rinse
s	salt
s	water

Superscripts

f	final
in	initial

Bibliography

[1] J. A. Slutz, J. A. Anderson, R. Broderick, P. H. Horner, et al., Key shale gas water management strategies: An economic assessment, in: International Conference on Health Safety and Environment in Oil and Gas Exploration and Production, Society of Petroleum Engineers, 2012.

[2] R. Vidic, S. Brantley, J. Vandenbossche, D. Yoxtheimer, J. Abad, Impact of shale gas development on regional water quality, Science 340 (6134).

[3] M. E. Mantell, Produced water reuse and recycling challenges and opportunities across major shale plays, in: Proceedings of the Technical Workshops for the Hydraulic Fracturing Study: Water Resources Management. EPA, Vol. 600, 2011, pp. 49–57.

[4] S. Shipman, D. McConnell, M. P. Mccutchan, K. Seth, et al., Maximizing flowback reuse and reducing freshwater demand: Case studies from the challenging marcellus shale, in: SPE Eastern Regional Meeting, Society of Petroleum Engineers, 2013.

[5] J.-P. Nicot, B. R. Scanlon, R. C. Reedy, R. A. Costley, Source and fate of hydraulic fracturing water in the barnett shale: A historical perspective, Environmental science & technology.

[6] Proceedings and Minutes of the Hydraulic Fracturing Expert Panel XTO Facilities, Fort Worth September 26th, 2007.

[7] V. Fedotov, D. Gallo, P. M. Hagemeijer, C. Kuijvenhoven, et al., Water manage-

ment approach for shale operations in north america, in: SPE Unconventional Resources Conference and Exhibition-Asia Pacific, Society of Petroleum Engineers, 2013.

[8] S. Rassenfoss, From flowback to fracturing: water recycling grows in the marcellus shale, Journal of Petroleum Technology 63 (7) (2011) 48–51.

[9] J. Bryant, I. Robb, T. Welton, J. Haggstrom, Maximizing friction reduction performance using flow back water and produced water for waterfrac applications, in: AIPG Marcellus Shale Hydraulic Fracturing Conference, 2010.

[10] A. Kamel, S. N. Shah, Effects of salinity and temperature on drag reduction characteristics of polymers in straight circular pipes, Journal of petroleum Science and Engineering 67 (1) (2009) 23–33.

[11] J. Paktinat, O. Bill, M. Tulissi, Case studies: Improved performance of high brine friction reducers in fracturing shale reserviors, Society of Petroleum Engineers (2011) 1–12.

[12] C. W. Aften, Study of friction reducers for recycled stimulation fluids in environmentally sensitive regions, in: SPE Eastern Regional Meeting, Society of Petroleum Engineers, 2010.

[13] M. J. Zhou, M. Baltazar, Q. Qu, H. Sun, Water-based environmentally preferred friction reducer in ultrahigh-tds produced water for slickwater fracturing in shale reservoirs, in: SPE/EAGE European Unconventional Resources Conference and Exhibition, Society of Petroleum Engineers, 2014.

[14] J. K. Hallock, R. L. Roell, P. B. Eichelberger, X. V. Qiu, C. C. Anderson, M. L. Ferguson, Innovative friction reducer provides improved performance and greater flexibility in recycling highly mineralized produced brines, in: SPE Unconventional Resources Conference-USA, Society of Petroleum Engineers, 2013.

[15] R. LeBas, P. Lord, D. Luna, T. Shahan, Development and use of high-tds recycled produced water for crosslinked-gel-based hydraulic fracturing, in: 2013 SPE Hydraulic Fracturing Technology Conference, 2013.

[16] H.-J. Lee, F. Sarfert, H. Strathmann, S.-H. Moon, Designing of an electrodialysis desalination plant, Desalination 142 (3) (2002) 267–286.

[17] R. McGovern, S. Zubair, J. Lienhard V, Hybrid electrodialysis reverse osmosis system design and its optimization for treatment of highly saline brines, IDA Journal of Desalination and Water Reuse 6 (1) (2014) 15–23.

[18] T. Brown, C. D. Frost, T. D. Hayes, L. A. Heath, D. W. Johnson, D. A. Lopez, D. Saffer, M. A. Urynowicz, J. Wheaton, M. D. Zoback, Produced water management and beneficial use, Tech. rep., DOE Award No.: DE-FC26-05NT15549 (2009).

[19] M. Turek, Electrodialytic desalination and concentration of coal-mine brine, Desalination 162 (2004) 355–359.

[20] L. Dallbauman, T. Sirivedhin, Reclamation of produced water for beneficial use, Separation science and technology 40 (1-3) (2005) 185–200.

[21] T. Sirivedhin, J. McCue, L. Dallbauman, Reclaiming produced water for beneficial use: salt removal by electrodialysis, Journal of membrane science 243 (1) (2004) 335–343.

[22] PCCell GmbH, ED 200, Lebacher Strasse 60, D-66265 Heusweiler, Germany. URL `http://www.pca-gmbh.com/pccell/ed200.htm`

[23] R. F. Stiles, M. S. Slezak, Strategies for reducing oilfield electric power costs in a deregulated market, SPE production & facilities 17 (03) (2002) 171–178.

[24] P. Tsiakis, L. G. Papageorgiou, Optimal design of an electrodialysis brackish water desalination plant, Desalination 173 (2) (2005) 173–186.

[25] M. S. Peters, K. D. Timmerhaus, R. E. West, K. Timmerhaus, R. West, Plant design and economics for chemical engineers, Vol. 4, McGraw-Hill New York, 1968.

[26] M. Fidaleo, M. Moresi, Optimal strategy to model the electrodialytic recovery of a strong electrolyte, Journal of Membrane Science 260 (1) (2005) 90–111.

[27] R. K. McGovern, S. M. Zubair, J. H. Lienhard V, The cost effectiveness of electrodialysis for diverse salinity applications.Under review.

[28] R. Robinson, R. Stokes, Electrolyte Solutions, Courier Dover Publications, 2002.

[29] T. Shedlovsky, The electrolytic conductivity of some uni-univalent electrolytes in water at 25 c, Journal of the American Chemical Society 54 (4) (1932) 1411–1428.

[30] J. Chambers, J. M. Stokes, R. Stokes, Conductances of concentrated aqueous sodium and potassium chloride solutions at 25, The Journal of Physical Chemistry 60 (7) (1956) 985–986.

[31] T. Hayes, B. F. Severin, P. S. P. Engineer, M. Okemos, Barnett and appalachian shale water management and reuse technologies, Contract 8122 (2012) 05.

[32] S. A. Klein, Engineering Equation Solver, Academic Professional V9.438-3D (2013).

[33] M. Fidaleo, M. Moresi, Electrodialytic desalting of model concentrated nacl brines as such or enriched with a non-electrolyte osmotic component, Journal of Membrane Science 367 (1) (2011) 220–232.

[34] A. Sonin, R. Probstein, A hydrodynamic theory of desalination by electrodialysis, Desalination 5 (3) (1968) 293–329.

[35] O. Kuroda, S. Takahashi, M. Nomura, Characteristics of flow and mass transfer rate in an electrodialyzer compartment including spacer, Desalination 46 (1) (1983) 225–232.

[36] E. R. Association, Viscosity of Water and Steam, Edward Arnold Publishers, 1967.

[37] A. Corporation, Neosepta, uRL: http://www.astom-corp.jp/en/en-main2-neosepta.html (2013).

[38] K. Kontturi, L. Murtomaki, J. A. Manzanares, Ionic Transport Processes In Electrochemistry and Membrane Science, Oxford, 2008.

[39] N. Berezina, N. Gnusin, O. Dyomina, S. Timofeyev, Water electrotransport in membrane systems. experiment and model description, Journal of membrane science 86 (3) (1994) 207–229.

Chapter 7

The benefits of hybridising electrodialysis with reverse osmosis

Abstract

A cost analysis reveals that hybridisation of electrodialysis with reverse osmosis is only justified if the cost of water from the reverse osmosis unit is less than 40% of that from a standalone electrodialysis system. In such cases the additional reverse osmosis costs justify the electrodialysis cost savings brought about by shifting salt removal to higher salinity, where current densities are higher and equipment costs lower. Furthermore, the analysis suggests that a simple hybrid configuration is more cost effective than a recirculated hybrid, a simple hybrid being one where the reverse osmosis concentrate is fed to the electrodialysis stack and the products from both units are blended, and a recirculated being one hybrid involving recirculation of the electrodialysis product back to the reverse osmosis unit. The underlying rationale is that simple hybridisation shifts salt removal away from the lowest salinity zone of operation, where salt removal is most expensive. Further shifts in the salinity at which salt is removed, brought about by recirculation, do not justify the associated increased costs of reverse osmosis.

Contributions

This chapter was co-authored by Prof. Syed Zubair and Prof. John Lienhard V. The work received financial support from the Hugh Hampton Young Memorial Fund Fellowship and the King Fahd University of Petroleum and Minerals through the Center for Clean Water and Clean Energy at MIT and KFUPM under project number R15-CW-11.

7.1 Introduction

Based on a comparison of the cost of water, we establish guidelines for choosing between standalone electrodialysis (ED) and hybrid electrodialysis-reverse osmosis (ED-RO) systems. By modelling the energy and equipment costs of electrodialysis as a function of product salinity we demonstrate the opportunity to reduce costs by shifting salt removal to higher salinity. Hybridisation of electrodialysis with reverse osmosis allows such a shift. Therefore, we model hybrid electrodialysis-reverse osmosis systems to establish when the benefits of hybridisation outweigh the costs of the reverse osmosis unit. We frame our models such that the decision between hybrid and standalone systems is based upon a cost ratio between reverse osmosis and electrodialysis systems, and consider this as a variable in our analysis.

Our interest in hybrid ED-RO systems is to further minimise the environmental impact and economic cost of brackish desalination, of which the latter has grown at an estimated annualised rate of 12% over the past 10 years[1] (see 7.A). Brackish desalination involves the treatment of waters of slight (1,000-3,000 ppm total dissolved solids, TDS) to moderate salinity (3,000-10,000 ppm TDS)[2] present in naturally saline inland aquifers or coastal aquifers that have become subject to the intrusion of seawater[3] (see Fig. 7-1).

From environmental and cost perspectives, the ratio of water recovered to that withdrawn, known as the recovery ratio, RR, is an important consideration. A higher recovery ratio allows the following benefits: a reduction in the size of the desalination plant intake; a reduction in the volume of brine produced, which requires disposal to the sea, surface waters or confined aquifers below the aquifer from which water is withdrawn[5]; and a reduction in the rate of aquifer recharge required, which might be done continuously with treated waste water[4] or periodically with water sourced from another location during periods of low demand[6]. Conversely, a higher recovery ratio results in the production of higher salinity brine, which, depending upon the degree of dispersion and/or dilution employed at the point of disposal, can have adverse effects on plant and animal life[7]. We focus on scenarios where the benefits of reduced

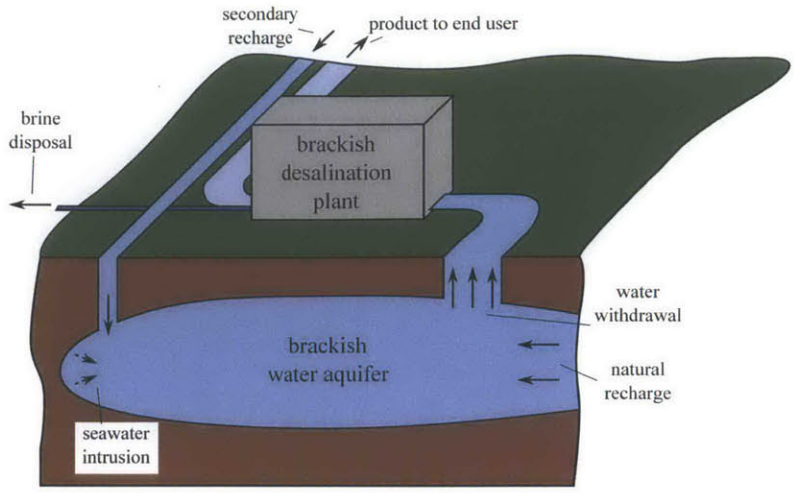

Figure 7-1 The supply of freshwater and mitigation of seawater intrusion with brackish desalination and secondary recharge. Based on an aquifer management system proposed by Koussis et al.[4].

volumes outweigh those of increased salinity and consider technologies offering high recovery ratios.

Electrodialysis is well suited to applications requiring high recovery ratios for at least three reasons. Firstly, electrodialysis is a salt removal rather than a water removal technology, and so the majority of the feed water is easily recovered as a product. This is in contrast to reverse osmosis, where high recovery ratios require multiple stages in a continuous process (Fig. 7-2a) or longer process times in a semi-batch (or batch) process[8]. Secondly, electrodialysis is capable of reaching brine concentrations above 10% total dissolved solids (TDS), which is beyond the osmotic pressures reachable by current reverse osmosis systems[9,10]. Thirdly, seeded precipitation of scalants in the ED process can in some cases circumvent the barrier on water recovery imposed by the solubility of feedwater solutes; this has been demonstrated by recirculating the electrodialysis concentrate loop through a crystalliser[9,11,12] or a combination of a crystalliser and an ultrafiltration unit[10].

Although ED enjoys the advantage of high water recovery, costs increase with the amount of salt removal required (Fig. 7-2b). This is particularly true at low

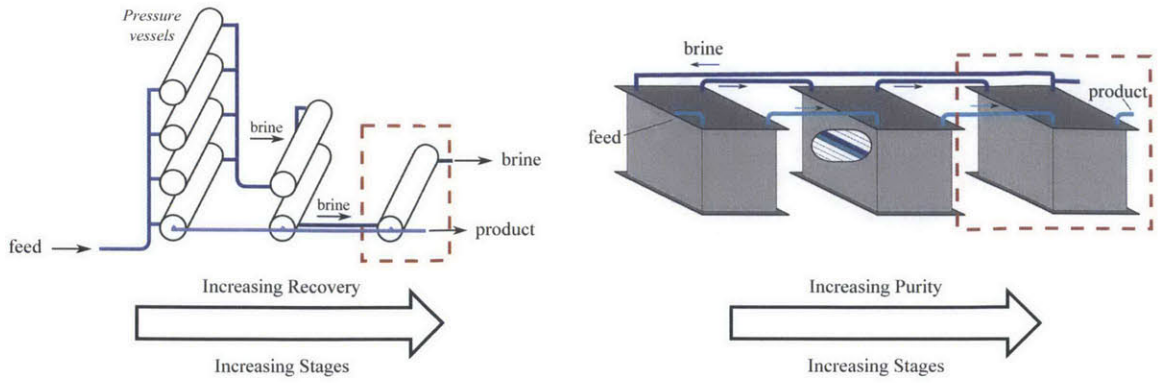

(a) Reverse osmosis **(b)** Electrodialysis

Figure 7-2 The ability of electrodialysis to achieve high recovery and reverse osmosis to achieve high purity points towards an opportunity for hybridisation.

salinity where salt removal rates, which scale with the electrical current, are limited by the rate of diffusion of ions to the membrane surface. This phenomenon, known as the limiting current density, as well as the high electrical resistance of solutions at low concentrations, increase the costs of electrodialysis at low salinity. Thus, it is the synergy of ED providing high recovery and RO providing final high product purity that gave rise to analyses of hybrid ED-RO systems. The technical feasibility of these systems has already been demonstrated[10,12–16], but there are a limited number of studies benchmarking hybrid ED-RO systems against other technologies. To date, one study has compared hybrid ED-RO to a reverse-osmosis-mechanical-vapour-compression system and concluded that the hybrid system has lower upfront capital costs and lower operational costs[13].

In summary, electrodialysis can offer the benefit of higher recovery relative to reverse osmosis systems. Although the cost of water from a reverse osmosis system operating at lower recovery may be smaller, when brine disposal costs are taken into account, electrodialysis can be more cost effective[17]. In this manuscript we focus on scenarios where, overall, ED is more cost effective than RO and analysis the question of when it is preferable to hybridise electrodialysis with reverse osmosis rather than operate with electrodialysis alone. We also compare simple hybrid and recirculated hybrid system configurations.

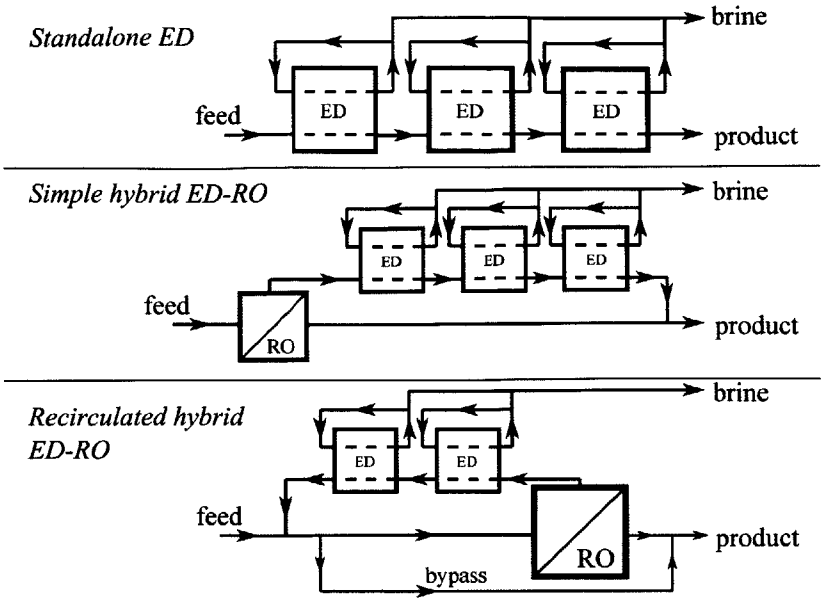

Figure 7-3 Standalone and hybrid ED configurations. The relative size of electrodialysis (ED) and reverse osmosis (RO) units is intended to illustrate the relative quantities of membrane area required in each, assuming the final product flow rate from all systems is the same.

7.2 The rationale for hybridising electrodialysis with reverse osmosis

The rationale for hybridising electrodialysis with reverse osmosis is to relax the product purity requirements on the electrodialysis unit. Later, we will demonstrate how these requirements can be relaxed by comparing simple hybrid and recirculated hybrid designs to a standalone ED system, Fig. 7-3. First, to understand why the relaxation of product purity requirements can reduce ED costs, we focus on the standalone ED system and consider the dependence of the specific cost of water on product purity.

We consider a steady-state 1-dimensional model for the performance and cost of a standalone electrodialysis system. The total system area is divided, in the direction of the flow, into twenty stacks within which salt and water transport are approximated as uniform. These stacks serve the numerical purpose of discretisation and do not relate to the number of stacks within a real system. The key salt, water and charge transport equations, which are based on the approach of Fidaleo and Moresi[18], and

McGovern et al.[19] are then applied to each stack. Membrane properties, flow rates and cell pair parameters are also taken from Fidaleo and Moresi[18] and are provided in 7.B. The process is designed and costed according to the following specifications and assumptions:

1. the feed is aqueous NaCl;
2. the concentrate concentration within each sub-region is determined by the net rates of salt and water transport across the membranes;
3. the system is operated at voltage of 0.8 V which corresponds to just above 70% of the limiting current density[20] (see 7.B.2);
4. equipment and stack energy costs are considered but pumping power is neglected (see 7.F);
5. equipment is costed on the basis of membrane area at \$1500/m^2 of cell pair area (see 7.C), amortised at 10% over 20 years;
6. energy costs are computed on the basis of stack power consumption (see 7.D for validation of results) and a 0.065 \$/kWh cost of electricity; and
7. the product flow rate is set at 1,000 m^3/day.

Specifying the feed salinity along with the product salinity and flow rate, these equations are solved simultaneously using a non-linear equation solver[21] to compute concentrate concentration, total membrane area, energy consumption, specific equipment costs, specific energy costs, and specific water costs.

Figure 7-4a illustrates the dependence of the specific cost of water C upon the product salinity S_P while Fig 7-4b illustrates the dependence of the marginal cost,

$$MC = \frac{\partial C}{\partial S_d}, \tag{7.1}$$

upon the local diluate salinity S_d, the low salinity stream within an ED process (as opposed to the high salinity recirculated concentrate stream). These figures show

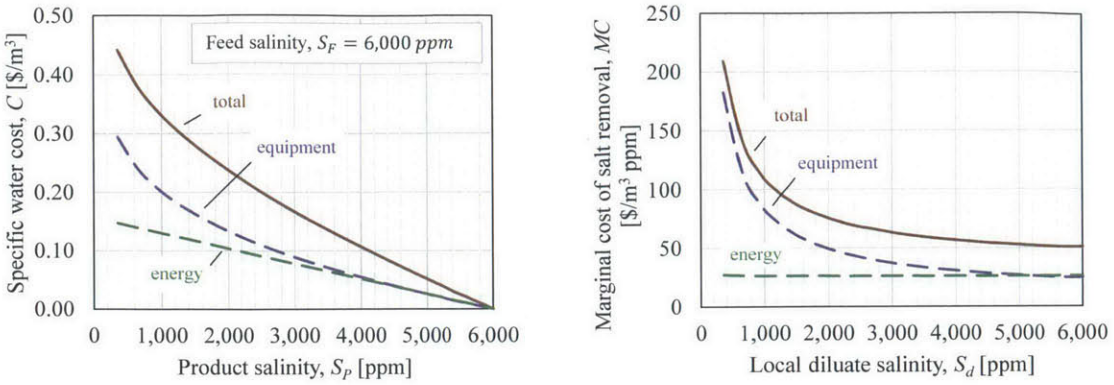

(a) Specific water cost **(b)** Marginal cost of salt removal

Figure 7-4 The falling marginal cost of salt removal with increasing local diluate salinity points to an opportunity to shift salt removal to higher salinities via hybridisation.

that the marginal cost of salt removal decreases with increasing diluate salinity. The marginal cost of equipment falls since the current density increases with salinity and more salt is removed per unit of membrane area. The marginal cost of energy per unit of salt removed equals the power density (current density times cell pair voltage iV^{cp}) divided by the rate of salt removal (which scales with the current density i). Therefore the marginal cost of energy is approximately constant and proportional to the cell pair voltage V^{cp}. Fig 7-4b illustrates an important opportunity to reduce ED costs by shifting salt removal to higher salinity.

Figure 7-5 illustrates the impact of shifting salt removal to higher salinity. In a standalone ED system salt is removed over a range from 3,000 ppm (the feed salinity) to 350 ppm (the product salinity). If, via hybridisation, salt could be removed at 3,000 ppm the specific cost of water would be represented by the rectangular area in Fig. 7-5 rather than the total area under the marginal cost curve. Figure 7-5 also shows that savings diminish as salt removal shifts to higher and higher salinity. This allows us to conclude that the percentage cost reduction in ED achieved through hybridisation:

1. is greatest when salt removal occurs at low salinity, *e.g.* when feed and product salinity are low

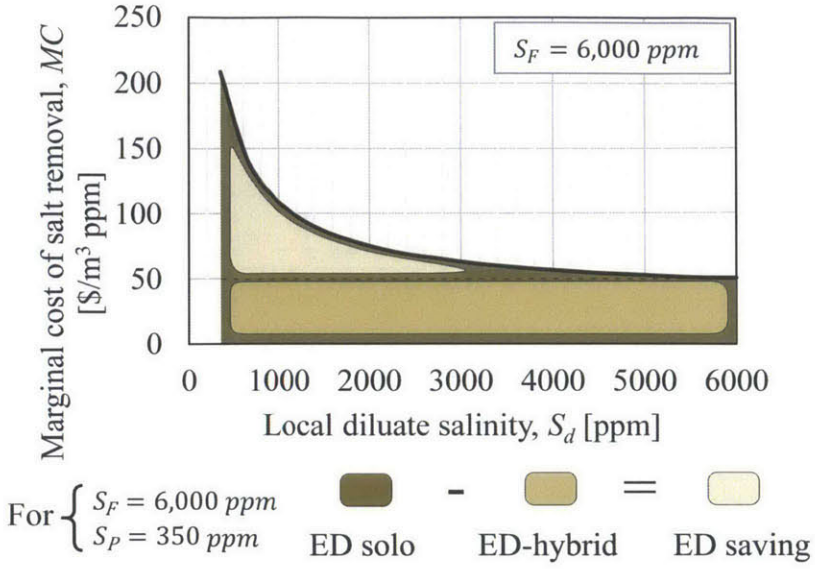

Figure 7-5 Cost savings can be achieved by shifting electrodialysis salt removal to higher salinity.

2. is smallest when salt removal occurs at high salinity, *e.g.* when feed salinity is high and especially when both feed and product salinity are high.

7.3 Reasons to prefer a simple ED-RO hybrid configuration

One way to shift salt removal to higher salinity is via the simple hybrid ED-RO configuration[12] illustrated in Fig. 7-3. This configuration has two benefits over a standalone electrodialysis system: the total membrane area (or number of stacks required) is reduced as higher rates of salt removal (current densities) are possible at higher salinities; and electrodialysis product requirements are relaxed since the final product consists of a blend of high purity RO permeate and the electrodialysis product. In practise, the recovery ratio of the reverse osmosis unit in the simple hybrid configuration would be a design variable. Increasing the recovery ratio leads to increasing reverse osmosis costs due to:

1. increased risks of scaling due to higher brine concentrations;

2. higher energy costs due to an increasing osmotic pressure;

3. the need for a 2nd stage of reverse osmosis if recoveries above 50% are required[8].

Increasing recovery ratios would also lead to reduced salt removal costs in the ED unit as the cost of salt removal falls at higher diluate salinities (see Fig. 7-5). This means that the recovery ratio would be set by a trade-off between reverse osmosis and electrodialysis costs. Furthermore, since, according to Fig. 7-5, there are diminishing returns as the ED feed salinity is increased the optimal recovery ratio is likely to be low if the system feed salinity is low and high if the system feed salinity is high. We leave the optimisation of the reverse osmosis recovery ratio to future work and, in this analysis, focus upon hybrid designs involving a single stage reverse osmosis unit treating feed streams of 3,000 ppm TDS and operating at 50% recovery. This puts the feed salinity to the ED unit at 6,000 ppm TDS, a point at which the change in salt removal costs with diluate salinity is already weak (Fig. 7-5).

To guide a decision between a standalone ED system and a simple ED-RO hybrid we require a measure of the relative cost of water from reverse osmosis and electrodialysis. In practise, one can envision costing a single-stage reverse osmosis unit operating at 50% recovery for a given feedwater flow rate and salinity. One can also envision costing (as we have done) water from a standalone electrodialysis system operating at a desired recovery ratio. Hence, in defining the cost ratio CR, we consider the the cost of water from a single-stage RO unit to that from a standalone ED unit. Specifically, the cost ratio is defined as the cost of water from an RO unit operating at 50% recovery $C_{RO}^{50\%}$ divided by the cost of water from an ED unit treating the same feedwater down to a desired product salinity, C_{ED}:

$$CR \equiv \frac{C_{RO}^{50\%}}{C_{ED}} \tag{7.2}$$

Applying equations describing the continuity of mass at the point of blending and across the reverse osmosis unit in Fig 7-5, and making the assumptions of:

- feed water at 3,000 ppm TDS,

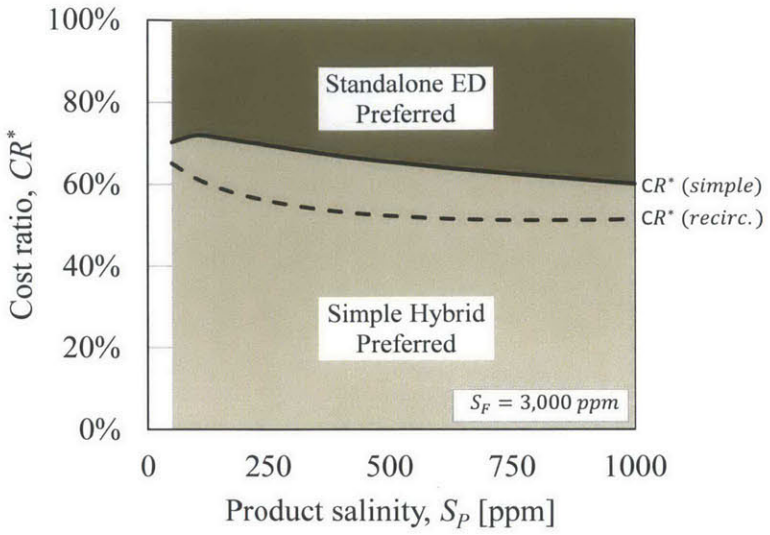

Figure 7-6 Dependence of the optimality of hybrid systems upon the cost ratio and the product salinity.

- a recovery ratio of 50% in the reverse osmosis unit, and

- a reverse osmosis product salinity of 50 ppm

we can compute value of CR at which the cost of water from a standalone ED and simple ED-RO hybrid systems are the same, which we define as the critical cost ratio CR^*. Detailed calculations are shown in 7.E.

Figure 7-6 shows that when high product purity is required ($S_P = 50$ ppm TDS) a simple hybrid ED-RO configuration is preferred when the cost of water from a single-stage RO unit is less than 70% of the cost of water from a standalone ED system. If potable water purity (500 ppm TDS) is required the relative cost of water from a single-stage RO system would have to be 65% of that from standalone ED to justify hybridisation. If product water requirements are even more relaxed (1,000 ppm TDS) the cost savings are smaller and it is even less likely for a hybrid to be preferred.

The dependence of the critical cost ratio CR^* upon product salinity, for the simple-hybrid, may be explained through consideration of the following equation equating

the cost of a standalone and a simple hybrid system:

$$C_{ED}^{solo}\dot{V}_P = C_{ED}^{hybrid}\dot{V}_{ED,P} + C_{RO}^{hybrid}\dot{V}_{RO,P}, \tag{7.3}$$

or, given a reverse osmosis recovery ratio of 50%:

$$C_{ED}^{solo} \approx \frac{1}{2}\left(C_{ED}^{hybrid} + C_{RO}^{hybrid}\right) \tag{7.4}$$

where C_{ED}^{solo}, C_{ED}^{hybrid} and C_{RO}^{hybrid} are the specific costs of water from electrodialysis units operating in standalone and hybrid configurations, and from the reverse osmosis unit in the hybrid configuration. $\dot{V}_P$, $\dot{V}_{ED,P}$ and $\dot{V}_{RO,P}$ are the volume flow rates of water from entire standalone or hybrid systems, from the ED unit within the hybrid and from the RO unit within the hybrid, respectively. Rearranging the above equation and introducing the critical cost ratio $CR^* \equiv C_{RO}^{hybrid}/C_{ED}^{solo}$, we see that the critical price ratio increases when the ratio of water costs from ED in the hybrid to the standalone system decreases:

$$CR^*\dot{V}_{RO,P} = \dot{V}_P - \frac{C_{ED}^{hybrid}}{C_{ED}^{solo}}\dot{V}_{ED,P} \tag{7.5}$$

$$CR^* \approx 2 - \frac{C_{ED}^{hybrid}}{C_{ED}^{solo}}. \tag{7.6}$$

Comparing ED units operating in stand-alone and simple-hybrid configurations, the ED unit within a stand-alone configuration will always have to desalinate the feed down to higher purity. Thus, considering Fig. 7-4b, the marginal cost of reducing ED product salinity will always be higher for the standalone system. This effect tends to decrease the cost ratio of ED in a simple-hybrid to a standalone ED unit, and thus increase the critical cost ratio CR^*. However, at low system product salinities an opposing effect becomes important. Due to the 50% recovery ratio of the RO unit, a marginal decrease in the system product salinity results in approximately double

that decrease in the ED product salinity in the hybrid configuration, since:

$$0.5(S_{RO,P} + S_{ED,P}) \approx S_P. \tag{7.7}$$

Therefore, at low system product salinity, where ED product salinities S_{ED}^{solo} and S_{ED}^{hybrid} are close, and thus their marginal costs of salt removal (in Fig. 7-4b) are close, the ratio of $C_{ED}^{hybrid}/C_{ED}^{solo}$ begins to rise and hence CR^* begins to fall.

While the critical price ratio by and large increases as system product salinity falls, there is a further reason why a simple hybrid system is likely to be preferred for high product purity. As product purity increases, ED costs will increase (according to Fig. 7-4a) and, as a consequence, increase relative to the cost of a single-stage RO system, resulting in a greater chance that CR will fall below CR^*. This is shown in Fig. 7-7 where the cost ratio is shown for a case where reverse osmosis water costs are \$0.20/m^3 (a reasonable value for brackish reverse osmosis[22]). In this scenario a simple hybrid would be preferred if product water salinity below approximately 300 ppm is required while a standalone ED system would be preferred for higher product salinities.

7.4 Reasons to prefer a recirculated hybrid ED-RO system

While the simple hybrid configuration of Fig. 7-3 can shift salt removal to higher salinities, the hybrid configuration[10,13–16] that incorporates recirculation can furthermore facilitate salt removal within a narrower band of higher salinity (closer to what is illustrated in Fig. 7-5). The effect of hybridising with recirculation is thus to cut down more drastically on ED costs than in the simple hybrid configuration, but at the expense of greater reverse osmosis costs, since a majority of product now comes from the reverse osmosis unit. As done for the simple hybrid system, by applying equations describing the continuity of mass at the point of blending and across the reverse osmosis unit in Fig. 7-6, and making the assumptions of

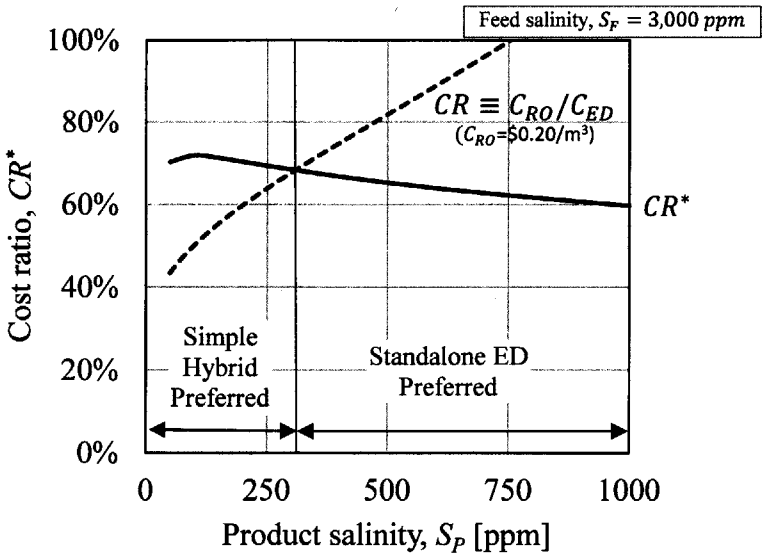

Figure 7-7 The ratio of water costs from single stage RO rise relative to ED as product salinity increases. At low product salinities a hybrid system can therefore be justified as the cost ratio falls below the critical cost ratio CR^* while at higher product salinities a standalone ED system is preferable.

- feed water at 3,000 ppm TDS,
- a recovery ratio of 50% in the reverse osmosis unit(s), and
- a reverse osmosis product salinity of 50 ppm,

we can illustrate in Fig. 7-6 the value of CR^* at which the cost of water from standalone ED and recirculated ED-RO hybrid systems are the same.

As with the simple hybrid system, the recirculated hybrid system is more strongly preferred over a standalone ED system when high product purities are required. However, regardless of product purity requirements, the recirculated system is inferior to the simple hybrid system, as indicated by a lower value of CR^*. In other words, if moving from a simple to a recirculated hybrid, the additional reverse osmosis costs do not justify the additional ED savings brought about by further shifting salt removal to higher salinity. One way to explain this is that, returning to Fig. 7-5, the greatest savings are made by shifting salt removal away from the lowest salinities and a simple ED-RO hybrid achieves just this. The reduced savings, achieved by further

increasing the concentration at which salt is removed, do not justify the additional reverse osmosis investment involved in a recirculated hybrid.

7.4.1 Implications of scaling and fouling on the selection of standalone versus hybrid systems

In addition to the preceding analysis, an assessment of the risks of membrane fouling and scaling are essential in guiding choice between standalone and hybrid systems.

In moving from a standalone ED system to a hybrid with reverse osmosis, pre-treatment will have to be adjusted to meet the requirements of reverse osmosis; the more sensitive of the two. Reverse osmosis feed requirements typically limit the Silt Density Index (SDI) to a maximum of 5 and the free chlorine content to a maximum of 0.1 ppm in the feed water[23]. Electrodialysis, by comparison, can tolerate an SDI of 10 and a free chlorine content of 0.5 ppm, as well as fluctuations up to an SDI of 15 and free chlorine of 30 ppm[24].

In the simple hybrid configuration, the concentration of non-ionic and weakly-ionised species will be almost unchanged between the feed to the system and the final product; since weakly-ionised compounds are poorly removed by electrodialysis. The suitability of the simple hybrid will then depend upon whether such species can be tolerated in the product or cost effectively removed after the process. In moving from a simple ED-RO hybrid to a recirculated configuration, weakly-ionised species in the feed would build up within the recirculation loop where their primary means of escape is via the RO bypass, Fig. 7-5. If such species are low in solubility (*e.g.* silica[10]) they can potentially precipitate within the electrodialysis or reverse osmosis units. In some cases, species may be encouraged to dissociate into ionic form by pH adjustment[25] which would then allow their removal via electrodialysis. The costs associated with this pH adjustment would have a bearing on the decision of whether to hybridise or not.

Since considerations of scaling and fouling tend to act in favour of standalone electrodialysis systems, the effective cost ratio that single-stage RO systems must

reach to make hybridisation viable, in particular with recirculation, is likely to be lower than those suggested by the present analysis.

7.5 Sensitivity analysis

Table 7.1 provides the sensitivity of the critical cost ratio, CR^*, to key input parameters for a simple hybrid system operating with a feed of 3,000 ppm, a product stream of 500 ppm and an applied voltage per cell pair corresponding to 70% of the limiting current density at 350 ppm. The sensitivity to each input parameter, X, is calculated according to:

$$\Sigma = \frac{X}{CR^*}\frac{\partial CR}{\partial X}. \tag{7.8}$$

CR^* is more sensitive to percentage changes in the feed salinity S_F than to percentage changes in the product salinity S_P. This is because, for the conditions at which these sensitivities are evaluated, the feed salinity is almost one order of magnitude greater than the product salinity. A 1% change in feed salinity will therefore affect the total salt removal required almost ten times as much as a 1% change in product salinity.

The sensitivity of CR^* to the specific cost of equipment, K_Q, and the specific cost of energy, K_E, may be understood via Fig. 7-4a. Since capital costs dominate energy costs at low product salinity, CR^* is more sensitive to K_Q than K_E.

Finally, to understand the sensitivity of CR^* to cell pair voltage, V_{cp}, we can consider the effect of cell pair voltage upon the marginal cost of salt removal. Three voltages are considered in Fig. 7-8 that correspond to 50%, 70% and 90% of the limiting current density at a point in the system where the diluate salinity is 350 ppm (see 7.B.2). The effect of increasing the cell pair voltage is to increase energy costs but to decrease capital costs, because the current drawn is higher. This results in a flattening of the marginal cost curve as the energy cost component becomes more significant (see Fig. 7-4b). Due to the opposing effects of rising energy costs

and falling equipment costs with voltage only a small change in the marginal cost curves is seen in Fig. 7-8, meaning that, over this range of voltages and for the chosen cost parameters, CR^* is weakly affected.

Figure 7-8 also helps explain the effect of changing specific equipment and electricity prices on CR^*. For the chosen set of cost parameters, Fig. 7-8 suggests that the optimal strategy is close to 90% of limiting current density. Were specific equipment costs (in \$/m^2 of cell pair area) to decrease relative to the cost of electricity (in \$/kWh) then the marginal cost curve would tend to flatten, thus weakening the benefit of shifting salt removal to higher salinity. However, this flattening would, to some extent, be mitigated since the optimal voltage would be driven down, serving to increase equipment relative to energy costs.

Table 7.1 Sensitivity of the critical cost ratio

Perturbed Variable	Sensitivity Σ
S_F	0.65
K_Q	0.42
V_{cp}	0.19
K_E	0.14
S_P	0.10

7.6 Conclusion

Hybrid ED-RO systems will be preferred over standalone ED systems where a high purity product is required *and* provided the cost of water from RO is low relative to ED. The break-even point between a hybrid ED-RO and a standalone ED system occurs when the cost of water from a single stage RO system, operating at 50% recovery, is between about 60-70% of the cost of water from a standalone ED system. At break-even, the savings in ED costs, brought about by the elimination of low salinity stages in a hybrid, justify the added costs of RO. The higher the product purity required, the greater the potential reduction in ED costs through hybridisation, and hence the higher the break-even cost ratio (cost of water from single stage RO relative to standalone ED).

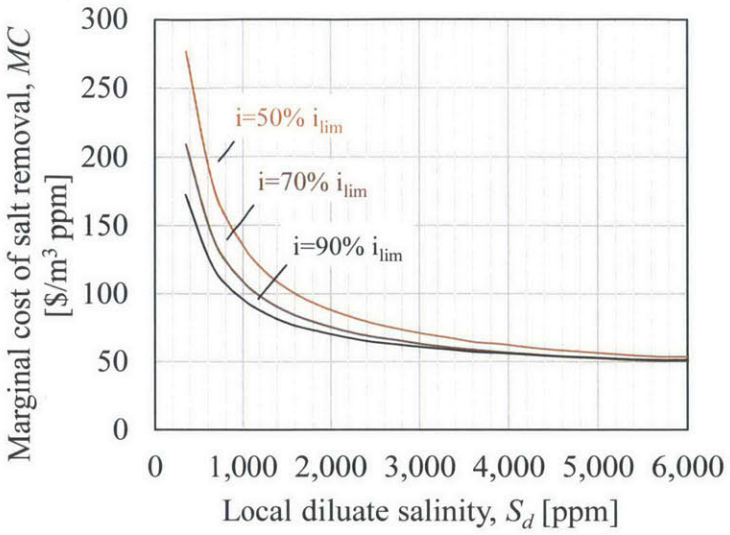

Figure 7-8 Illustration of the sensitivity of the marginal cost of salt removal to cell pair voltage.

7.A Estimation of the growth of world brackish water desalination

Annualised growth in brackish desalination over the past ten years was calculated by considering the online capacity in the years 2003 and 2013. Data for new capacity brought online in each of the years 1993 until 2013 was obtained by summing together the new capacity online of 'River or low concentrated saline water (TDS 500 ppm - 3,000 ppm)' and 'Brackish water or inland water (TDS 3,000 - 20,000 ppm)' of plants tracked by Desaldata[1]. Online capacity in 2003 was then computed by summing together new capacity brought online in the years from 1993 to 2003, while online capacity in 2013 was computed by summing together new capacity brought online in the years 1993 to 2013.

7.B Electrodialysis model details

7.B.1 Electrodialysis transport model

The total area of the electrodialysis system is broken into a series of cell-pair stacks. The diluate stream flows through these stacks in series. The concentrate streams are recirculated within each stack. To keep constant the volume of concentrate within each stack, a portion is bled off. The concentrate concentration in each stack is determined by the relative salt and water flux from diluate to concentrate:

$$x_c = \frac{J_s}{J_s + J_w} \tag{7.9}$$

where x_c is the mole fraction of salt in the concentrate, J_s is the net salt molar flux and J_w the net water molar flux from diluate to concentrate in a cell pair. The combination of the bleed streams from all stacks allows the computation of the outlet concentrate salinity from the ED system and the recovery ratio.

Salt, water and charge transport are modelled based upon the approach taken in previous work[19,26]. Salt transport is modelled by a combination of migration and diffusion:

$$J_s = \frac{T_s^{cp} i}{F} - L_s \left(C_{s,c,m} - C_{s,d,m}\right) \tag{7.10}$$

and water transport by a combination of migration (electro-osmosis) and osmosis:

$$J_w = \frac{T_w^{cp} i}{F} + L_w \left(\pi_{c,m} - \pi_{d,m}\right) \tag{7.11}$$

T_s^{cp} and T_w^{cp} are the overall salt and water transport numbers for the cell pair, L_s and L_w are the overall salt and water permeabilities of the cell pair and all four quantites are considered independent of diluate and concentrate salinity. C denotes concentration in moles per unit volume and π osmotic pressure (calculated employing osmotic coefficients for aqueous NaCl from Robinson and Stokes[27]). F is Faraday's constant and the subscripts s, c, d and m denote salt, the concentrate stream, the

diluate stream and the membrane-solution interface. The difference between bulk and membrane wall concentrations and osmotic pressures is accounted for by a convection-diffusion model of concentration polarisation:

$$\Delta C = -\frac{(\bar{T}_{cu} - t_{cu})}{D} \frac{i}{F} \frac{2h}{\mathrm{Sh}} \tag{7.12}$$

where D is the solute diffusivity (distance squared per unit time), h is the channel height and t_{cu} is the counter-ion transport number in the diluate and concentrate solutions and is approximated as 0.5 for both anions and cations. $\bar{T}_{cu}$ is the integral counter-ion transport number in the membrane that accounts for both migration and diffusion. $\bar{T}_{cu}$ is the integral counter-ion transport number in the membrane that accounts for both migration and diffusion.

$$\bar{T}_{cu} \approx \frac{T_s^{cp} + 1}{2}. \tag{7.13}$$

This expression would be exact were diffusion within the membrane to be negligible and the counter-ion transport number to be equal in anion and cation exchange membranes. Sh, the Sherwood number is computed using the correlation obtained by Kuroda et al.[28] for spacer A in their analysis:

$$\mathrm{Sh} = 0.5\mathrm{Re}^{1/2} Sc^{1/3} \tag{7.14}$$

where Sc is the Schmidt number, calculated using the limiting diffusivity of NaCl in water[27] and the kinematic viscosity of pure water ν[29], both at 25°C. Re is the Reynolds number defined as:

$$\mathrm{Re} = \frac{2hV}{\nu} \tag{7.15}$$

where V is the mass averaged velocity in the channel.

The cell pair voltage, is represented as the sum of ohmic terms and membrane

potentials:

$$V^{cp} = i\left(\bar{r}_{am} + \bar{r}_{cm} + \frac{h_d}{\sigma\Lambda_d C_d} + \frac{h_c}{\sigma\Lambda_c C_c}\right) + E_{am} + E_{cm} \tag{7.16}$$

where Λ is the molar conductivity, itself a function of concentration[30,31], h denotes channel height and σ denotes the spacer shadow factor. Membrane surface resistances, denoted $\bar{r}$, are considered to be independent of salinity. Junction potentials associated with concentration polarisation are neglected, while the sum of the anion and cation membrane potentials $E_{am} + E_{cm}$ is computed considering quasi-equilibrium migration of salt and water across the membranes (based on the approach of Prentice[32]):

$$E_{am}+E_{cm} = T_s^{cp}\frac{1}{F}(\mu_{s,c,m} - \mu_{s,d,m}) + T_w^{cp}\frac{1}{F}(\mu_{w,c,m} - \mu_{w,d,m}) \tag{7.17}$$

where μ_s denotes the chemical potential of salt and μ_w the chemical potential of water; both calculated employing osmotic coefficients and NaCl activity coefficient data from Robinson and Stokes[27].

Knowing the inlet and outlet salinities from each stack, the salt flux, water flux and cell pair voltage allow the computation of energy, area and concentrate salinity for each stack.

7.B.2 Evaluation of the stack voltage

The cell pair voltage is set such that the ratio of the current density to the theoretical limiting current density is approximately equal to 70% throughout the stack. This is done by considering a reference point in the system where the salinity is 350 ppm. The limiting current density at this point is calculated using:

$$i_{lim} = -\frac{D}{\bar{T}_{cu} - t_{cu}}\frac{\mathrm{Sh}}{2h}FC_d. \tag{7.18}$$

Given this limiting current density the cell pair voltage V_{cp}^{350ppm} is solved for by setting $i = 0.7i_{lim}$ within Eq (7.16). This cell pair voltage is then employed across the entire system. Employing the same cell pair voltage across the entire system approximately

maintains the same ratio of i/i_{lim} throughout. This is because both the current density and the limiting current density both scale approximately with the diluate concentration. At higher diluate concentrations this approximation breaks down as the cell pair resistance no longer scales with the diluate resistance when membrane resistances become important.

7.B.3 Electrodialysis cost model

The standalone electrodialysis system and the electrodialysis subsystem are costed on the basis of system size, represented by membrane area, and energy consumption. Equipment costs are assumed to scale with membrane area and are costed employing an equipment cost per unit cell pair area K_Q[20,33]. The equipment costs are amortised considering a plant life τ and an annualised cost of capital of r:

$$C_Q = \frac{1}{\dot{V}_{d,o}} \frac{K_Q \sum_i A_i}{\frac{1}{r}\left[1 - \left(\frac{1}{1+r}\right)^{\tau}\right]} \tag{7.19}$$

where A_i is the area of a single-stage and $\dot{V}_{d,o}$ is the volume flow-rate of diluate out of the final ED stage. Energy costs are computed by taking the product of stack power consumption and the cost of electricity K_E:

$$C_E = \frac{K_E}{\dot{V}_{d,o}} \sum_i V_{cp} i_i A_i \tag{7.20}$$

where i_i is the current density in stage i. Energy required for pumping power is neglected as it may be shown to be negligible relative to energy required to drive desalination (7.F). The combination of equipment and energy costs:

$$C = C_Q + C_E \tag{7.21}$$

gives the specific cost of water C. A summary of the membrane (validated experimentally by Fidaleo and Moresi[18]), cell-pair geometry and financial parameters employed are provided in Table 7.2.

7.C Estimation of specific equipment costs

Sajtar and Bagley[38] reviewed the capital costs of electrodialysis plants removing between 0 and 2,000 mg/L of total dissolved solids from a feed stream. They found capital costs to scale approximately linearly with product flow rate such that the capital cost per unit of production rate was \$568/(m^3/day).

Running the model of 7.B, with a feed salinity of 2,350 ppm, a product salinity of 350 ppm (*e.g.* approximately 2,000 mg/L of TDS removal), and the voltage set such that the current density is 70% of its limiting value in the final stage (0.8 V per cell pair), yields an area requirement of 0.39 m^2 of cell pair area/(m^3/day).

The combination of this information on capital cost from Sajtar and Bagley[38] with the area requirements predicted by the model results in estimated specific equipment costs of approximately \$1500/m^2 cell pair area.

7.D Validation of energy consumption

Sajtar and Bagley[38] reviewed the energy consumption of electrodialysis plants removing between 0 and 2,000 mg/L of total dissolved solids from a feed stream. Though there is a positive correlation between salt removal and electrical consumption there is significant scatter in the data at these levels of TDS removal, with energy consumption varying between 0.1 and 1 kWh/m^3. The ED model, run with the conditions described in 7.C, predicts energy consumption of 0.79 kWh/m^3, which falls between these limits. Of course, energy consumption will depend upon stack design parameters such as diluate channel height, the spacer shadow factor and the voltage applied per cell pair.

7.E Hybrid model details

Similar equations apply for the computation of masses and salinities within the simple and recirculated hybrid systems (Fig. 7-9). The conservation of total mass and salt

mass at the points of product blending,

$$\dot{m}_{RO,P} + \dot{m}_{ED,P} = \dot{m}_P \tag{7.22}$$

$$S_{RO,P}\dot{m}_{RO,P} + S_{ED,P}\dot{m}_{ED,P} = S_P\dot{m}_P, \tag{7.23}$$

and on the RO units,

$$\dot{m}_{RO,P} + \dot{m}_{ED,F} = \dot{m}_{RO,F} \tag{7.24}$$

$$S_{RO,P}\dot{m}_{RO,P} + S_{ED,F}\dot{m}_{ED,F} = S_{RO,F}\dot{m}_{RO,F}, \tag{7.25}$$

are the same for both hybrids, as is the consideration of the recovery ratio of the RO system,

$$\dot{m}_{RO,P}(1 - S_{RO,P}) = 50\% \times \dot{m}_{RO,F}(1 - S_{RO,F}). \tag{7.26}$$

The main difference arising is that the determination of masses and salinities is fully specified by the above equations in the case of the recirculated hybrid system whereas the simple hybrid system requires the above equations to be simultaneously solved with the set of coupled non-linear equations describing the ED system, which may be written as:

$$\dot{m}_{ED,P} = \text{fn}(\dot{m}_{ED,F}, S_{ED,F}, S_{ED,P}). \tag{7.27}$$

For both hybrid systems and the standalone ED system the specific cost of water (based on the ED diluate outlet flow rate) is available from the ED model and may be written:

$$C_{ED} = \text{fn}(\dot{m}_{ED,F}, S_{ED,F}, S_{ED,P}) \tag{7.28}$$

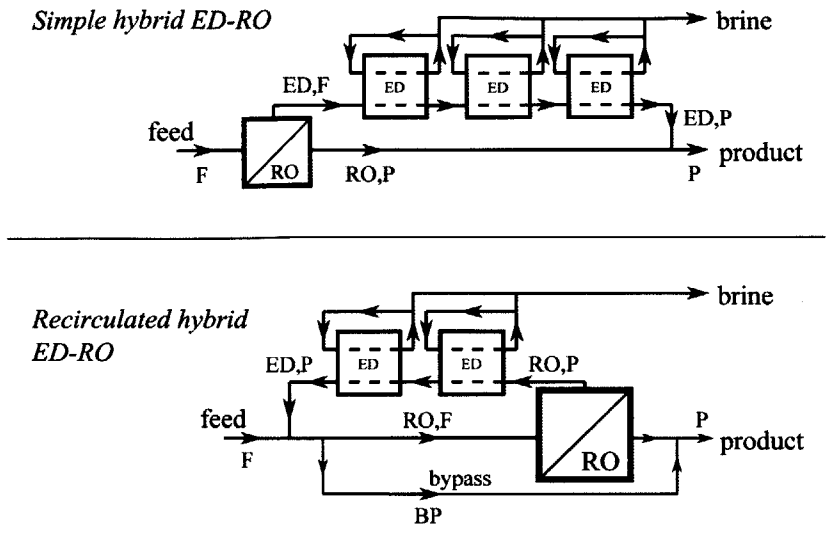

Figure 7-9 Simple and recirculated hybrid systems with streams labelled

The overall specific water cost for the either hybrid system C_{ED}^{hybrid} and for a standalone ED system, C_{ED}^{solo}, are then equated:

$$C_{ED}^{solo}\frac{\dot{m}_P}{\rho_P} = C_{ED}^{hybrid}\frac{\dot{m}_{ED,P}}{\rho_{ED,P}} + C_{RO}\frac{\dot{m}_{RO,P}}{\rho_{RO,P}} \tag{7.29}$$

and divided across by C_{ED}^{solo} to yield:

$$\frac{\dot{m}_P}{\rho_P} = \frac{C_{ED}^{hybrid}\dot{m}_{ED,P}}{C_{ED}^{solo}\rho_{ED,P}} + CR^*\frac{\dot{m}_{RO,P}}{\rho_{RO,P}} \tag{7.30}$$

where CR^* is the quantity of interest, the critical cost ratio of water from the single-stage RO system to the standalone ED system.

7.F Assessment of electrodialysis power requirements for pumping

The power consumption associated with drawing a current and pumping fluid through the channels may be compared on the basis of unit cell pair area. Power consumption

associated with salt removal,

$$p_I = V_{cp} i, \tag{7.31}$$

where V_{cp} is the cell pair voltage and i is the current density, is minimum in the final ED stack where the diluate salinity is lowest (350 ppm), the resistance highest and thus, for a constant cell pair voltage, the current density lowest. Power consumption associated with pumping may be quantified by considering viscous dissipation per unit cell pair area:

$$p_{pump} = 2Vh\frac{\Delta P}{L} \tag{7.32}$$

where the factor of 2 accounts for viscous dissipation in the diluate and concentrate channels, the product Vh is the volumetric flow rate per unit channel width through a cell pair and $\frac{\Delta P}{L}$ is the pressure drop per unit length, which may be found via the friction factor, defined as:

$$f = \frac{\Delta P}{0.5\rho V^3 \frac{L}{2h}} \tag{7.33}$$

where ρ, the fluid density, is approximated by the density of pure water[35]. A friction factor correlation, such as that obtained by Kuroda et al.[28] for spacer A in their analysis,

$$f = 9.6Re^{-1/2}, \tag{7.34}$$

allows the computation of p_{pump}. Given the parameters of Table 7.2, the power associated with drawing current at 350 ppm TDS is over 620 times that associated with viscous dissipation.

Nomenclature

Acronyms

ED	electrodialysis
ppm	parts per million, mg solute per kg solution
RO	reverse osmosis

Roman Symbols

A	area, m^2
C	cost/concentration, $\$/m^3$/ mol/m^3
D	diffusion coefficient, m^2/s
E	potential, V
F	Faraday's constant, C/mol
h	channel height, m
i	current density, A/m^2
J	molar flux, $mol/m^2 \cdot s$
K_E	specific cost of electricity, \$/kWh
K_Q	specific cost of equipment, $\$/m^2$
L_w	permeability to water, $mol/m^2 \cdot s \cdot bar$
MC	marginal Cost, $\$/m^3$-ppm
$\dot{m}$	mass flow rate, kg/s
r	rate of return on capital, -
Re	Reynolds number, -
$\bar{r}$	area resistance, Ωm^2
p	power density, -
CR	cost ratio, -
S	salinity, kg salt/kg solution
Sc	Schmidt number, -
Sh	Sherwood number, -

t	solution transport number, -
T_s	membrane salt transport number, -
T_w	membrane water transport number, -
$\bar{T}$	integral ion transport number, -
V	flow velocity, m/s
V_{cp}	cell pair voltage, V
$\dot{V}$	volume flow rate, m^3/s
w	water
x	mole fraction, -
X	input parameter, various

Greek Symbols

Δ	difference
Λ	molar conductivity, Sm^2/mol
μ	chemical potential, J/mol
ν	viscosity, -
π	osmotic pressure, bar
ρ	density, kg/m^3
Σ	sensitivity, -
τ	time, years

Subscripts

am	anion exchange membrane
BP	bypass
c	concentrate
cm	cation exchange membrane
cu	counter ion
d	diluate
ED	electrodialysis

F	feed
m	at membrane surface
i	counting index
I	associated with current
$pump$	pump
P	product
RO	reverse osmosis
s	salt
w	water

Superscripts

hyb	hybrid
solo	standalone
*	optimal
50%	operating at 50% recovery

Symbol	Value	Ref.
Membrane Performance Parameters		
T_s	0.97	[18]
T_w	10	[18]
L_w	1.4×10^{-4} mol/bar-m^2-s	[18]
L_s	1.4×10^{-8} m/s	[18]
$\bar{r}_{am}, \bar{r}_{cm}$	2.8 Ω cm^2	[18]
Solution Properties		
D	1.61×10^{-9} m^2/s	[27]
t_{cu}	0.5	[34]
ν	8.9×10^{-7} m^2/s	[29]
ρ	9.97×10^{2} kg/m^3	[35]
Flow Properties/Geometry		
h	0.4 mm	[18,20a]
V	0.05 m/s	[20b]
σ	0.7	[26]
N	20	-
Re	44.8	calc.
Sh	27.5	calc.
Cost Parameters		
K_Q	1,500 \$/m^2 cell pair	7.C
τ	20 yr	-[c]
r	10%	[36d]
K_E	0.065 \$/kWh	[37e]
Operational Conditions		
S_F	3,000 ppm	-
V^{cp}	0.8 V	[20]

[a] Lee et al.[20] suggest 0.65 mm, while Fidaleo et al.[18] employ 0.7 mm;
[b] Lee et al.[20] suggest 0.075 m/s
[c] increased from Lee et al.[20] and Tsiakis et al.'s[33] suggestion of a 6 year plant life
[d] Returns on an entire project are assumed to be twice the 4.78% rate paid on bonds issued to finance the Carlsbad desalination plant[36].
[e] based on conventional combined cycle natural gas plants coming online in 2018 at 0.067 \$/kWh

Table 7.2 Electrodialysis Model Parameters

Bibliography

[1] Desaldata, Analysis, desaldata.com (2013).

[2] S. C. McCutcheon, J. L. Martin, T. Barnwell Jr, D. Maidment, Water quality., McGraw-Hill Inc., 1992.

[3] M. Radmor, J. Strauss, J. Bishop, G. Piatt, K. DeGroat, D. Fargo, D. Eisemann, C. Mulligan, Desalination and water purification technology roadmap, Tech. rep., DTIC Document (2003).

[4] A. Koussis, E. Georgopoulou, A. Kotronarou, D. Lalas, P. Restrepo, G. Destouni, C. Prieto, J. Rodriguez, J. Rodriguez-Mirasol, T. Cordero, A. Gomez-Gotor, Cost-efficient management of coastal aquifers via recharge with treated wastewater and desalination of brackish groundwater: general framework, Hydrological Sciences Journal–Journal des Sciences Hydrologiques 55 (7) (2010) 1217–1233.

[5] N. Wolthek, K. Raat, J. A. de Ruijter, A. Kemperman, A. Oosterhof, Desalination of brackish groundwater and concentrate disposal by deep well injection, Desalination and Water Treatment 51 (4-6) (2013) 1131–1136.

[6] D. A. Blair, W. D. Spronz, K. W. Ryan, Brackish groundwater desalination: A community's solution to water supply and aquifer protection, JAWRA Journal of the American Water Resources Association 35 (5) (1999) 1201–1212.

[7] D. A. Roberts, E. L. Johnston, N. A. Knott, Impacts of desalination plant discharges on the marine environment: A critical review of published studies, water research 44 (18) (2010) 5117–5128.

[8] R. L. Stover, Industrial and brackish water treatment with closed circuit reverse osmosis, Desalination and Water Treatment 51 (4-6) (2013) 1124–1130.

[9] R. Rautenbach, W. Kopp, C. Herion, Electrodialysis-contact sludge reactor and reverse osmosis-phase separator, two examples of a simple process combination for increasing the water recovery rate of membrane processes, Desalination 72 (3) (1989) 339–349.

[10] Y. Oren, E. Korngold, N. Daltrophe, R. Messalem, Y. Volkman, L. Aronov, M. Weismann, N. Bouriakov, P. Glueckstern, J. Gilron, Pilot studies on high recovery BWRO-EDR for near zero liquid discharge approach, Desalination 261 (3) (2010) 321–330.

[11] R. Rautenbach, R. Habbe, Seeding technique for zero-discharge processes, adaption to electrodialysis., Desalination. 84 (1-3) (1991) 153–161.

[12] E. Korngold, L. Aronov, N. Daltrophe, Electrodialysis of brine solutions discharged from an RO plant, Desalination 242 (1-3) (2009) 215–227.

[13] E. R. Reahl, Reclaiming reverse osmosis blowdown with electrodialysis reversal, Desalination 78 (1) (1990) 77–89.

[14] S. Thampy, G. R. Desale, V. K. Shahi, B. S. Makwana, P. K. Ghosh, Development of hybrid electrodialysis-reverse osmosis domestic desalination unit for high recovery of product water, Desalination 282 (SI) (2011) 104–108.

[15] Y. Zhang, K. Ghyselbrecht, B. Meesschaert, L. Pinoy, B. Van der Bruggen, Electrodialysis on ro concentrate to improve water recovery in wastewater reclamation, Journal of Membrane Science 378 (1) (2011) 101–110.

[16] Y. Zhang, K. Ghyselbrecht, R. Vanherpe, B. Meesschaert, L. Pinoy, B. Van der Bruggen, Ro concentrate minimization by electrodialysis: Techno-economic analysis and environmental concerns, Journal of Environmental Management 107 (2012) 28–36.

[17] M. Badruzzaman, J. DeCarolis, A. Subramani, W. Pearce, J. Jacangelo, Performance and cost effectiveness of reverse osmosis and electrodialysis reversal for desalination of brackish groundwater containing high silica, in: AWWA and AMTA Membrane Technology Conference, Memphis, TN, American Water Works Association and American Membrane Technology Association, 2009.

[18] M. Fidaleo, M. Moresi, Electrodialytic desalting of model concentrated nacl brines as such or enriched with a non-electrolyte osmotic component, Journal of Membrane Science 367 (1) (2011) 220–232.

[19] R. K. McGovern, S. M. Zubair, J. H. Lienhard V, The cost effectiveness of electrodialysis for diverse salinity applications, Under review.

[20] H.-J. Lee, F. Sarfert, H. Strathmann, S.-H. Moon, Designing of an electrodialysis desalination plant, Desalination 142 (3) (2002) 267–286.

[21] S. A. Klein, Engineering Equation Solver, Academic Professional V9.438-3D (2013).

[22] J. E. Miller, Review of water resources and desalination technologies, Sandia National Labs Unlimited Release Report SAND-2003-0800.

[23] Hydranautics, (2014) [cited 2014.03.11].
URL

[24] General Electric Company, GE 2020 EDR Systems (2013).

[25] A. J. Giuffrida, Electrodialysis process for silica removal (1981).

[26] M. Fidaleo, M. Moresi, Optimal strategy to model the electrodialytic recovery of a strong electrolyte, Journal of Membrane Science 260 (1) (2005) 90–111.

[27] R. Robinson, R. Stokes, Electrolyte Solutions, Courier Dover Publications, 2002.

[28] O. Kuroda, S. Takahashi, M. Nomura, Characteristics of flow and mass transfer rate in an electrodialyzer compartment including spacer, Desalination 46 (1) (1983) 225–232.

[29] E. R. Association, Viscosity of Water and Steam, Edward Arnold Publishers, 1967.

[30] T. Shedlovsky, The electrolytic conductivity of some uni-univalent electrolytes in water at 25 C, Journal of the American Chemical Society 54 (4) (1932) 1411–1428.

[31] J. Chambers, J. M. Stokes, R. Stokes, Conductances of concentrated aqueous sodium and potassium chloride solutions at 25 C, The Journal of Physical Chemistry 60 (7) (1956) 985–986.

[32] G. Prentice, Electrochemical engineering principles, Vol. 1, Prentice Hall Englewood Cliffs, NJ, 1991.

[33] P. Tsiakis, L. G. Papageorgiou, Optimal design of an electrodialysis brackish water desalination plant, Desalination 173 (2) (2005) 173–186.

[34] A. Sonin, R. Probstein, A hydrodynamic theory of desalination by electrodialysis, Desalination 5 (3) (1968) 293–329.

[35] E. R. Association, Thermodynamic Properties of Water and Steam, Edward Arnold Publishers, 1967.

[36] San Diego County Water Authority, Carlsbad desalination project (2012).

[37] U.S. Energy Information Administration, Annual energy outlook 2013, Tech. rep. (2013).

[38] E. T. Sajtar, D. M. Bagley, Electrodialysis reversal: Process and cost approximations for treating coal-bed methane waters, Desalination and Water Treatment 2 (1-3) (2009) 284–294.

Chapter 8

Summary and Impact

8.A Seawater desalination and the future of forward osmosis

Until now forward osmosis was often seen as a technology with the potential to reduce the energy requirements of forward osmosis. The analysis of chapter 2 draws attention to the energy penalty involved in the draw-dilution step of forward osmosis, a factor that has not yet been identified in literature. This energy penalty is shown to be important to the extent that it puts a theoretical limit upon the energy required for forward osmosis putting it it at a significant disadvantage to reverse osmosis for seawater desalination. These findings are significant to the field of forward osmosis research as they suggest the need for a realignment of research away from seawater and towards alternate applications such as fertiliser irrigation or the treatment of waters of a salinity that is beyond reverse osmosis.

In all forward osmosis applications there is a perception that, in choosing whether to orient the membrane's active layer towards the feed or the draw solution, one is forced to choose between low flux and high fouling. The analysis of chapter 3 shows that this is not always the case. For fertiliser irrigation and the concentration of flowback waters the active-layer-to-feed may well give maximum flux and minimum fouling. Furthermore, chapter 3 provides an intuitive framework that allows a practi-

tioner to understand, for a given application, how strongly membrane orientation will affect flux. In doing so practitioners will be better informed when making trade-offs between fouling and flux.

8.B Desalination of produced waters via electrodialysis

While the conventional thinking is that electrodialysis is most cost effective at low salinity, Chapter 4 reveals that the effect of salinity on cost is more subtle. From a thermodynamic perspective, ED is most effective removing salt from streams in the range of 1,000 ppm TDS to 20,000 ppm TDS. This finding should encourage the development of electrodialysis for further applications where treatment is required in this range, such as the food and beverage industry and the mining industry.

Again, while conventional thinking might suggest that the cost of salt removal from high salinity produced waters with electrodialysis might be prohibitive, Chapter 6 demonstrates that this need not be the case. From the perspective of energy consumption and equipment size, ED can compete with incumbent thermal technologies, albeit because the cost of incumbent technologies is high. This work takes important steps towards the commercialisation of ED for such applications by providing a numerical system model that has been validated over a range of 250 ppm to 192,000 ppm and also a means of optimising the stack voltage to achieve costs savings of up to 30%.

8.C Desalination of brackish waters via hybrid electrodialysis - reverse osmosis systems

While hybrid electrodialysis-reverse osmosis systems previously existed, their design and optimisation has not been investigated or understood. Given the understanding developed in Chapters 4 and 6 of how salt removal costs with electrodialysis fall as

the feed water salinity rises, C1hapter 7 provides an intuitive framework to explain how hybrid ED-RO systems can leverage this characteristic. Furthermore, this work provides a simple rule of thumb allowing practitioners to rapidly identify the economic benefit or disbenefit of adopting a hybrid configuration.